

CUTTINGS TRANSPORT IMPLICATIONS FOR DRILL STRING DESIGN:
A STUDY WITH COMPUTATIONAL FLUID DYNAMICS

by
Gregory B. Dykes, Jr.

Copyright by Gregory B. Dykes, Jr. 2014

All Rights Reserved

A thesis submitted to the Faculty and the Board of Trustees of the Colorado School of Mines in partial fulfillment of the requirements for the degree of Master of Science (Petroleum Engineering).

Golden, Colorado

Date _____

Signed: _____

Gregory B. Dykes, Jr.

Signed: _____

Dr. Alfred William Eustes III

Thesis Advisor

Golden, Colorado

Date _____

Signed: _____

Dr. Ramona M. Graves

Professor, Petroleum Engineering

Dean, College of Earth Resource Sciences and Engineering

ABSTRACT

Modern drilling programs require a variety of drilling equipment over a variety of well paths. Changes in equipment and parameters greatly affect the process of cuttings transport in the wellbore. While extensive experimental work has explored a multitude of drilling parameters, a firm methodology for using computational fluid dynamics to model this process has not been established. Moreover, computational models more easily compare different drilling geometries than experimental apparatuses that require significant equipment exchange. This thesis first establishes a methodology for utilizing computational fluid dynamics to model cuttings transport in a drilling annulus. The results establish qualitatively comparable results to prior experimental work. Therefore, the tool is made useful by isolating and studying the effects of changing parameters. The second part of the thesis consists of a parameter study to determine effects of drill pipe rotation, drilling fluid velocity, drill pipe eccentricity, wellbore inclination, and rate of penetration on cuttings accumulation over different drill pipe and borehole sizes. Results include both individual parameter effects as well as combined effects of the parameters in a single scenario, some of which suggest more complex mechanisms of cuttings transport than previously postulated.

TABLE OF CONTENTS

CHAPTER 1: INTRODUCTION	1
1.1 Motivation	1
1.2 Background	2
1.2.1 Drilling with Coiled Tubing.....	2
1.2.2 Composite Coiled Tubing.....	6
1.2.3 Cuttings Transport	10
1.2.4 Computational Fluid Dynamics (CFD).....	11
1.3 Objectives.....	11
1.4 Methodology	12
CHAPTER 2: MODEL VALIDATION	13
2.1 Overview of FVM and CFD Processes	13
2.2 Geometry	14
2.3 Mesh.....	16
2.4 CFD General Parameters.....	18
2.5 CFD Models	18
2.5.1 Multiphase.....	18
2.5.2 Viscosity	19
2.6 Materials.....	20
2.6.1 Drilling Fluid	20
2.6.2 Drill Cuttings	20
2.7 Phases.....	20
2.7.1 Phase Definitions	21
2.7.2 Phase Interaction.....	22

2.8	Boundary Conditions.....	23
2.8.1	Inlet	23
2.8.2	Outlet.....	24
2.8.3	Walls	24
2.9	Solution Settings	25
2.10	Results and Discussion	25
2.10.1	Simulation 1	25
2.10.2	Simulation 2	27
2.10.3	Sensitivities and Accuracy	31
2.10.4	CFD Limitations and Future Studies	35
2.11	Conclusions	36
CHAPTER 3: PARAMETER IMPLICATIONS.....		37
3.1	General Methodology.....	37
3.2	Flow Rate and Velocity Study	38
3.2.1	Study Design.....	38
3.2.2	Results.....	39
3.3	Eccentricity Study	42
3.3.1	Study Design.....	42
3.3.2	Results.....	44
3.4	Inclination Study	45
3.4.1	Study Design.....	45
3.4.2	Results.....	47
3.5	Rate of Penetration Study.....	48
3.5.1	Study Design.....	48
3.5.2	Results.....	50

CHAPTER 4: DISCUSSION AND CONCLUSIONS	53
4.1 Discussion	53
4.2 Future Work	53
4.3 Conclusions	54
LIST OF SYMBOLS	55
REFERENCES CITED.....	56
APPENDIX A: SUMMARY OF INPUTS	58
A.1 Simulation 1.....	58
A.2 Simulation 2.....	60
APPENDIX B: DETERMINATION OF TURBULENCE	62
APPENDIX C: LIST OF PARAMETERS FOR IMPLICATION STUDY SIMULATIONS.....	64
APPENDIX D: CUTTINGS VOLUME FRACTION PROFILES FOR PARAMETER IMPLICATIONS	67

LIST OF FIGURES

Figure 1.1: An example of a CTD rig site used in the arctic (Leising and Rike 1994).	3
Figure 1.2: Conceptual rendition of a piece of composite coiled tubing. The left figure represents a cross section, and the right demonstrates the layers.	7
Figure 1.3: Example of an electric, self-propelled BHA.	7
Figure 1.4: Operation of the hydraulically driven tractor unit with inflatable anchoring devices. This section of the BHA is used to apply normal force to the drill bit.	9
Figure 2.1: Schematic of the experimental apparatus used in Experiment 1 (Tomren et al. 1986).	15
Figure 2.2: Dimensioned drawings of the geometries used in Simulations 1 and 2. The figures are internally to scale only.	16
Figure 2.3: View of the mesh on the outlet of the two models. The effect of the inflation properties is visible.	17
Figure 2.4: Comparison of experimental and simulation results for the first validation case.	26
Figure 2.5: Cross-sectional view of the volumetric cuttings fraction rendering shown on the outlet of each trial. The flow rate increases from left to right, and the rotary speed increases from top to bottom.	28
Figure 2.6: Comparison of the experimental and simulation results for Simulation 2. While the majority of the parameters are identical, the simulation uses a different drilling fluid, different cutting density, and a shorter test section.	30
Figure 2.7: Volumetric cuttings fraction renderings for Simulation 2. The cross-sections shown are on the outlet faces.	32
Figure 2.8: Velocity profiles of the drilling fluid at the outlet face. The top figure is from the 200 gpm, 0 rpm trial, and the bottom figure is from the 200 gpm, 175 rpm trial.	33
Figure 2.9: Side views of the volumetric cuttings fraction renderings for the short and long test sections. The entire test section is shown for both trials with a magnification on the inlet side of the long section. Vertical exaggeration has been added to both models for a clearer representation.	34
Figure 2.10: Comparison of the Simulation 2 results (middle) to simulation results for two experiments executed by Sanchez et al. (1999)	35
Figure 3.1: Results of the total cuttings concentration for the constant flow rate study.	40

Figure 3.2: Resulting cuttings concentrations for different geometries at a constant average annular fluid velocity with and without drill pipe rotation.	41
Figure 3.3: Example of eccentricity terminology used in this study.	43
Figure 3.4: Resulting cuttings concentration for concentric, negatively eccentric, and positively eccentric cases.	45
Figure 3.5: Results for applying drill pipe rotation to negatively and positively eccentric cases. The top plot shows the results for negative eccentricity, and the bottom plot shows the results for positive eccentricity.	46
Figure 3.6: Cuttings concentration results for the study of the effect of inclination.	48
Figure 3.7: Results for applying drill pipe rotation at different wellbore inclinations. The top-left is at 0°, the top-right at 30°, the bottom-left at 60°, and the bottom-right at 90°.	49
Figure 3.8: Resulting cuttings concentrations at low, moderate, and high rates of penetration. ..	51
Figure 3.9: Results for applying drill pipe rotation at different rates of penetration. The top plot shows the effect at low (10 ft/hr) drilling rates, and the bottom shows the effect at high (200 ft/hr) drilling rates.	52
Figure D.1: Volume fractions of cuttings for the figures in Table D.1.	95

LIST OF TABLES

Table 1.1: Summary of the effects of different parameters and internal states on hole cleaning.	10
Table 2.1: Experiment 1 and 2 apparatus specifications.....	15
Table 2.2: Original data from Tomren et al. used for comparison to Simulation 1 (1986)	25
Table 2.3: Results from Simulation 1	26
Table 2.4: Experimental data presented by Sanchez et al. (1999).....	29
Table 2.5: Resulting total cuttings concentrations for Simulation 2.....	29
Table 3.1: List of parameters that are varied in the parameter implication study	37
Table 3.2: List of constant parameters for simulations conducted in the parameter implication study	38
Table 3.3: Model parameters for the constant flow rate/ constant annular velocity study	39
Table 3.4: Model parameters for the eccentricity study	43
Table 3.5: Model parameters for the inclination study	47
Table 3.6: Model parameters for the ROP study	50
Table B.1: Table of parameters used to determine minimum Reynolds number	63
Table C.1: List of the parameters and results for each simulation in Chapter 3.....	64
Table D.1: Volume fraction renderings	67

CHAPTER 1

INTRODUCTION

Rotary drilling equipment gained popularity within the oil and gas industry at the end of the 19th century (Mitchell and Miska 2011). Although vast technological improvements have been made in the rig equipment, oil and gas wells around the world are currently being drilled using the same systems that were developed over a century ago. As time has progressed, conventional, easily reached oil and gas deposits have been largely discovered and produced. The industry is faced with more challenging drilling tasks in order to economically produce oil and gas.

To meet these challenges, many new technologies have been developed to lower drilling costs and improve well delivery. Many of these technologies are considered niche technologies that are advantageous for very specific purposes. One of these technologies is coiled tubing drilling (CTD) (Samuel 2007). With its ability to drill underbalanced through slim holes, it has been primarily used to drill for previously bypassed hydrocarbons. Further capitalizing on this profitable idea, companies such as Statoil and Halliburton have invented new forms of composite coiled tubing with self-propelled bottom hole assemblies (BHA's), ushering in a new realm of drilling possibilities. However, many of these projects have since been terminated with the determination that, at the time they were developed, they were not economic for re-drilling in the offshore environment, the original intent of the system. Since their termination, the oil and gas industry has seen an enormous upturn in so-called "shale plays" since the time they were conceived. Now, constructing wellbores onshore has become an assembly-line factory-type affair, and new technologies are aimed at lowering drilling costs, primarily by drilling faster.

1.1 Motivation

Drilling with coiled tubing, particularly composite coiled tubing, may hold different economic value than it did 15 years ago, when the technology was first conceived. With drilling automation receiving heavy focus in the industry, the system may make sense simply for its ability to be automated. However, CTD still has many technical challenges that need to be addressed. One of these challenges is cuttings transport. The coiled tubing method of drilling does not allow for pipe rotation and can have large annular space in some scenarios, resulting in

slower fluid velocity. These parameters have independently been shown to be less than ideal in experimental work on conventional drilling (Nazari et al. 2010). However, no study has combined the properties of CTD to thoroughly understand cuttings transport. One of the first steps to understanding the full extent to which CTD may be applied is understanding the extent of the limitation cuttings transport imposes, particularly in horizontal wellbores. Although the scope of this thesis is much broader than simply understanding the limitations of cuttings transport pertaining to drilling with coiled tubing, establishing the methodology to test some of these new drilling systems and drawing some first-pass observations of their implications is a primary motivation for the project.

1.2 Background

In order to understand both the motivation for the project and the area of research to which it is channeled, a better background for the terminology must be established. First, the topic of drilling with coiled tubing is discussed, followed by its modern evolution of composite coiled tubing. Next, cuttings transport is discussed, followed by its primary means of investigation in this thesis, computational fluid dynamics.

1.2.1 Drilling with Coiled Tubing

Coiled tubing is a string of continuous pipe that is capable of being wound around spools for transportation and deployment. The first use of modern coiled tubing dates back to World War II where several long pipes were constructed by welding 4000 ft sections together and winding them around hubs with 40 ft diameters. The pipelines were strung across the English Channel to supply fuel to the allied forces after the French coast was secured. Shortly afterwards various patents were awarded to ideas involving injecting continuous pipe and cable into a pressurized well in the 1940's and 1950's. The first modern coiled tubing injector heads were constructed and used for workovers in the 1960's (Sas-Jaworsky II 1993).

To date, coiled tubing is still commonly used as a workover tool. In 1993, the most common use for coiled tubing was sand or solids washing (Sas-Jaworsky II 1993). However, many of the same advantages offered by a continuous string of tubing for workovers apply for drilling as well. Coiled tubing is especially suited to drilling in underbalanced conditions. The deployment system includes an injector head that mechanically feeds coiled tubing into the well under pressure. A stuffing box seals around the coiled tubing to allow for control of annular

fluids, and as with a conventional drilling system, blow out prevention equipment is employed under the stuffing box (Samuel 2007). Figure 1.1 shows a schematic of a typical CTD rig site. Drilling underbalanced provides two primary advantages. First, it allows for higher rates of penetration (ROP) because the net pressure of the system is into the wellbore. Therefore, less energy is required to remove a quantity of rock from the formation and into the well bore. Second, it prevents unnecessary formation damage. In overbalanced conditions, wellbore fluids are pushed into the formation. Depending on the properties of the reservoir and the fluid, those fluids can hinder reservoir fluid flow into the wellbore after completion.

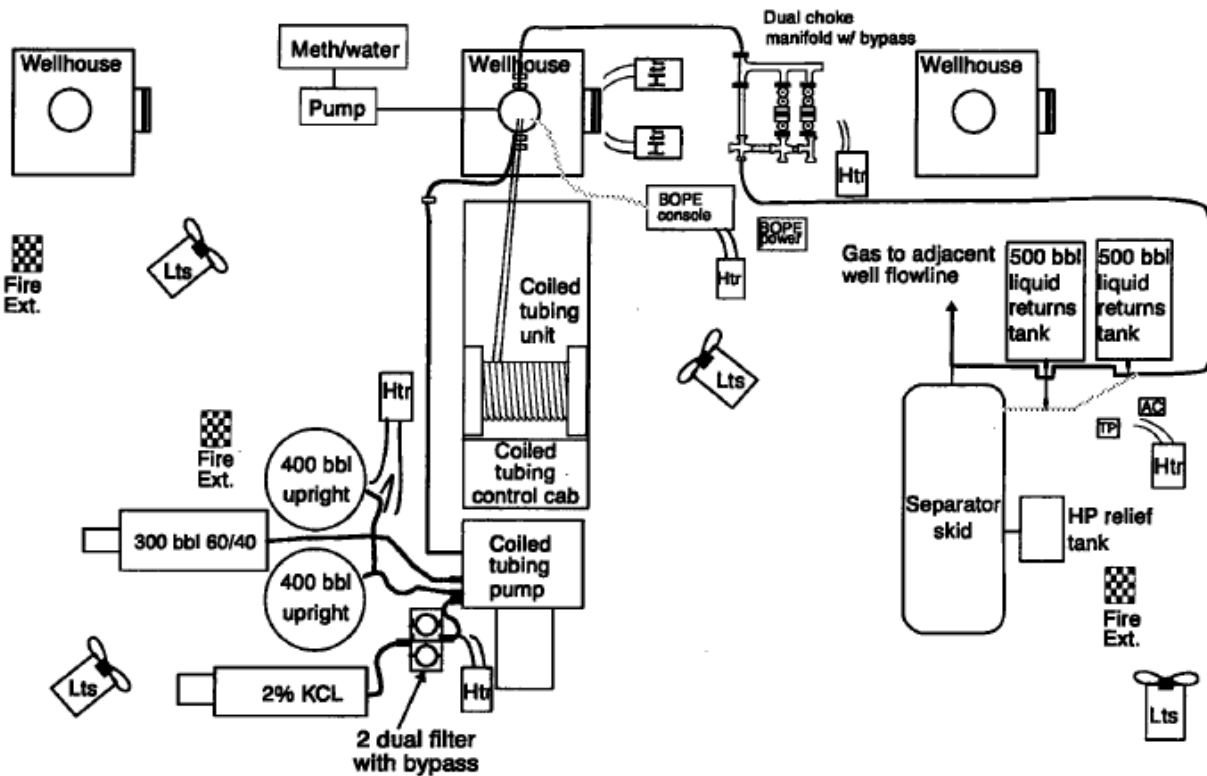


Figure 1.1: An example of a CTD rig site used in the arctic (Leising and Rike 1994).

CTD evolved as a way to economically improve recovery from existing wellbores. Known as through-tubing CTD, wells are either deepened through the existing casing or liner shoe, or they are side-tracked. Deepening an existing well involves drilling out the cement and casing or liner shoe at the end of the well bore. From there, the well is drilled continuously to total depth (TD). Side tracking through the existing tubular utilizes a deflection technique, either

cement sidetrack, whipstock in cement, or through-tubing whipstock. The tubular is milled out prior to drilling ahead (Samuel 2007).

The CTD BHA is typically composed of a drill bit, a positive displacement motor (PDM) known as a bent housing mud motor, various measuring and transmission devices (MWD), a check valve, and an emergency disconnect. The coiled tubing is composed of carbon steel alloy and is available in different grades for different properties. Usually an electrical cable, often 7/16 of an inch, is run through the coiled tubing before operations. This allows for real-time, high resolution communication with the BHA in comparison to slower, lower resolution data transmission techniques such as mud pulse telemetry. Common MWD sensors include weight on bit (WOB), bit torque, internal and external pressure, directional data, temperature, vibrations, and optional formation evaluation tools such as gamma ray and resistivity. With an electric cable connection to these devices, the information is transmitted to surface nearly instantaneously while drilling (Samuel 2007).

Drilling with coiled tubing offers both significant advantages and disadvantages to conventional drilling. As such, it has become a niche application for specific conditions. Some advantages of coiled tubing include (Samuel 2007):

- Lack of connections - Coiled tubing does not require making up threaded connections between stands of pipe. The result is significantly less off-bottom time.
- Continuous circulation - Connecting threaded pipe requires shutting down the pumps. When drilling underbalanced, this can create well control issues. Because coiled tubing is continuous, the pumps can continue to run, providing more stable bottom hole conditions.
- Underbalanced drilling - As previously mentioned, the stuffing box, in combination with continuous circulation, allow for ideal underbalanced drilling conditions.
- Data acquisition - The continuous two-way communication with the BHA by means of electric cable provides much higher quality data than other methods. It also is not limited by the wellbore fluid type.
- Slim-hole capability - Coiled tubing is available in small outer diameters (OD's). This makes it well-suited for drilling through narrow tubulars.

In juxtaposition, coiled tubing presents the following drawbacks (Samuel 2007):

- Inability to rotate - Unlike conventional drilling, coiled tubing is not rotated on the surface. The rotational energy for the system is provided solely by the PDM to the drill bit. The coiled tubing itself never rotates. In conventional drilling, this mode of drilling is known as sliding. However, conventional rigs have the capability of rotating the pipe. Some studies suggest rotation is one of the most important factors to hole cleaning (Sanchez et al. 1999), and insufficient hole cleaning could result in stuck pipe problems. Wiper trips with coiled tubing are common, and other hole cleaning factors such as drilling fluid rheology must be finely tuned.
- Buckling - Coiled tubing is made less rigid than conventional drill pipe to allow it to spool. As a tradeoff, the lack of rigidity causes the pipe to buckle more easily. This can limit the amount of WOB that can be applied.
- Operating limits - As with any tubular, coiled tubing has burst, collapse, tensile, and compressive ratings that can limit the range of drilling parameters used.
- Hydraulics - In common CTD applications, hydraulics can be a significant concern. The narrow internal diameter (ID) of the pipe results in significant pressure loss due to friction. In addition, fluid is pumped through the entire coil, regardless of the amount of tubing in the hole. The potential remedy of increasing the pump pressure could exceed the burst rating. Similarly, narrow clearances in the annulus could result in significant frictional losses. The PDM also requires enough hydraulic energy to turn the bit. Each of these factors could result in insufficient hydraulics to use CTD. On the other end of the spectrum, a large annulus may result in an insufficient fluid velocity to transport the cuttings. 7 in. wellbores are considered the upper limit for coiled tubing sizes up to 3-1/2 in.
- Wear and fatigue - Spooling and unspooling pipe wears the pipe. The gooseneck, where the coiled tubing is fed into the injector, inflicts the most wear. Both thinning and deformation are issues as both affect the operational limitations of the tubular.

In addition to these technical advantages and disadvantages, coiled tubing has several positive and negative logistical aspects (Campbell 2001). For example, coiled tubing is designed to be highly portable and typically requires less total space than conventional drilling equipment.

However, the spool is the largest single piece of equipment, and space for the spool can be limited, particularly offshore (Campbell 2001).

Overall, economics dictate the viability of any technology. In 2001, the only known location in the world where directional CTD proved to cost less money than conventional drilling was in Alaska. Despite the additional expense, some wells are drilled with coiled tubing simply to improve wellbore delivery by underbalanced drilling. In this case, the additional cost is justified by production. As of 2001, CTD accounted for less than 10% of coiled tubing service revenue and a very small portion of the drilling market as a whole (Campbell 2001).

1.2.2 Composite Coiled Tubing

CTD has brought out other ideas over the past two decades. One of those is drilling with composite coiled tubing. In the late 1990's, Halliburton and Statoil worked on a joint venture project known as the Anaconda project. The objective of this project was to develop a new method of finding and economically drilling bypassed hydrocarbon zones offshore Norway. Traditional offshore drilling equipment is very expensive to operate and is inefficient at drilling through-casing sidetracks, yielding many potential projects uneconomic. Therefore, the companies decided to design an entirely new drilling system that did not require a traditional drilling rig. The result was composite coiled tubing in conjunction with an electrically powered BHA. The system eliminated the need for traditional surface hoisting and rotating equipment (Marker et al. 2000). The team conducted several laboratory experiments and field trials on the system near the beginning of the new millennium. The trials succeeded in technical performance; however, at that time the project did not hold favorable economics (Feechan et al. 2003).

The composite coiled tubing developed by Fiberspar as part of the Anaconda project contains layers of various polymer and fiberglass-epoxy mixtures. The pipe also imbeds several electric conductors for the conveyance of power and transfer of information to and from the BHA (Feechan et al. 2003). Figure 1.2 depicts a cross sectional view and layered view of the pipe. The ability to convey electric power in addition to sending and receiving information to the BHA unlocks several new possibilities.

The Anaconda project resulted in a new type of CTD system. The design outlined in this paper builds upon the design created in the Anaconda project (Terry et al. 2004), proposing a more speculative apparatus. One of the implications of composite coiled tubing is the ability to create a self-propelled BHA. An example of a simple, self-propelled BHA for a composite CTD

system is shown in Figure 1.3. Starting with the bit, the first few components are similar to those used in standard coiled tubing and conventional drilling. Polycrystalline diamond compact (PDC) bits are common in all forms of drilling, and they are suited for CTD due to their ruggedness and durability (Samuel 2007). Similarly to standard coiled tubing system, a bent housing mud motor could be used for directional control in this apparatus. However, because the mud motor does not have to create the rotational energy for the drill bit, a rotary steerable system (RSS) could be used in conjunction with an electric drilling motor, potentially allowing for better directional control. The MWD or logging while drilling (LWD) tools can measure a wide variety of parameters and transmit them continuously to surface through the electric cables embedded in composite pipe.



Figure 1.2: Conceptual rendition of a piece of composite coiled tubing. The left figure represents a cross section, and the right demonstrates the layers.

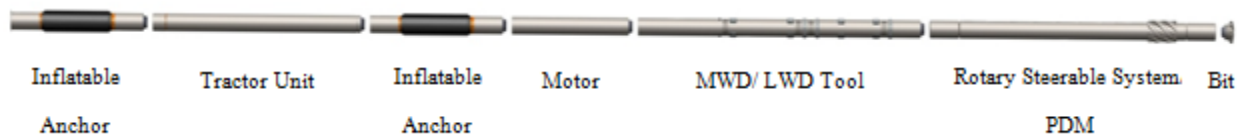


Figure 1.3: Example of an electric, self-propelled BHA.

The differences in a conventional BHA and the proposed BHA begin with the electric drilling motor. As previously discussed, PDM's require hydraulic energy to operate. They also have a limited life depending on the operating conditions. An electric drilling motor would eliminate the additional pressure drop through the mud motor and potentially offer a longer life expectancy. CTES prepared a report on the viability of electric drilling motors for standard CTD, concluding that although they may be more expensive to include in a drilling apparatus, they are technically feasible and hold significant advantages to other rotating methods (Newman and Stone 1995).

Complementary to the electric motor, a hydraulically driven tractor system can be used to apply a normal force to the drill bit. Many open hole tractor designs have been proposed for different purposes (Hallundbæk 1994). The design chosen for the Anaconda project was created by Western Well Tools, Inc. (Moore et. al 1999). A similar concept is proposed here but with inflatable anchoring elements instead of expanding metal components. In all, the tractor system includes a front inflatable anchor, a tractor unit, and a rear inflatable anchor. The anchoring elements operate similarly to inflatable bridge plugs conveyed by electric line (Osorio and Frisby 2013). However, the elastomeric element is custom molded to allow annular capacity for fluids and drill cuttings to pass up the well bore. The function of the hydraulically driven tractor is shown in Figure 1.4. The following steps correspond to the arrow numbers:

1. The completely deflated anchors and compressed tractor are lowered into the borehole. When it reaches the bottom, the rear element is inflated.
2. The hydraulic tractor is extended as the hole is drilled.
3. Once completely inflated, the front element is inflated.
4. The rear element is deflated.
5. The tractor is compressed.
6. The rear element is inflated once again.
7. The front element is deflated, and drilling continues.

The surface equipment for the proposed drilling system works similarly to a standard coiled tubing rig. The spooled tubing can be mounted to a truck and backed up to a borehole. The blowout prevention equipment, injector system, and goose neck all function identically to a

coiled tubing system. As proposed by Statoil, proper sensors and control systems allow for automated drill string deployment (Marker et al. 2000).

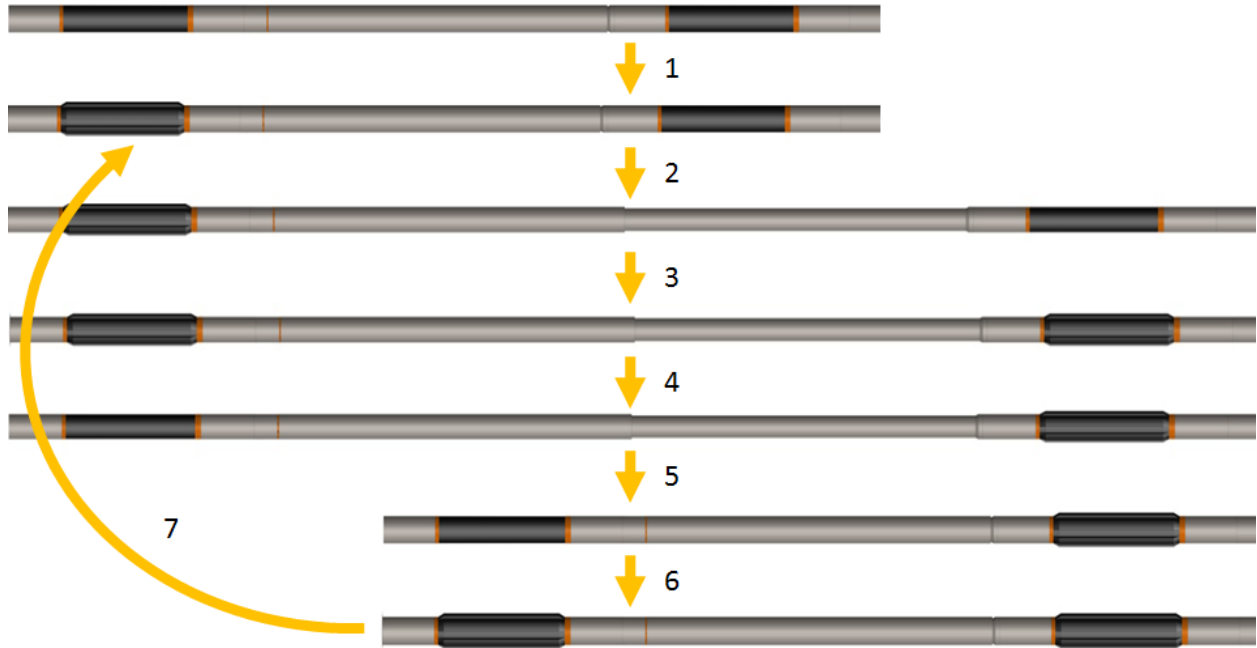


Figure 1.4: Operation of the hydraulically driven tractor unit with inflatable anchoring devices. This section of the BHA is used to apply normal force to the drill bit.

Composite CTD offers some different advantages and disadvantages to standard CTD. Using an electric motor in place of a PDM, which consumes significant hydraulic energy, provides a greater pressure margin for frictional losses inside the tubing while still providing sufficient rotational energy to the bit. The tractor system provides additional, direct, normal force to the bit, allowing for a wider range of WOB control. The composite coiled tubing is neutrally buoyant in most drilling fluids (Marker et al. 2000). The buoyancy significantly reduces drag. In combination with the tractor system, the limiting factor to well bore length is hydraulics. Additionally, it holds a high capacity for automation and control loops as the system is electrically linked to both sensors and the downhole equipment.

The system does not eliminate all of the disadvantages of standard coiled tubing. Hole cleaning and hydraulics are still a concern. The composite coiled tubing requires thick walls to achieve the required ratings. The small ID contributes to significant pressure loss that requires high pump pressures. The pipe also does not rotate, which makes cuttings transportation more

difficult. Such a system has not yet been made economic, and very few field trials have been conducted (Feechan et al. 2003).

1.2.3 Cuttings Transport

Cuttings transport is defined as the process of carrying pieces of rock cut by the drill bit from the bottom of the hole to the surface by circulating drilling fluid (Nazari et al. 2010). It is affected by a variety of factors, and one of the greater factors is wellbore inclination. With an increase in directional drilling in the onshore United States, great efforts have been made recently to better understand cuttings transport and how to optimize it. Without proper hole cleaning, drillers run the risk of stuck pipe and excessive torque and drag. The University of Tulsa owns an experimental apparatus for simulating a wellbore and has defined the contributions of many drilling inputs and internal states to the system (Nazari et al. 2010). A summary of the findings from experiments conducted with this apparatus are shown in Table 1.1.

Table 1.1: Summary of the effects of different parameters and internal states on hole cleaning

Property	Contribution	Relationship
Mud flow rate	Significant	Positive with greater flow rates
Mud rheology	Moderate	Positive or negative depending on other variables
Hole angle	Significant	Negative with greater angle
Mud weight	Small	Positive with increased mud weight
Mud type	Small to moderate	Depends on other variables
Hole size	Small to none	Negligible assuming equal annular velocity
Rotation speed	Significant	Positive with higher speeds
Eccentricity	Significant	Negative with more eccentricity
ROP	Moderate	Negative with higher ROP
Drill bit type	Unknown	Unknown due to regrinding
Cutting size	Small	Negative or positive depending on other variables

Of the greatest interest for the purposes of this paper are the effects of pipe size and rotation in directional wells. Pipe size and hole size combined with the pump rate define the mud flow rate in the annulus. A smaller drill pipe will greatly affect this system. In highly inclined and horizontal wells, drill pipe rotation sweeps the cuttings from the bottom of the wellbore into the higher velocity profile above the drill pipe. It has been demonstrated that the contribution of this effect to hole cleaning in horizontal wells can be significant (Sanchez et al. 1999).

1.2.4 Computational Fluid Dynamics (CFD)

Computational fluid dynamics (CFD) utilizes computational algorithms to solve equations, usually partial differential equations, pertaining to the flow of fluid. Finite volume methods (FVM) utilize discrete partitions, combined to form a mesh, in order to simulate large scale physics. FVM allows a computer to solve each element over a time interval and repeat for a complete model. The combination of CFD and FVM allow for a complete model of a fluid system (Pletcher et al. 2013).

ANSYS Fluent is commercial software capable of building and running such CFD/FVM models. It contains multiphase capabilities that allow the user to model solid-liquid systems. Bilgesu et al. applied this program in previous studies to simulate cuttings transport. Their study successfully modeled an annular section of wellbore and allowed them to vary five parameters (2007).

Zhou and Shah (2003) used Fluent to study the fluid flow inside coiled tubing. Their objective was to understand the friction pressure gradients that result from the curved geometries of the tubing. They were able to use Fluent to successfully apply the model to both Newtonian and non-Newtonian fluids.

Although application to the drilling sector of the oil and gas industry has, to date, been rare, these limited applications are used as a starting point for developing a more thorough methodology. Similarities between prior work with CFD, both within and outside of the industry, can be exploited to put together a system of models for the solid-liquid drilling system.

1.3 Objectives

There are two primary objectives for this thesis. The first objective is to establish the specific methodology used to model cuttings transport in an annulus while drilling. To complete this objective, a means of creating a geometry, a mesh, and various fluid models are suggested and tested against experimental data to establish validity. The objective is considered successfully completed if the results suggest that CFD can be used to test drilling parameters.

The second objective is to compare the effects of different drilling parameters on cuttings transport using the methodology established by the first objective. More specifically, the effects of drill pipe rotation, fluid velocity, drill pipe eccentricity, well bore inclination, and ROP over a variety of drill pipe and casing sizes are observed and compared. The objective is considered to

be complete if conclusions and recommendations can be drawn regarding different drilling geometries and the parameters affecting cuttings transport.

1.4 Methodology

The studies conducted are broken into two categories, each corresponding to an objective. The first set of studies seeks to establish a specific CFD methodology for modeling cuttings transport in a wellbore. ANSYS Fluent and the associated pre- and post-processing ANSYS software are used to establish the methodologies. The proposed practices include creation of a geometry, division of that geometry into a mesh of cells, and all of the fluid models. The results are compared to selected experiments to validate the model as a tool for CFD modeling. Additionally, helpful post-processing techniques are presented as a means of analyzing the generated data. This model validation is presented in Chapter 2.

The second set of studies support the objective of parameter implications. The same programs and methodology that are used to validate the model are used for this study. Each of the parameters established in the objectives are isolated and varied to determine the effect it has on cuttings transport. The specific parameter implication study details and their results are presented in Chapter 3.

CHAPTER 2

MODEL VALIDATION

Before creating CFD models that compare different parameters and drilling equipment, the modelling techniques and parameters used to simulate a borehole environment must be validated. Many experiments have been performed using apparatuses that simulate annuli for cuttings transport. Two particular experiments, published by Tomren et al. and Sanchez et al., were conducted on two different apparatuses and provide pertinent data for CFD simulations (1986; 1999). Therefore, they are used for computational model validation and are referred to as Experiment 1 and Experiment 2 respectively throughout this chapter. The CFD simulations modeled after the experiments will be known as Simulations 1 and 2 respectively. The following sections describe the processes and parameters used for the Fluent models that correspond to the experiments.

2.1 Overview of FVM and CFD Processes

ANSYS offers a full package of software that allows the user to conduct every step of creating a FVM model for the purposes of CFD. The package is titled Workbench, and the CFD modeling software is Fluent. Other programs within Workbench create the geometry, mesh, and post-processing results. CFD can also be performed with other commercial software as well as user-programmed software for specific situations. These other programs may have altered workflows, and only the workflow for the ANSYS suite is defined here. It consists of five major steps. They are:

1. Creating geometry
2. Meshing geometry
3. Defining CFD models
4. Executing
5. Post-processing

The geometry of a model can be two or three dimensional and simply represents the physical area or volume of the system under study. All of the geometries in this thesis are three dimensional. As with any CAD drawings, the geometry must be properly dimensioned for consistent results.

Meshing is the process of dividing the geometries into smaller areas or volumes for computation. Generally, the mesh is kept as coarse as possible while maintaining accurate results. If the mesh is not finely tuned, especially in asymmetric systems, mathematical convergence will not be obtained when running the model.

CFD is the process of applying all of the fluid and boundary conditions to mass, energy, and momentum balances over the meshed geometry. Each simulation requires many different models. These models have been primarily empirically derived over the years for use under specific conditions. This thesis details which models are used for the simulations and why they are used over other available models. The references cited describe the specifics of those models, including their equations and applicability.

Executing a simulation includes defining the desired accuracy for convergence, the desired outputs, and the desired timing if transient results are desired. Once running, various means can be used for determining whether a simulation has converged. Residuals from the equations being solved are commonly observed as well as user defined observed values. Post-processing can be used to verify convergence by visualizing the generated data to see if expected results are obtained.

Post-processing is any form of analyzing the vast amounts of data generated from a simulation. Many variables such as volume fractions and velocities are recorded for each meshed element at the final iteration of the simulation. ANSYS provides a means of accessing that data and visualizing it in many ways. Post-processing is essential to understanding how effective the user-defined models are at modeling reality and the implications that the modeled physics may have about reality.

2.2 Geometry

The first step toward creating a FVM is creating the geometry. The system being modeled for cuttings transport is the drill pipe to bore hole annulus. The drill pipe is concentric with bore hole for both validation cases. Simulating a bore hole with realistic rugosity is challenging both experimentally and computationally, and prior work has used a smooth outer boundary with constant diameter, which resembles casing. This type of outer boundary is also used for this project. While undoubtedly oversimplifying the system, this assumption is essential to obtain consistent results between experiments and simulations.

The apparatuses for the two experiments operate similarly but have different dimensions. Figure 2.1 shows a schematic for Experiment 1 that is also generally representative of Experiment 2. Specifications for the apparatus dimensions are shown in Table 2.1.

Table 2.1: Experiment 1 and 2 apparatus specifications

Experiment	Test Section Length	Wellbore Diameter	Drill Pipe Diameter	Drill Pipe Rotation	Liquid Flow Rate	Angle of Inclination
1	40 ft	5 in	1.9 in	0-100 rpm	0-225 gpm	0-90°
2	100 ft	8 in	4.5 in	0-140 rpm	0-700 gpm	10-90°

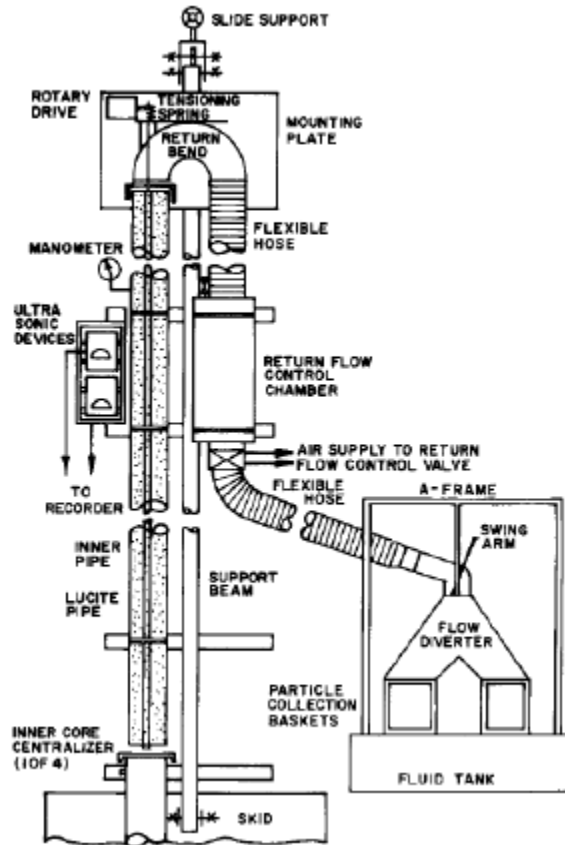


Figure 2.1: Schematic of the experimental apparatus used in Experiment 1 (Tomren et al. 1986).

A full scale geometry of Experiment 1 was created for Simulation 1, but the 100 ft length of Experiment 2 proved to be computationally demanding. Therefore, a 25 ft section with the same diameters was created for Simulation 2, and a study was conducted to determine if

shortening the wellbore is valid to compare with the experimental results. The study is presented in Section 2.10.3. A diagram for the two geometries and their dimensions is shown in Figure 2.2.

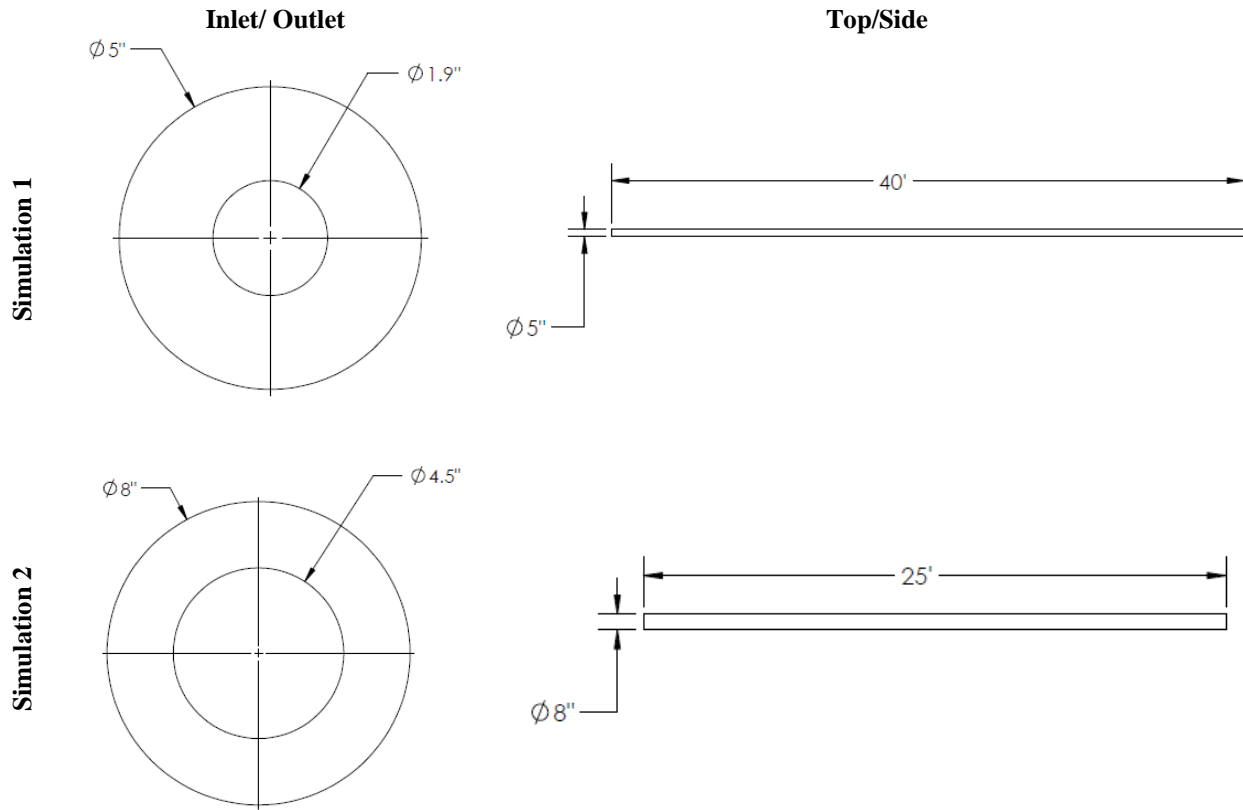


Figure 2.2: Dimensioned drawings of the geometries used in Simulations 1 and 2. The figures are internally to scale only.

Both experiments conducted trials at different inclinations. For the purposes of validation, only horizontal trials with an inclination angle of 90° were selected for simulation. Because the formation of a cuttings bed in horizontal wells is of particular importance to this project, these cases provide the most pertinent data and clear visualization.

2.3 Mesh

Once the geometry is established, it must be divided into volumetric elements for computation. The divided geometry is known as a mesh. The quality of the mesh can greatly affect the CFD results.

Zhou and Shaw used Fluent to model flow through coiled tubing (2003). They suggest hexahedral cells for accuracy, convergence, and speed. They also suggest using finer cells near boundary walls and a swept mesh through the tubular. These suggestions were utilized for meshing the simulation geometries.

Both experiments used the same meshing methods. The inlet face was meshed first using two inflation techniques, one from the outer boundary and one from the inner boundary. For Simulation 1, each inflation used five layers and a growth rate of 1.8. Simulation 2 used eight layers and a growth rate of 1.2. Simulation 1 used a first layer thickness criterion of 1 in, and Simulation 2 used a smooth transition criterion with a 0.3 transition ratio. Radially, both were divided into 10° intervals. The faces were swept using a “quad/tri” mesh type and 3 in. elements in length. The meshes on the outlet faces for the two experiments are shown in Figure 2.3. In total, the mesh for Simulation 1 contains 54,219 elements, and the mesh for Simulation 2 contains 64,260 elements. The values used for the meshing methods are derived from the work published by Zhou and Shah (2003), which consists of a detailed analysis of the mesh on the results of a liquid flowing through pipe.

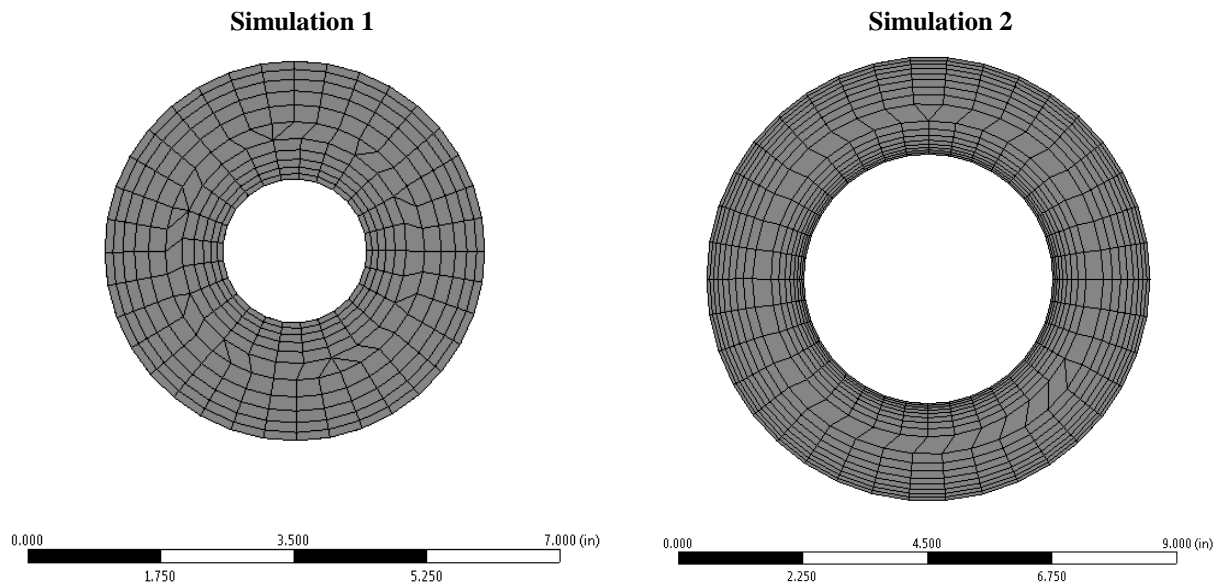


Figure 2.3: View of the mesh on the outlet of the two models. The effect of the inflation properties is visible.

2.4 CFD General Parameters

Several general solver parameters are important before determining specific CFD models to solve. First, there are two solver types, pressure-based and density based. The primary difference between the two is whether the density field or the pressure field is determined from the continuity and momentum equations. Historically, the pressure-based solver is better suited for low-speed, incompressible flows while the density-based solver is better suited for high-speed, compressible flows (ANSYS 2013a, 625). Thus, the pressure-based solver is appropriate for cuttings transport modeling in liquid drilling fluids and is used for both simulations.

Another important solver parameter is velocity formulation, which can be absolute or relative. The objective of selecting velocity formulation type is to minimize numerical diffusion and provide faster, more accurate results. The relative formulation is more appropriate when nearly the entire domain contains moving fluid whereas the absolute formulation is adequate when some fluid is not moving (ANSYS 2013b, 541). For the varying parameters used in the validation study, an absolute formulation was selected to accommodate different flow profiles. However, future studies could evaluate the effect of a relative velocity profile.

Next, the time dimension is defined for the simulation. The two solvers, steady and transient, are used to observe the steady-state result and the effect of fluid simulations over time respectively. The goal of the simulations is to observe the steady-state of the cuttings transport system, and the steady time domain is used. Finally, gravity is enabled for the model, and the standard gravitational acceleration of 32.14 ft/s^2 is applied orthogonally to well bore.

2.5 CFD Models

Fluent solves mass and momentum conservation equations for all flow models. Several other models are available that add equations or modify the continuity equations (ANSYS 2013a, 1-2). Two additional models are utilized in the validation simulations.

2.5.1 Multiphase

The first additional model enables multiphase flow. Two types of multiphase flow allow for a solid-liquid system: the Euler-Lagrange discrete phase model and the Euler-Euler multiphase model. The discrete phase model is used to simulate a dilute, dispersed phase in which discrete particles are modeled (ANSYS 2013b, 1131, 1134). The Euler-Euler models the second phase as a continuum where restrictions on dilution and dispersion are reduced but

individual particle tracking is not possible (ANSYS 2013a, 512-513). Because a cuttings bed involves low dispersion and dilution of the solid phase, a two phase Euler-Euler model is used for these simulations. Additionally, the Euler-Euler model allows for the designation of a granular solids phase. The granular designation primarily pertains to packing and is further discussed in the phase section. The Euler-Euler model allows for volume fraction parameters to be calculated explicitly or implicitly. The implicit scheme is appropriate for steady-state models (ANSYS 2013b, 1247-1249).

2.5.2 Viscosity

The second model pertains to modeling turbulence. Reynolds number calculations were performed for both simulations to determine if the flow is laminar or turbulent. They are shown in Appendix C. For all of the flow rates used in both simulations, the flow is fully turbulent. Therefore, a turbulence model must be used in Fluent, where turbulence is defined as “three-dimensional unsteady random motion observed in fluids at moderate to high Reynolds numbers” (ANSYS 2013b, 695). Although computationally more costly than simpler models, the Reynolds Stress Model is most effective for forms of rotating flows. The Reynolds Stress Model is formulated by calculating Reynolds stresses and dissipation rate rather than implementing the isotropic eddy-viscosity hypothesis of other models. For 3D flows, the model uses an additional seven transport equations that are more capable of handling complex flows (ANSYS 2013a, 83). Rotating flow is present when the drill pipe is rotated, so the Reynolds Stress Model is used for these simulations. Additionally, models of stirred vessels have shown that some flow characteristics due to rotation are only captured by the Reynolds Stress Model (Montante and Bakker 2004).

Several options are available with the Reynolds Stress Model. A linear pressure-strain model with included wall reflection effects and standard wall functions were selected. Little difference was observed in special considerations for these options, implying that the models in this project are not sensitive to the parameters that these models and functions tune. Therefore, the default values were used. In addition, 11 model constants are available for modification in the Reynolds Stress Model. However, modification is not necessary in most applications, and the default values were used for these models (ANSYS 2013b, 730).

Two additional models are available when using the Reynolds Stress Model in multiphase systems: mixture and dispersed. The dispersed assumes that the secondary phase is

dilute and the primary phase drives the turbulence parameters. The mixture applies mixture parameters to the turbulence modeling (ANSYS 2013a, 554-556). Most turbulence occurs in the dilute flow stream of cuttings where the fluid velocity is high. Very little turbulence occurs in the cuttings bed where the cuttings concentration is the greatest. Therefore, the dispersed model was used in the validation simulations.

2.6 Materials

Only two materials are used to create a CFD model of a simple drilling annulus. One material corresponds to the drilling fluid, and the other material corresponds to the drill cuttings.

2.6.1 Drilling Fluid

Modelling non-Newtonian fluids in turbulent flow regimes is difficult in Fluent. Therefore, fresh water is used as the drilling fluid in the validation models. Tomren et al. used five different drilling fluids in their work (1986). One of the five was fresh water with no additives, providing comparable data. Sanchez et al., however, used bentonite or polymer in all five of their selected muds (1999). The lowest viscosity bentonite mud they used had a plastic viscosity (PV) of 7 cp and a yield point (YP) of 7 lb/ 100ft². This mud was used in Experiment 2 and is compared to the simulation data for qualitative purposes. The two material properties of fresh water that are important to the simulations are density and viscosity, which are 62.3 lb/ft³ (8.33 ppg) and 6.74x10⁻⁴lb/ft/s (1.00 cp).

2.6.2 Drill Cuttings

The only significant material property for the drill cuttings is the density. Other properties of the drill cuttings that are pertinent to flow behavior, such as size, are defined as phase properties, not as a material properties. Experiment 1 used cuttings that had a density of 165.5 lb/ft³, which is employed in Simulation 1. Experiment 2 used river gravel and limestone cuttings that had densities of 164.8 lb/ft³ and 159.8 lb/ft³ respectively. The river gravel density is used in Simulation 2.

2.7 Phases

In these simulations, each material corresponds to a phase. Defining the phases and their interaction is one of the most vital components for creating a realistic multiphase CFD model.

2.7.1 Phase Definitions

The primary phase is the drilling fluid, or fresh water, for Simulations 1 and 2. No additional parameters are required for the primary phase. However, the second phase, which is the drill cuttings, requires further description.

First, the phase was set to a granular phase. A continuous granular phase is modeled with various viscous and packing properties. Next, a granular viscosity model was selected. The following subsection includes the selection of the Gidaspow drag model used for phase interaction. The Gidaspow granular viscosity model, which provides the viscosity of the suspension of the granular phase in the liquid phase, was used in the phase definition for consistency (ANSYS 2013a, 505; ANSYS 2013b, 2078). The granular bulk viscosity model was enabled next. The Lun et al. model is the only model built into Fluent and was used for the simulations (ANSYS 2013a, 542; ANSYS 2013b, 2078).

Frictional viscosity models the friction between solid particles. By default, it is disabled by Fluent. However, once the cuttings begin to form a bed, the frictional interaction between particles becomes significant. Therefore, the Johnson et al. model, one of the two available models, is utilized (ANSYS 2013a, 543; ANSYS 2013b, 2074). No difference in results was observed between the two available models; however, disabling the frictional viscosity greatly reduces accuracy. The default angle of friction was used, which is approximately 30°. The frictional pressure was defined by kinetic theory, and the derived frictional modulus model was used, which are also default values that apply to most situations (ANSYS 2013b, 2074-2075). The friction packing limit was set to 0.05 based on trial and error of determining the point at which a cuttings bed formed. This limit is the volume fraction of the granular phase at which the frictional viscosity becomes dominant (ANSYS 2013b, 1322).

Radial distribution corrects for particle collisions when the granular phase becomes dense. The default Lun et al. model was used for this parameter and no difference was observed when trying other available models (ANSYS 2013b, 2079). Similarly, the default, derived option was used for the elasticity modulus (ANSYS 2013b, 2079).

One quarter inch drill cuttings (ASTM-size designation) were used in Experiment 1, so the granular diameter was set to 0.25 in for Simulation 1. The distribution of sizes between sieves was neglected for simplicity. The validity of the simplification is discussed in Section 2.10.4. Experiment 2 used 0.25 in. limestone cuttings and 0.10 in. river gavel. Due to an input

error, the diameter of the limestone cuttings was used in conjunction with the river gravel density in Simulation 2. The results in Section 2.10.3 include discussion of model sensitivity to granular density and diameter. Because the cuttings are modeled as spheres, the packing limit is 0.63 (ANSYS 2013b, 2079).

The granular temperature model can either be set as a phase property or utilize a partial differential equation. Because these models assume thermal equilibrium, heat transfer is inconsequential. The temperature model can be set as a phase property, utilizing an algebraic strategy (ANSYS 2013a, 506).

2.7.2 Phase Interaction

When simulating a solid-liquid system as two continuous phases, models describing how the phases interact are necessary. The first property that must be modeled is the drag function. This function is used to determine the momentum exchange coefficients (ANSYS 2013b, 1325). Most drag coefficient models are more applicable to granules in still fluids than turbulent fluids (Montante and Bakker 2004). However, the Gidaspow model has worked well for stirred-tank simulations (Gohel et al. 2012). Additionally, it is possible to modify the drag coefficient with a drag factor, which is a multiplication factor to the drag coefficient (ANSYS 2013b, 1328). The Brucato, or Magelli, correction factor, which is traditionally used for gas-liquid flows (ANSYS 2013a, 528), has yielded positive results in stirred tanks as well (Monante and Bakker 2004). Therefore, the Gidaspow model with the Brucato drag modification was used for the cuttings transport simulations.

Another important phase interaction property is turbulent dispersion, which replaces the interfacial momentum force with a diffusion term (ANSYS 2013a, 536). Stirred tank simulations have shown that the property can be essential to properly predicting the movement of a granular phase (Gohel et al. 2012). Several models are available, and the Diffusion in Volume of Fluid (VOF) model was selected based on consistent results by trial and error. Other models appeared to have very little impact or cause instability in convergence. The default diffusion coefficient of 0.75 was used for the model, and no limiting function was applied.

Fluent provides the ability to modify the model for collisions between particles. The user modifies the restitution coefficient, which applies to the solid-solid exchange coefficient (ANSYS 2013a, 527-528). The default coefficient of 0.9 was used for the validation models.

Additional phase interaction properties can be added to the model as necessary. Those properties include the virtual mass force, lift force, turbulent interaction, mass transfer mechanisms, and surface tension. In comparison to the drag force, the lift force is usually negligible and was not included (Montante and Backer 2004; ANSYS 2013b, 1328-1329). The turbulent interaction option allows the user to include the effect of the dispersed phase turbulence on the primary phase (ANSYS 2013a, 556). By default, this impact is neglected. After trying several simulations with different turbulent interaction models, no discernable differences were observed, so the term was neglected for the validation models. The mass transfer mechanisms apply to phase changes, which do not apply to this model (ANSYS 2013b, 1351-1552). Similarly, no fluid-fluid phase interfaces are present in the model, and surface tension is neglected.

2.8 Boundary Conditions

The wellbore model consists of one fluid region and four boundaries. The boundaries include an inlet where drilling fluid and drill cuttings are fed into the system, an outlet at the opposite end of the model, an outer wall that represents the casing, and an inner wall that represents the drill pipe. Separate boundary conditions describe each of these physical locations.

2.8.1 Inlet

Fluent allows several methods for the definition of a fluid inlet. The mass flow method, in which the mass flow rate and direction of each phase are specified, was selected for this application. The direction was specified as normal to the boundary.

The mass flow rate for each phase varied for Simulations 1 and 2. The cuttings rate remained constant within Simulation 1 and Simulation 2, but the drilling fluid flow rate varied to compare the effect of flow velocity on hole cleaning. Experiment 1 used a cuttings mass flow rate of 20 lb/min (0.33 lb/s), which was directly fed into Fluent for Simulation 1. Experiment 2 maintained a constant simulated drill rate of 35 ft/hr. With a bit size of 8 in., that drill rate corresponds to a mass flow rate of 0.56 lb/s. The initial gauge pressure was set to zero at the inlet. The steady-state inlet pressure is low, and Fluent calculates the actual pressure once the simulation begins to run.

The drilling fluid rates for Simulation 1 ranged from 125 to 225 gpm in 25 gpm intervals to match experimental data. For Simulation 2, flow rates ranged from 200 to 500 gpm in 100 gpm intervals. These volumetric flow rates were converted to mass flow rates using the density

of water. The velocity ratio of the secondary phase to the primary phase was set to one, specifying that the two phases enter the model at the same velocity.

A turbulence condition for the primary phase is required at the inlet. A turbulent intensity of 5% and a turbulent viscosity ratio of 10 were used for both simulations. Those default parameters are sufficient for most situations and usually work well when more information is not known (ANSYS 2014).

2.8.2 Outlet

A pressure boundary condition is applied to the outlet of the model. The specified outlet pressure is 0 psig. Paired with the mass flow inlet condition, ANSYS determines the pressure required at the inlet to maintain the specified flows.

Some backflow criteria are also required in the event that one or more cells produces flow back into the model during simulation. Before convergence, this condition is likely and reasonable inputs are required to prevent divergence. Like the inlet turbulent conditions, the primary phase backflow turbulent intensity and turbulent viscosity ratio maintained the default values of 5% and 10 respectively. The granular phase backflow volume fraction is set to zero, and the back flow granular temperature was left at its default value.

2.8.3 Walls

The wellbore model consists of an outer wall that represents the casing and the inner wall that represents the drill pipe. Both walls employ a no slip condition to both phases, no roughness height, and a roughness constant of 0.5. Unfortunately, modeling roughness is difficult and finer tuning of the roughness parameters could be part of future work. The outer wall is stationary, and these are the only necessary boundary conditions.

Both Simulation 1 and 2 use drill pipe rotation. Simulation 1 rotates the pipe at 0, 50, and 100 rpm, and Simulation 2 rotates it from 0 to 175 rpm in 25 rpm intervals. These rotation speeds are easily input into the boundary conditions in Fluent. The models employ counter-clockwise rotation, the opposite direction to which drill pipe is rotated while drilling. While this is a parameter that can be changed for convenience in the future, it has no impact on the results of CFD studies.

2.9 Solution Settings

Fluent offers two algorithms to solve Euler-Euler multiphase systems. Both algorithms couple the pressure and momentum equations, but the SIMPLE algorithm segregates the velocities prior to reconstructing for overall continuity. No discernable difference between the solvers was observed in execution of the simulations, so the SIMPLE algorithm was used for all reported results. Within the spatial discretization properties, the least squares cell based method was used for the gradient, and first order upwind was used for all other properties.

A volume monitor was included while solving to observe either the total volume or total mass of the second phase in the test section. This allowed for identifying steady-state and calculating the steady-state volumetric cuttings concentration, which is used to represent hole cleaning efficiency.

2.10 Results and Discussion

Both simulations were run as described in the preceding methodology. The inputs are defined to correspond with experimental data. The results from these trials are reported in the following subsections.

2.10.1 Simulation 1

The purpose of Simulation 1 is to create a comparable case to Experiment 1. The experiment consists of trials at five flow rates and three drill pipe rotation speeds. In all, 12 data points are considered and shown in Table 2.2. The quality of cuttings removal is reported in terms of the total volumetric cuttings concentration in the test section. Experimentally, this data was derived from the total cuttings weight remaining in the annular test section after the pump was shut off.

Table 2.2: Original data from Tomren et al. used for comparison to Simulation 1 (1986)

Rotary Speed (RPM)	Total Cuttings Concentration, C_{VT} (Percent)				
	At 125 gpm	At 150 gpm	At 175 gpm	At 200 gpm	At 225 gpm
0	10.7	8.1	6.9	3.7	2.5
50	-	8.9	6.2	4.2	2.5
100	-	-	5.8	4.2	1.7

The experimental trials support two conclusions. First, the total cuttings concentration decreases with increased pump rate, indicating that hole cleaning efficiency increases with

increased flow rate. This is consistent with accepted transport theory. Second, the rotary speed produces a no discernable trend. This conclusion is in direct opposition to other authors. Other experiments have shown that rotary speed can have a dramatic positive effect on hole cleaning (Nazari et al. 2010, Sanchez et al. 1999).

Simulation trials were conducted for each of the 12 data points. The results are shown in Table 2.3, and both experimental and simulation results are shown in Figure 2.4.

Table 2.3: Results from Simulation 1

Rotary Speed (RPM)	Total Cuttings Concentration, C_{VT} (Percent)				
	At 125 gpm	At 150 gpm	At 175 gpm	At 200 gpm	At 225 gpm
0	3.49	2.21	1.44	1.08	0.81
50	-	2.14	1.43	1.05	0.78
100	-	-	1.41	0.99	0.74

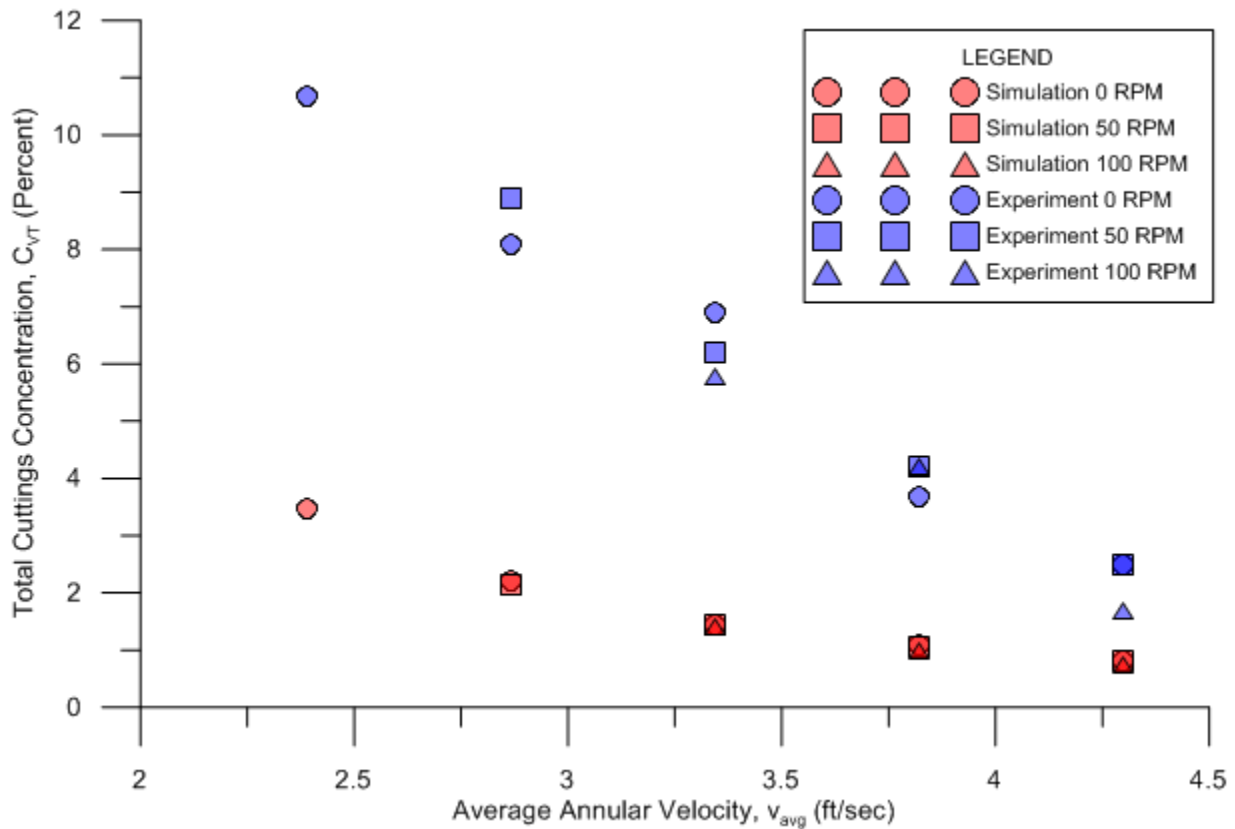


Figure 2.4: Comparison of experimental and simulation results for the first validation case.

The simulation results show the same general trend as the experimental results. Quantitatively, however, the simulated cuttings concentration values are approximately one quarter of the experimental values. Several reasons for this discrepancy are discussed in detail in the CFD Limitations subsection.

The simulations match the reliance of hole cleaning on flow rate. They also show a very slight improvement due to drill pipe rotation. At all flow rates, the total cuttings concentration decrease with increased rotary speed although the significance in comparison to the effect of flow rate is minor.

ANSYS provides a post-processing program that allows for detailed graphical analysis of the simulation results. The cuttings bed height and distribution throughout the drilling annulus is particularly important to hole cleaning. Figure 2.5 shows a cross section of the cuttings volume fraction at the model outlet.

The cross sections clearly show the trends previously described and add some insight to the processes underlying the bulk observations. In the simulations, the cuttings bed nearly disappears by the highest flow rate. The dispersion of the cuttings is also noted as the colors smooth to the blue shades throughout the annulus. Additionally, rotation affects the symmetry of the system. The motion shifts the cuttings bed to the left and causes a higher cuttings concentration to the left of the drill pipe, which would be flipped horizontally in reality because the rotation is opposite of convention. It is difficult to discern a difference in cuttings bed height due to rotation, but the dispersion appears to increase, which would suggest slightly less overall cuttings concentrations. This is consistent with the numerical results.

2.10.2 Simulation 2

While Simulation 1 provides more information on the flow rate effect, Simulation 2 provides more information on the rotary effect. The original data for Experiment 2 is taken from Sanchez et al (1999). Two of the data sets were obtained from trials with horizontal well sections, the same flow rates, the same rotary speeds, and the same drilling fluid ($PV = 7$ cp, $YP = 7$ lb/ 100ft²). The difference between the two was the cuttings used. The first used 0.25 in. limestone cuttings, and the second used 0.10 in. gravel. As previously mentioned, the trials conducted for Simulation 2 use the gravel density with the limestone cutting size due to an input error. A sensitivity test shows that the data gathered is more comparable to the limestone

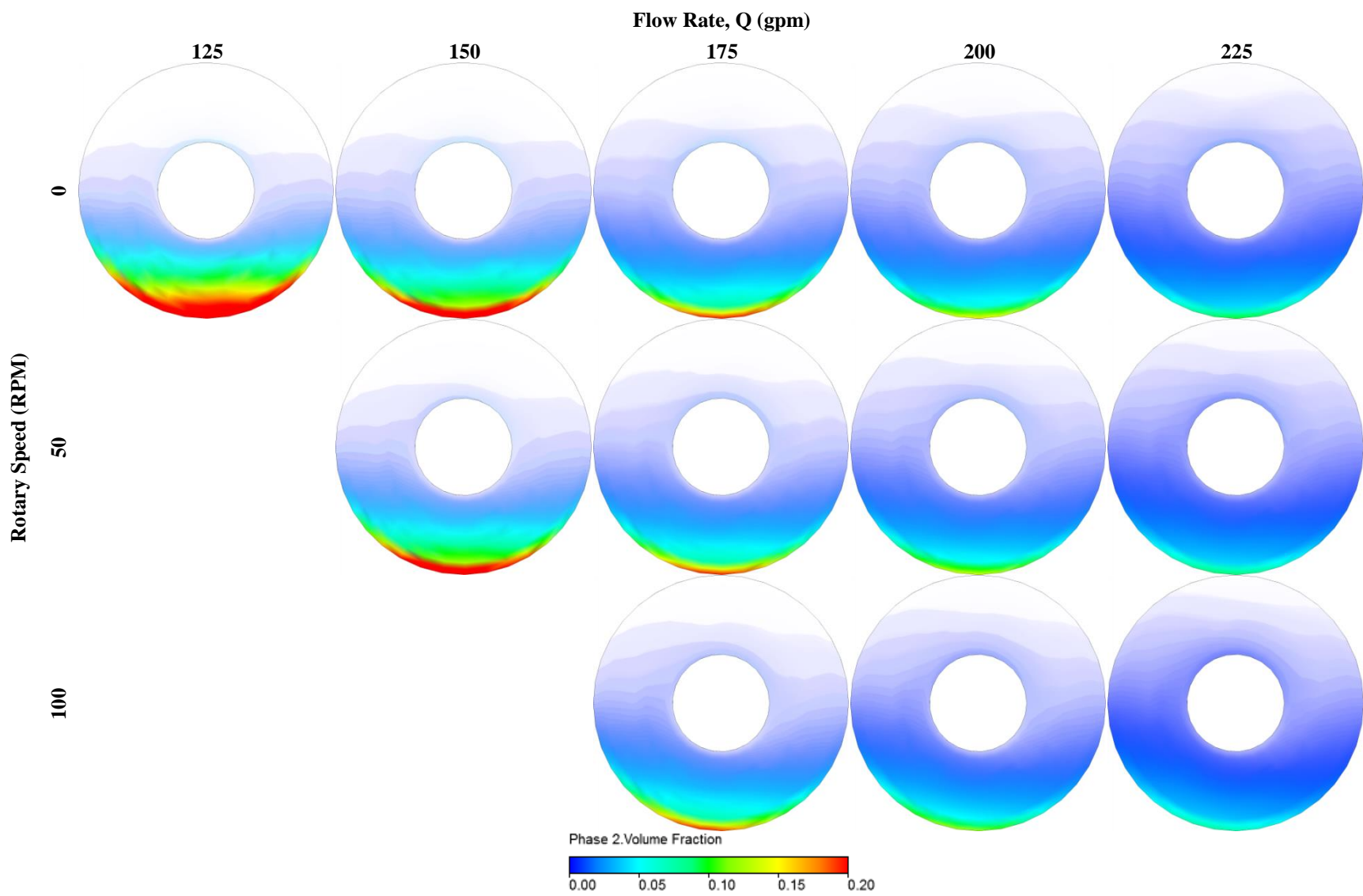


Figure 2.5: Cross-sectional view of the volumetric cuttings fraction rendering shown on the outlet of each trial. The flow rate increases from left to right, and the rotary speed increases from top to bottom.

experimental data. Therefore, experimental data reported in this section is extracted from the limestone data set. More details on the sensitivity test are discussed in the following section.

Experiment 2 reported the total cuttings mass in the test section at four flow rates and eight rotary speeds. These values are divided by the density of the cuttings to achieve the volume of cuttings, and then divided by the total section volume to determine the total volumetric cuttings concentration. Those values are reported in Table 2.4 for consistency with Simulation 1. Table 2.5 shows the corresponding results from simulation. Both results are shown graphically in Figure 2.6.

Table 2.4: Experimental data presented by Sanchez et al. (1999)

Rotary Speed (RPM)	Total Cuttings Concentration, C_{VT} (Percent)			
	At 200 gpm	At 300 gpm	At 400 gpm	At 500 gpm
0	19.63	13.10	9.28	7.83
25	18.66	8.82	5.90	4.20
50	18.26	8.09	4.96	3.41
75	17.80	7.58	4.63	3.28
100	17.29	7.12	4.40	3.03
125	16.58	6.74	4.27	2.75
150	15.38	6.41	4.20	2.49
175	14.34	6.36	4.07	2.29

Table 2.5: Resulting total cuttings concentrations for Simulation 2

Rotary Speed (RPM)	Total Cuttings Concentration, C_{VT} (Percent)			
	At 200 gpm	At 300 gpm	At 400 gpm	At 500 gpm
0	12.10	2.25	1.34	0.61
25	14.48	2.36	1.32	0.59
50	11.77	2.40	1.17	0.54
75	9.31	2.44	0.94	0.49
100	7.39	2.32	0.76	0.46
125	5.89	1.43	0.67	0.44
150	3.30	1.12	0.62	0.42
175	2.40	0.99	0.59	0.41

The simulated values ranged between 8% and 74% of the experimental values. Simulation 2 and the experiment it is modeled after have large areas of potential differences and

error. The sources for these are discussed in the CFD limitations section. Despite the numerical discrepancy, many of the overall trends are exhibited in both results. One of the most dramatic results is the effect of flow rate on the cuttings concentration. Each increase in flow rate resulted in lower concentrations with the greatest effect taking place between flow rates of 200 and 300 gpm.

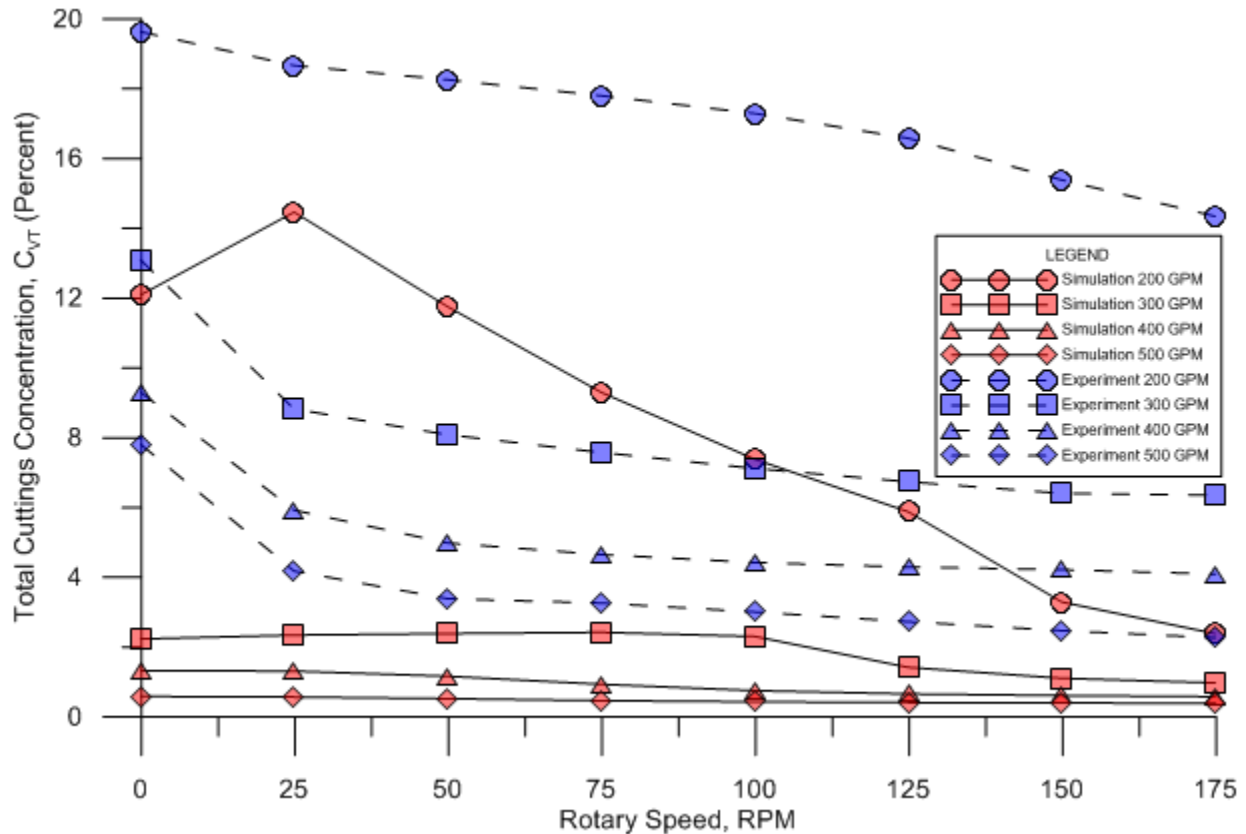


Figure 2.6: Comparison of the experimental and simulation results for Simulation 2. While the majority of the parameters are identical, the simulation uses a different drilling fluid, different cutting density, and a shorter test section.

The experimental results reflect a strong influence from the rotary speed of the drill pipe, particularly the difference between stationary and 25 rpm. While simulation results do reflect a positive influence from drill pipe rotation, the initial impact is less dramatic. At most flow rates, positive results from drill pipe rotation do not occur until between 75 and 125 rpm. In fact, at 300 gpm, the drill pipe rotation shows a slight negative impact on cuttings concentration.

Simulation results also indicate that drill pipe rotation has a much stronger influence at lower flow rates than higher flow rates. The experimental data suggests a more even impact at all flow rates. The proportional impact is also reflected in almost all of the data reported by Sanchez et al., even at different inclinations, cutting types, and mud properties (1999). However, experimental data on this effect is not consistent throughout literature, and it has been suggested that the effect of drill pipe rotation is dependent on several other drilling conditions (Sifferman and Becker 1992).

Figure 2.7 shows the cuttings concentration across the outlet of the simulation model at different flow rates and rotational speeds. Careful attention to the changes in the cuttings bed yields some insights as to why cuttings concentrations changed with changes in the parameters. The dominating trends are clear. Increase in flow rate has a dramatic effect on the cuttings bed, particularly between 200 gpm and 300 gpm. Drill pipe rotation as a whole tends to erode the bed. Looking more carefully, it is clear that the rotation also causes the cuttings to gather on the left side of the borehole while looking toward the bit. At low flow rates and low rotational speeds, it appears that the rotation is not enough to carry the cuttings into the higher flow regime. This seems to allow more room for cuttings to settle on the right side of the well bore, allowing for an increase in overall bed volume. This explains the increase in the simulation data that is not reflected in the experimental data.

Figure 2.8 shows two velocity vector plots on the outlet face of the model. The top plot shows the steady-state velocity profile with a 200 gpm pump rate and no pipe rotation. The bottom plot is at the same pump rate, but with no pipe rotation. The plot shows the dramatic change in the velocity profile of the wellbore with the added pipe rotation. For the top model, the highest flow regime is at the top of the wellbore, and it is centered azimuthally. The bottom model has a more even velocity distribution, and the highest flow regime has shifted to the right side of the wellbore. When compared to the volume fraction renderings, a more even velocity field suggests more dispersed cuttings that are easier to transport.

2.10.3 Sensitivities and Accuracy

Two additional studies were conducted to reconcile the differences between Experiment 2 and Simulation 2. First, a 100 ft model was built to compare to the 25 ft model. The 300 gpm pump rate trial with no rotation was repeated for the long section. The result is a cuttings concentration of 1.60% for the long model in comparison to 2.25% for the short model, which is

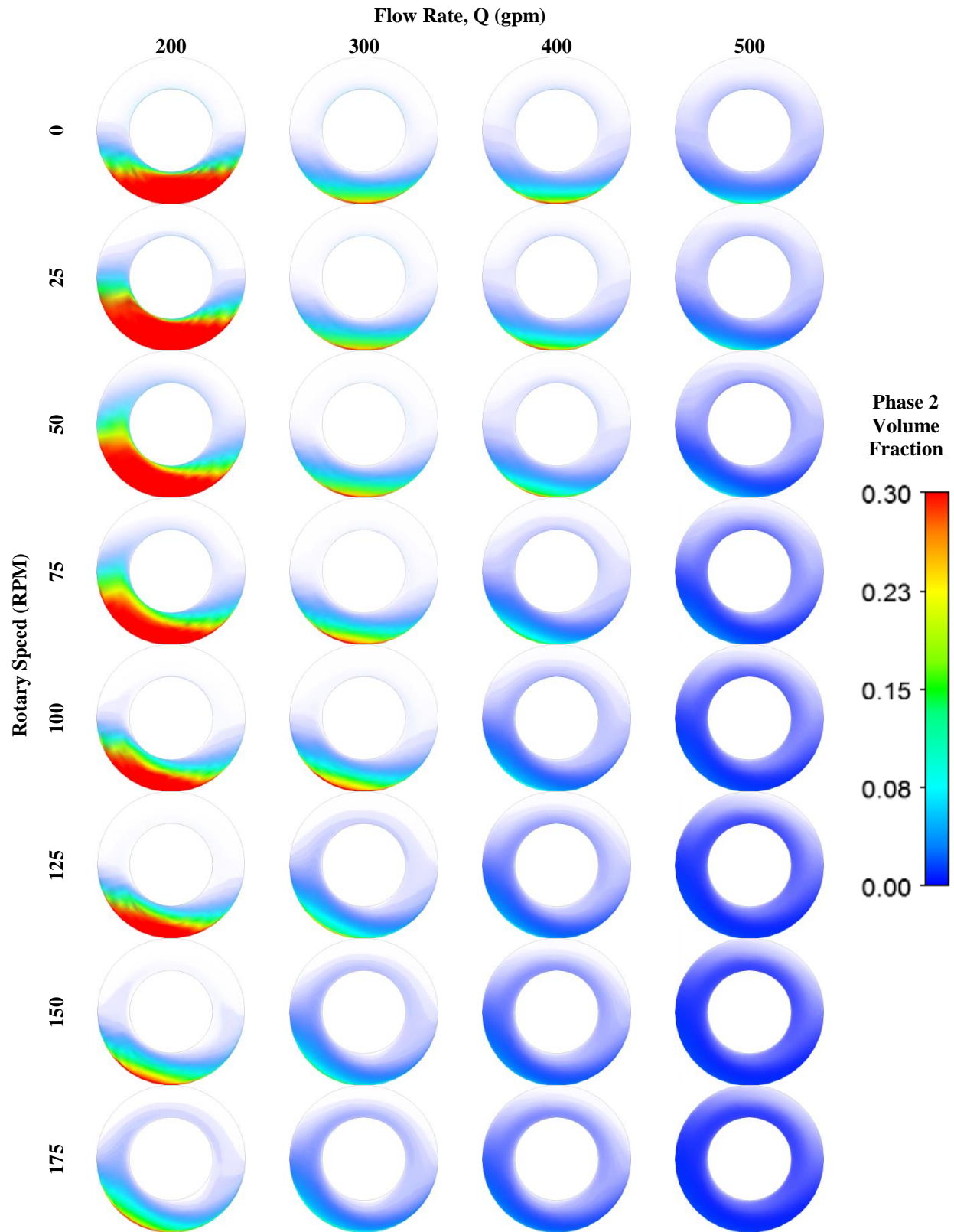


Figure 2.7: Volumetric cuttings fraction renderings for Simulation 2. The cross-sections shown are on the outlet faces.

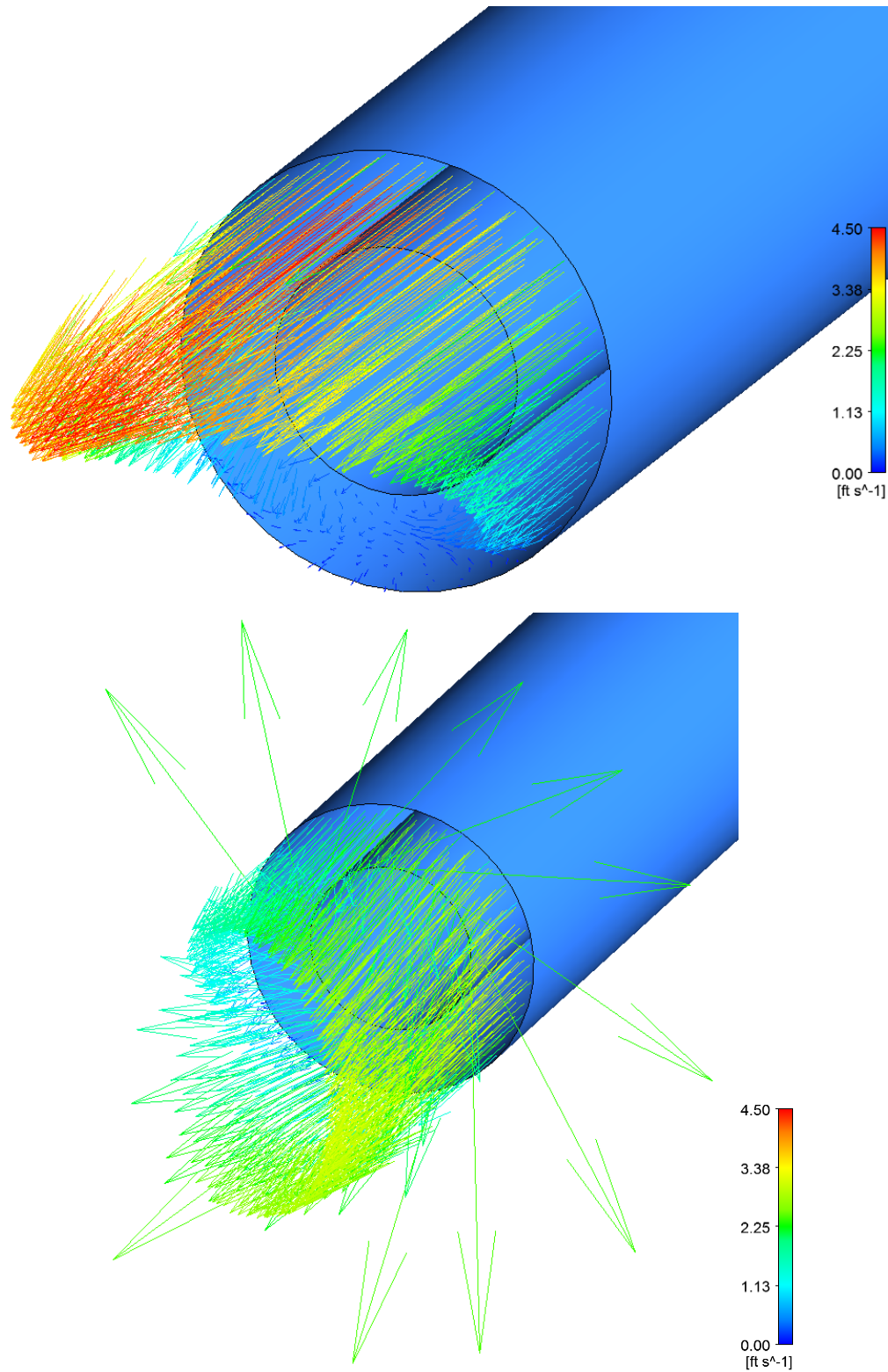


Figure 2.8: Velocity profiles of the drilling fluid at the outlet face. The top figure is from the 200 gpm, 0 rpm trial, and the bottom figure is from the 200 gpm, 175 rpm trial.

about 70% of the 25 ft model. Figure 2.9 shows a cuttings fraction comparison of the side views. At the inlet of the model, the cuttings tend to drop out in a form that resembles a dune. The profile then drops into an even cuttings bed for the rest of the model. For the 25 ft section, the initial cuttings bed makes up a significant portion of the model. It is much less significant over 100 ft. This effect is likely the largest contributor to the lower cuttings concentration in the 100 ft model.

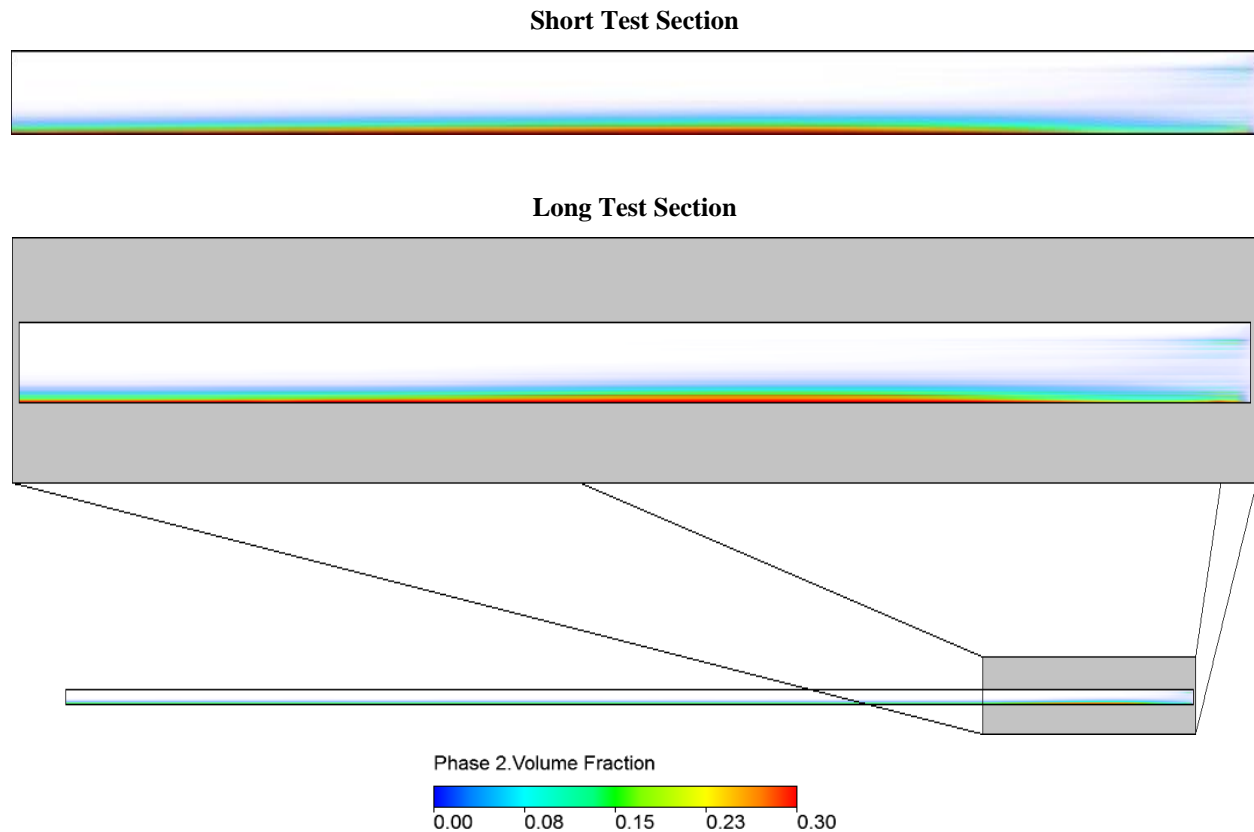


Figure 2.9: Side views of the volumetric cuttings fraction renderings for the short and long test sections. The entire test section is shown for both trials with a magnification on the inlet side of the long section. Vertical exaggeration has been added to both models for a clearer representation.

The second study seeks to observe the contribution of cutting size and density to the model. Because the cuttings in Simulation 2 utilized the size of one experiment and the density of another of the Sanchez et al. experiments, a sensitivity study is necessary to determine which, if either, data set is comparable to the simulation (1999). The 400 gpm flow rate, 125 rpm rotary speed was selected to test the two variables because of its fast convergence. Two trials were run that represented the actual data sets provided in the work by Sanchez et al (1999). The first used

0.25 inch limestone cuttings, and the second used 0.10 inch gravel. The results are shown with the Simulation 2 data in Figure 2.10.

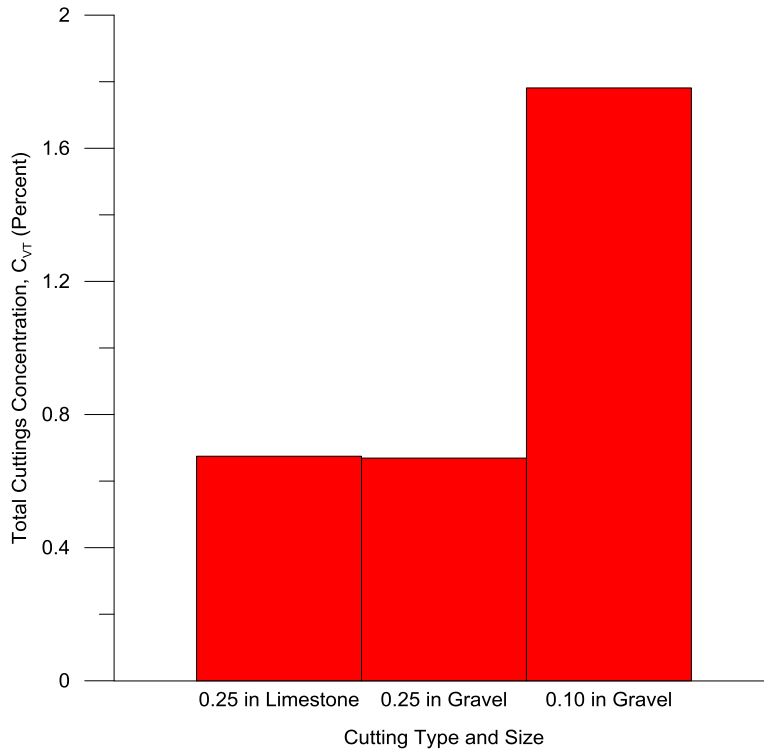


Figure 2.10: Comparison of the Simulation 2 results (middle) to simulation results for two experiments executed by Sanchez et al. (1999)

The cutting density has a negligible effect while the cutting size has a dramatic effect, increasing the cuttings concentration by a factor of 2.7. The volume rendered cutting concentration profiles are the same shape but much greater in concentration values than the original simulation. The smaller cutting size likely has the largest impact on the drag and dispersion models. Future work could study this effect in more detail, and finer tuning could result in quantitative agreement with experiments.

2.10.4 CFD Limitations and Future Studies

Modeling a solid-liquid system as two continuous phases has some limitations. Modeling a highly heterogeneous system such as oil and gas well drilling adds to the challenges. First, many simplifying assumptions are necessary. Highly idealized boundary conditions are required

for numerical modeling. While they are easily transferable to well-controlled experiments, they are less transferable to actual drilling conditions.

Drill cuttings are usually highly asymmetrical and present a distribution of sizes. The shape and size of the cuttings are critical to modeling drag as is shown by the second sensitivity study. While a constant granule size is employed in the presented models, Fluent is capable of incorporating a distribution of sizes. If cutting size distribution data is available, future studies could attempt to study this parameter more effectively. Additionally, the user has the option to adjust the packing factor, which is capable of incorporating some of the effect shape has on cutting bed density. Increasing the packing factor decreases the effective porosity of the cuttings bed, which represents perfect spheres of equal size in the presented simulations.

Studies in other fields have shown the importance of drag models and dispersion models on turbulent, granular flows (Montante and Bakker 2004, Gohel et al. 2012). While extensive effort has been made in selecting these models, future work could ensure that the physics of cuttings transport are properly captured.

Finally, it is difficult to model turbulent, non-Newtonian fluids in Fluent. If a robust user defined function is developed, the viscous properties of bentonite and other muds could be incorporated. Simulation 2 data is not directly comparable to the experimental data because of the differing rheological properties.

2.11 Conclusions

The following conclusions are drawn from the methodology and results produced in this chapter:

1. The trends of two experiments were successfully reproduced using CFD.
2. Quantitative agreement is not exact between the experiments and the simulations, and finer details of the trends vary.
3. The qualitative results suggest that the CFD modeling methodology developed in this chapter for the cuttings transport process can produce useful results.
4. Phase specific volumetric fraction rendering and velocity profiles add tremendous values to understanding the processes driving the formation, or lack thereof, of a cuttings bed.
5. The methodology and techniques developed in this chapter are capable of being applied to more involved studies on different drilling parameters and internal state variables.

CHAPTER 3

PARAMETER IMPLICATIONS

As stated in Chapter 1, the effect of different drilling parameters on cuttings transport have been thoroughly explored experimentally (Nazari et al. 2010). However, almost all experimental work uses fixed geometries to test the different parameters. It is difficult to change drill pipe and casing sizes, and doing so introduces variable control concerns. This chapter utilizes the CFD methodology developed in the previous chapter to explore the effect of different wellbore geometries on several drilling parameters. The goal of this set of studies is to compare the relative effect of different drilling parameters on cuttings accumulation in a wellbore across different casing and drill pipe sizes.

3.1 General Methodology

In order to properly test the effect of different parameters on cuttings transport, a careful list of trials was prepared prior to creating models, ensuring that each test variable is isolated for comparison to a control group. Table 3.1 below summarizes which variables are varied in this study and which values are used for each variable. Appendix C lists each trial and the parameters used for each as well as the resulting cuttings volume percent. In total, this study includes 111 computer simulations.

Table 3.1: List of parameters that are varied in the parameter implication study

Parameter	List of Values
Drill Pipe OD (in.)	4.5, 3, 1.5
Casing ID (in.)	12, 8, 5
Eccentricity	Concentric, positively eccentric, negatively eccentric
Drilling Fluid Flow Rate (gpm)	300, constant fluid velocity of 2.5 ft/s
Rotary Speed (rpm)	0, 100
Inclination (degrees)	0, 30, 60, 90
Rate of Penetration (ft/hr)	10, 50, 200

The trials were designed around four major studies:

1. Flow rate and velocity
2. Eccentricity
3. Inclination
4. ROP

Each study tested these parameters on varied model geometries. Additionally, each study tested the effect of rotation in combination with that parameter. The following sections describe the specifics of each study and the results.

Other than the parameters listed in Table 3.1, all model and drilling parameters remain constant throughout each of the studies. Table 3.2 lists the values of the constant parameters.

Table 3.2: List of constant parameters for simulations conducted in the parameter implications study

Parameter	Value
Model Length (ft)	30
Cutting Diameter (in.)	0.25
Cutting Density (lb/ft ³)	165.5
Drilling Fluid Type	Water
Drilling Fluid Density (lb/ft ³)	62.31
Drilling Fluid Viscosity (ft ² /s)	1.08E-05

3.2 Flow Rate and Velocity Study

Drilling fluid flow rate is the most important parameter in cuttings transport. The resulting average annular fluid velocity through the annular geometry determines how effectively a specific piece of formation can be carried up the wellbore. Therefore, this parameter makes a logical starting place for exploring cuttings transport via CFD.

3.2.1 Study Design

There are three objectives for studying the effect of flow rate and velocity on cuttings transport. First, this study compares CFD results to the expected results from solid-liquid flow systems. The results should show that residual cuttings concentrations are proportional to the square of the cross-sectional area at a constant flow volumetric flow rate and constant at constant

average fluid velocity. If the theoretical behavior is displayed in the results, this study provides additional validity to using the methodology developed in Chapter 2 with the new drilling parameters.

Second, this study provides the first comparison of different drilling geometries. Holding all other drilling parameters constant in their simplest forms provides a control group for comparison of future parameters. Results obtained by adding additional parameters such as pipe eccentricity can be compared to the results for this study to determine the relative effects of that parameter.

The final objective is to observe the effect of drill pipe rotation on the different geometries in a constant average velocity system. As previously stated, each study includes the addition of drill pipe rotation to the parameter being tested. This study isolates drill pipe rotation to the simplest parameters, and the results of the following studies are compared to these results.

Table 3.3 lists the parameters used to study the effects of constant flow rate and constant average annular fluid velocity on cuttings transport. First, the average annular fluid velocity is allowed to vary for each drill pipe and casing combination, holding the flow rate constant. Then, the velocity is set to a constant value, and the flow rate is allowed to vary. In each of the future studies, the average annular fluid velocity is held constant, and the results are compared to the second set of results from this study.

Table 3.3: Model parameters for the constant flow rate/ constant annular velocity study

Parameter	List of Values
Drill Pipe OD (in.)	4.5, 3, 1.5
Casing ID (in.)	12, 8, 5
Eccentricity	Concentric
Drilling Fluid Flow Rate (gpm)	300, constant fluid velocity of 2.5 ft/s
Rotary Speed (rpm)	0, 100
Inclination (degrees)	90
Rate of Penetration (ft/hr)	50

3.2.2 Results

The first nine simulations, as shown in Appendix C, make up the constant volumetric flow rate component of this study. The flow rate of the drilling fluid, which is water in this case,

is set to 300 gpm for each of the nine different wellbore geometries. Figure 3.1 shows the results of each simulation by plotting the residual cuttings concentration in the wellbore as a function of cross-sectional flow area.

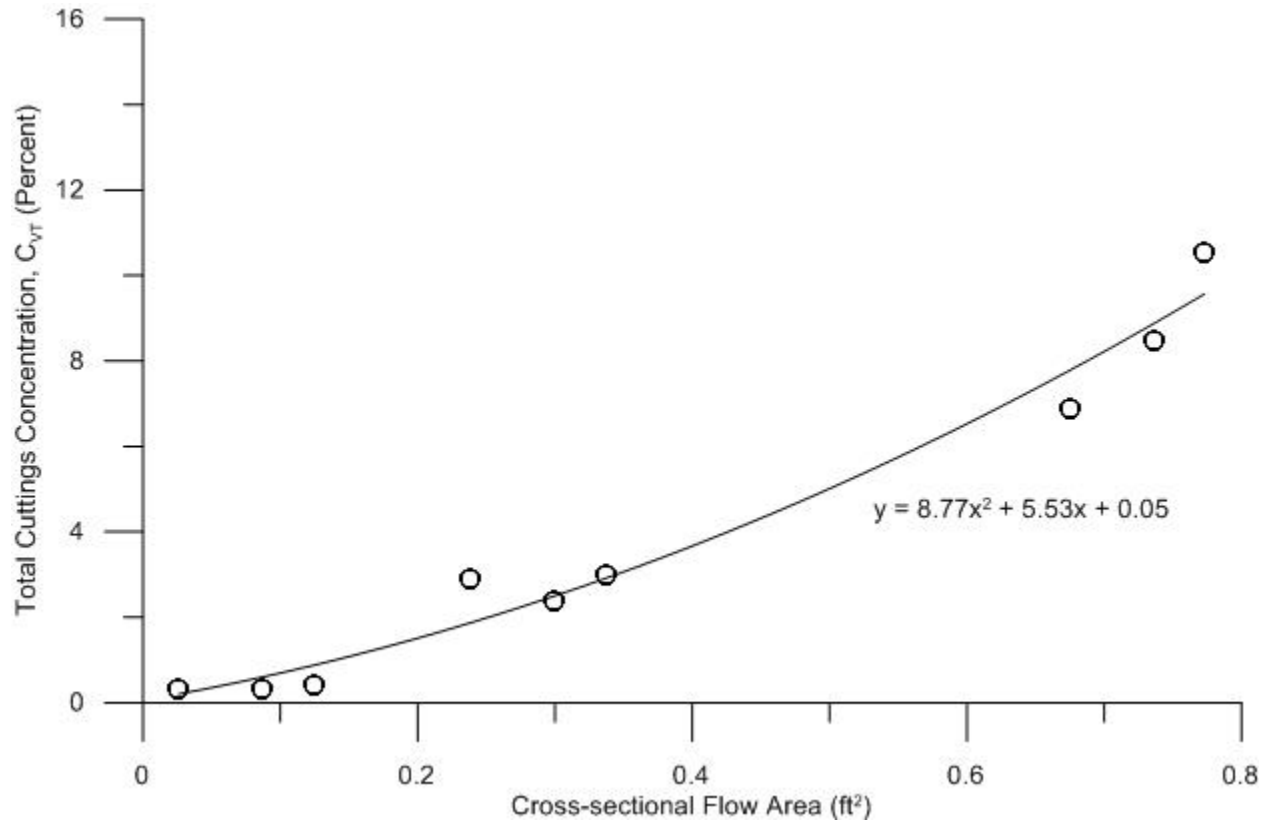


Figure 3.1: Results of the total cuttings concentration for the constant flow rate study.

The second order polynomial shown in Figure 3.1 fits the data quite well with a coefficient of determination of 0.97. Therefore, the data matches the expectation of a second order relationship between cuttings concentration and flow area at constant flow rate. These initial results suggest that the methodology developed in Chapter 2 applies to different model geometries. Although it is difficult to determine a critical cuttings concentration, combining the results from Figure 3.1 with those obtained in Chapter 2 suggests that average annular flow velocities below approximately 2.0 ft/s can contribute to rapid increases in cuttings accumulations.

The second part of this study holds a constant average fluid velocity instead of a constant flow rate. The results are shown in Figure 3.2.

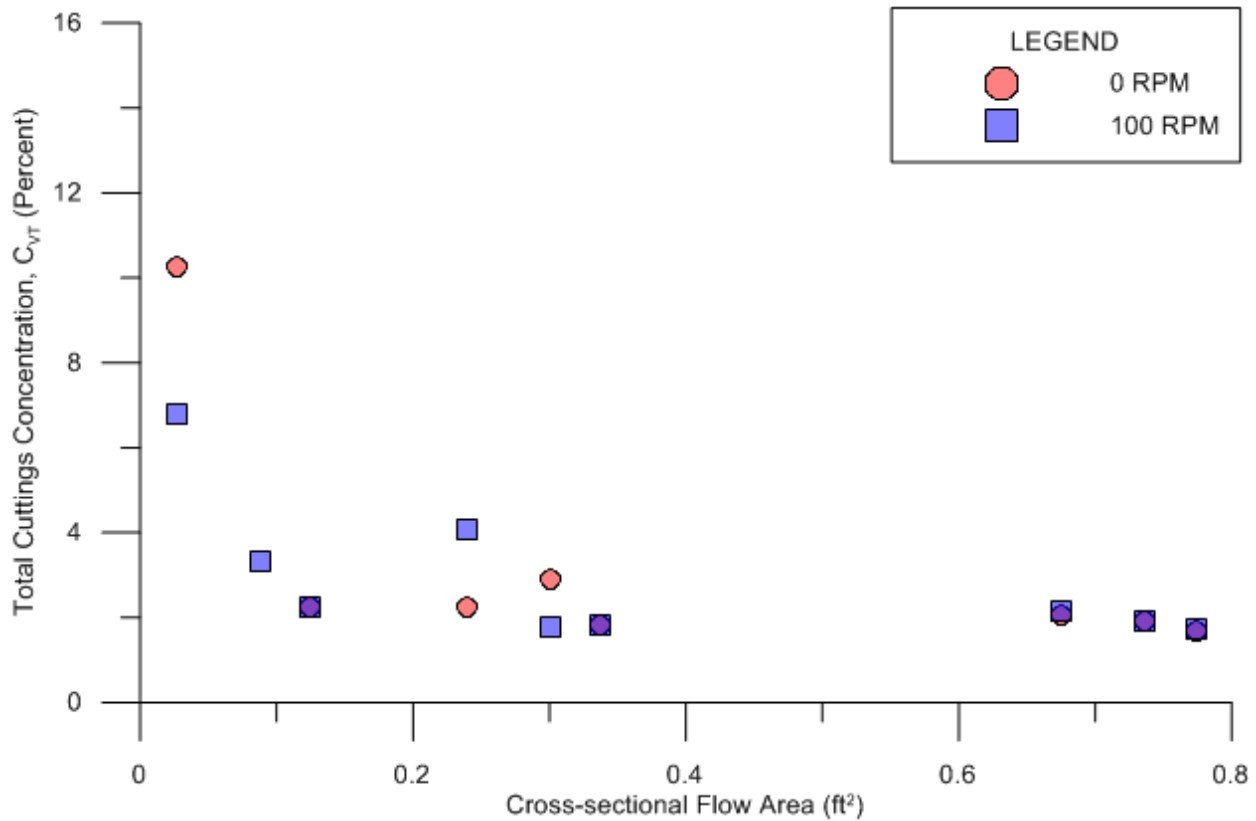


Figure 3.2: Resulting cuttings concentrations for different geometries at a constant average annular fluid velocity with and without drill pipe rotation.

At a constant average annular fluid velocity, the cuttings concentration should remain constant across all model geometries. With the exception of the smallest cross-sectional area, the expected trend is shown very well. The smallest cross-sectional area, 3.7 in.^2 for a 4.5 in. by 5 in. annulus, introduces extreme frictional interactions, causing additional cuttings to accumulate within the wellbore. Smaller geometries can also be more difficult simulate. One model, Simulation 15, is not included in Figure 3.2 because it did not properly mathematically converge. The cuttings volume fraction profiles shown in Appendix D reveal that the parts of the model had difficulties converging. The unrealistically small flow areas are not part of the following studies. While interesting to observe the extremes, they serve no purpose to overall trend observation, and it is difficult to verify that the models actually converged to a real solution.

Figure 3.2 reveals no clear effect of rotation. Most of the geometries retain nearly identical results with the addition of rotation. In some cases, there is improvement, and in some cases the rotation seems to have a negative effect. Similarly to some of the results obtained in Chapter 2, negative effects tend to occur when the frictional component of the drill pipe is insufficient to bring the cuttings all the way into the higher flow regime, simply creating more accommodation space. The positive effect occurs when the friction of the drill pipe is able to move the cuttings into the higher flow regime and out of the annulus. Which models benefit from drill pipe rotation also depends on the drill pipe roughness. This is further discussed in the future studies section.

3.3 Eccentricity Study

In reality, the drill pipe never remains perfectly concentric while drilling. It is a difficult parameter to control, but its natural occurrence deems it essential to understand. This study seeks to understand the effects of vertical eccentricity on cuttings transportation in various geometries, both with and without drill pipe rotation.

3.3.1 Study Design

For the purposes of this study, the eccentricity fraction reported in Appendix C is calculated using the following equation.

$$\varepsilon = \frac{y_{dp}}{r_{csg}}$$

Where

ε	=	Eccentricity (dimensionless)
y_{dp}	=	Y-component of drill pipe center coordinate (in)
r_{csg}	=	Casing radius (in)

Figure 3.3 depicts the vertical eccentricity values. The origin is defined as the center point of the casing. For all except one geometry, the models are defined as either 0.50 or -0.50 eccentricity. That eccentricity is not possible with a 4.5 in. drill pipe and an 8 in. casing, so 0.375 and -0.375 eccentricities are used.

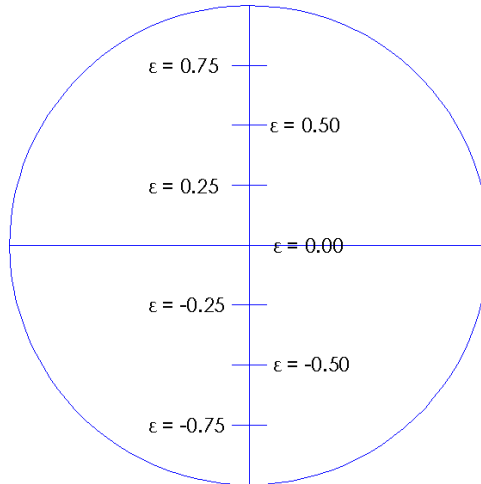


Figure 3.3: Example of eccentricity terminology used in this study.

To more efficiently obtain results, only one geometry and mesh were created for both the positive and the negative eccentricity simulations. The direction of the gravity term was switched instead. In Appendix D, the positive eccentricity simulations appear to collect cuttings on the roof of the borehole instead of the floor because of this.

In total the eccentricity study consists of 24 simulations with six geometries, divided evenly between positive and negative eccentricities, with and without drill pipe rotation. The results are also compared to the results from the fluid velocity study for the concentric case with and without drill pipe rotation. Table 3.4 details the parameters used in the eccentricity study simulations.

Table 3.4: Model parameters for the eccentricity study

Parameter	List of Values
Drill Pipe OD (in.)	4.5, 3, 1.5
Casing ID (in.)	12, 8, 5
Eccentricity	Concentric, positively eccentric, negatively eccentric
Average fluid velocity (ft/s)	2.5
Rotary Speed (rpm)	0, 100
Inclination (degrees)	90
Rate of Penetration (ft/hr)	50

3.3.2 Results

Modeling the negative eccentricity case is a difficult task. Simulations 29, 32, and 98 did not properly converge and are removed from the following results. Many of the negative eccentricity models resulted in very small spaces between the drill pipe and the casing. The mesh, despite being adjusted for these spaces, did not have the cell quantities between the two boundaries that the concentric cases had. When these few cells contained high volume fractions of cuttings, the solver had difficulty properly resolving the models. As so, it is difficult to draw firm conclusions for the negatively eccentric case.

Figure 3.4 shows the results for the eccentricity studies without drill pipe rotation. The concentric and positively eccentric cases are clear and consistent. The concentric case produces the greatest residual cuttings concentration followed by the positively eccentric case. The data does not support a clear trend for the negatively eccentric case. Prior work indicates that the concentric case yields the lowest cuttings concentration with negatively eccentric and positively eccentric cases yielding incrementally more cuttings (Tomren et al. 1986). However, these experiments were conducted at significantly lower annular fluid velocities.

The cuttings profiles shown in Appendix D reveal that the positively eccentric cases allow for higher velocity fluid to flow directly over the cuttings bed. The concentric case blocks much of the higher velocity fluid from directly removing cuttings from the bed surface, rendering it worse than the positively eccentric case. Simulation 28 is responsible for the high cuttings concentration result for the negatively eccentric case. It appears that certain geometries can produce catastrophic results when combined with no rotation and negative eccentricity. The velocity profile is sufficiently lowered around the drill pipe to allowing cuttings to accumulate while simultaneously allowing for large accumulation space. The result is a completely buried drill pipe. Other geometries, such as those in simulations 30 and 31, allow high enough velocity profiles around the drill pipe to continue to allow cuttings removal. Because this observation is based on only three data points, confirmation will be reserved for future studies.

Figure 3.5 shows the results of adding rotation to the positively and negatively eccentric cases. The results of the concentric case are shown in Figure 3.2 and discussed in Section 3.2.2. The positively eccentric case shows negligible impact from drill pipe rotation. The drill pipe is too far removed from the bottom of the wellbore where the cuttings accumulate to affect the forming bed. The concentric case shows mixed results as discussed in the previous section.

Overall, no trend is distinguishable. The addition of rotation allowed all of the negatively eccentric simulations to converge. With only three data to compare with the rotational case, no distinct trend is observed. However, simulation 38, in correspondence to simulation 28, shows that rotation may provide significant improvements under certain conditions. This particular geometry has high surface area contact between the drill pipe and the cuttings bed, increasing the frictional interaction between the two and contributing to improved cuttings removal.

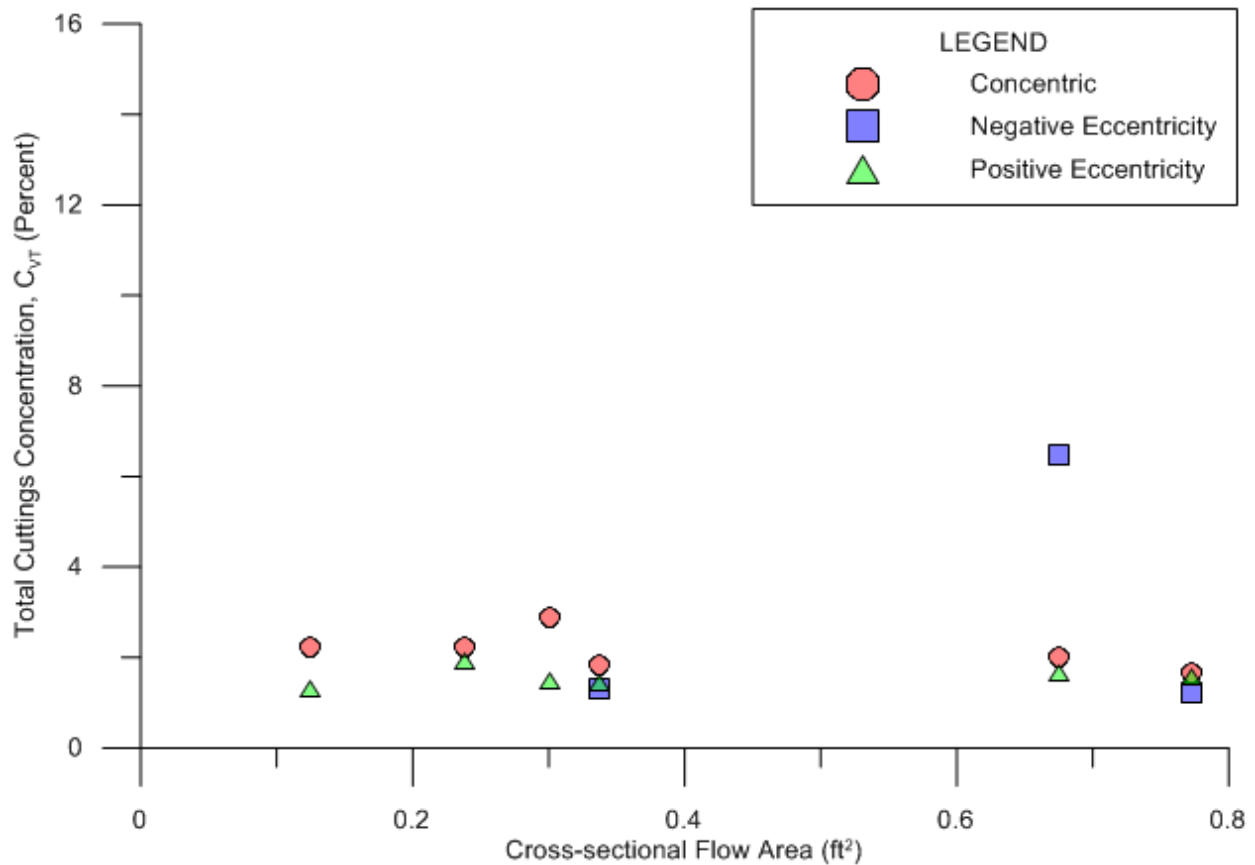


Figure 3.4: Resulting cuttings concentration for concentric, negatively eccentric, and positively eccentric cases.

3.4 Inclination Study

So far, all of the cases have been limited to a horizontal wellbore. The inclination study compares the horizontal case to a vertical case, a 30° inclination case, and a 60° inclination case.

3.4.1 Study Design

In total, the inclination study includes 36 simulations in addition to the 12 simulations already conducted at horizontal conditions. Table 3.5 contains the parameters used for the

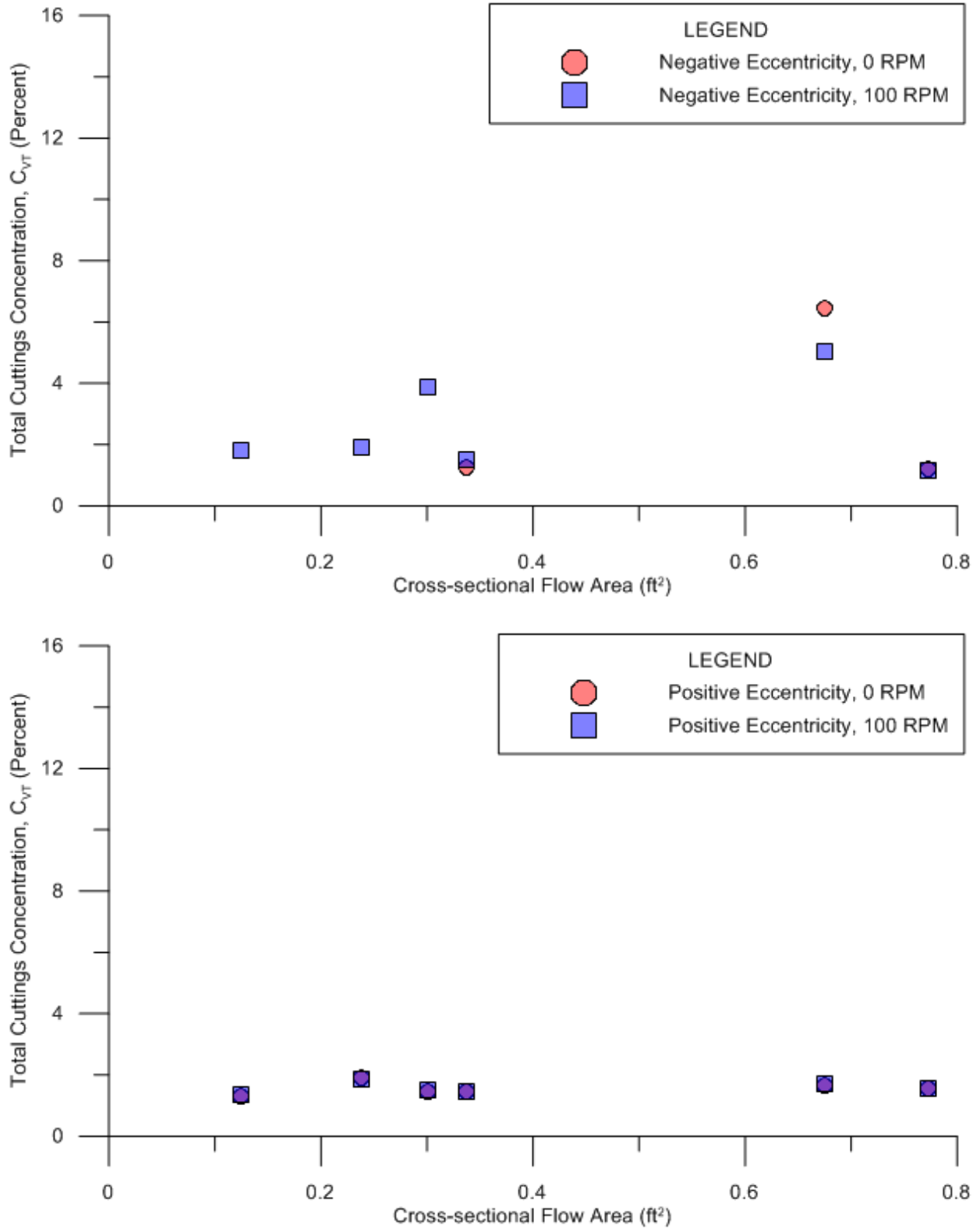


Figure 3.5: Results for applying drill pipe rotation to negatively and positively eccentric cases. The top plot shows the results for negative eccentricity, and the bottom plot shows the results for positive eccentricity.

inclination study. As in the eccentricity study, the direction of gravity is adjusted instead of creating new geometries and meshes for each of the inclinations.

Table 3.5: Model parameters for the inclination study

Parameter	List of Values
Drill Pipe OD (in.)	4.5, 3, 1.5
Casing ID (in.)	12, 8, 5
Eccentricity	Concentric
Average fluid velocity (ft/s)	2.5
Rotary Speed (rpm)	0, 100
Inclination (degrees)	0, 30, 60, 90
Rate of Penetration (ft/hr)	50

3.4.2 Results

Figure 3.6 shows the results for each inclination without drill pipe rotation. The results are clear and consistent. In order from most cuttings remaining in the wellbore to least, the cases are 60°, 30°, 90°, and 0°. This agrees very well with experimental studies (Nazari et al. 2010).

Figure 3.6 also shows that the vertical and horizontal cases are much less dependent on specific wellbore geometry than the 30° and 60° cases. More specifically, the simulations with larger drill pipe sizes result in greater cuttings concentration for those two cases but not in the horizontal and vertical cases. The cuttings profiles in Appendix D show large accumulations in parts of the wellbore for the larger drill pipe cases. A possible explanation could be that the drill pipe stabilizes the cuttings bed and prevents it from sliding.

Figure 3.7 contains the results of drill pipe rotation for each of the four inclinations. Neither the vertical nor the horizontal case benefit explicitly from the drill pipe rotation. However, the 30° and 60° both show cases of improvement from the added rotation. The improvement corresponds directly to the cases where high build ups occur without rotation. Rotating the pipe destabilizes the cuttings bed, allowing the cuttings to slide or transport with the drilling fluid. The exact mechanism of the cuttings removal is unclear from the steady-state simulation. The figures in Appendix D show the reduction in cuttings accumulations in the corresponding simulations to those with high accumulations without rotation.

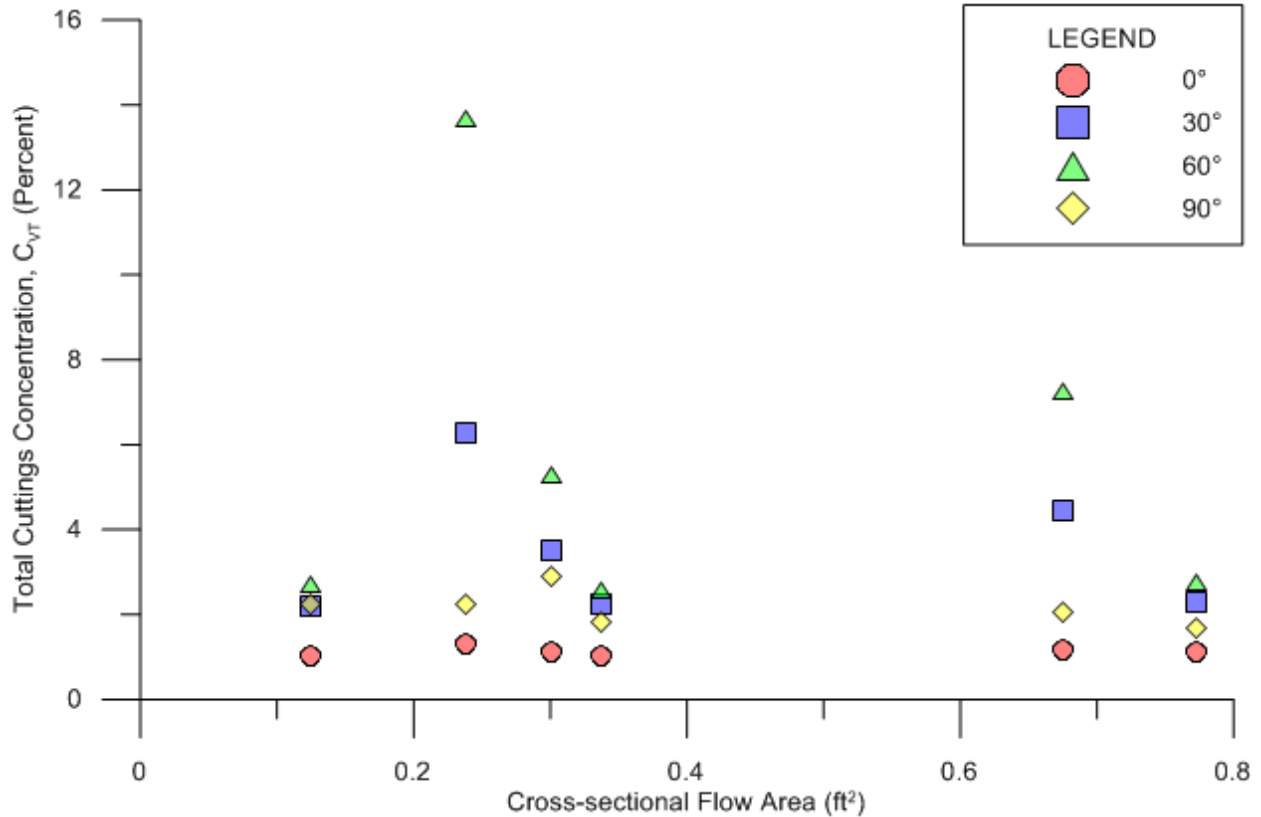


Figure 3.6: Cuttings concentration results for the study of the effect of inclination.

3.5 Rate of Penetration Study

The final study seeks to determine the impact of the ROP, or cuttings flow rate, on cuttings accumulation in a horizontal wellbore. This study compares three cases aimed to represent low, medium, and high ROP situations.

3.5.1 Study Design

The low, medium, and high ROP situations respectively utilize 10, 50, and 200 ft/hr ROP equivalents. The mass inlet rate of the cuttings phase is adjusted for each simulation to account for the amount of cuttings that would be created by drilling at those rates with a bit the size of the casing for that model.

The ROP study consists of 24 simulations in addition to the 12 simulations previously conducted at 50 ft/hr. Table 3.6 details the parameters used for this study.

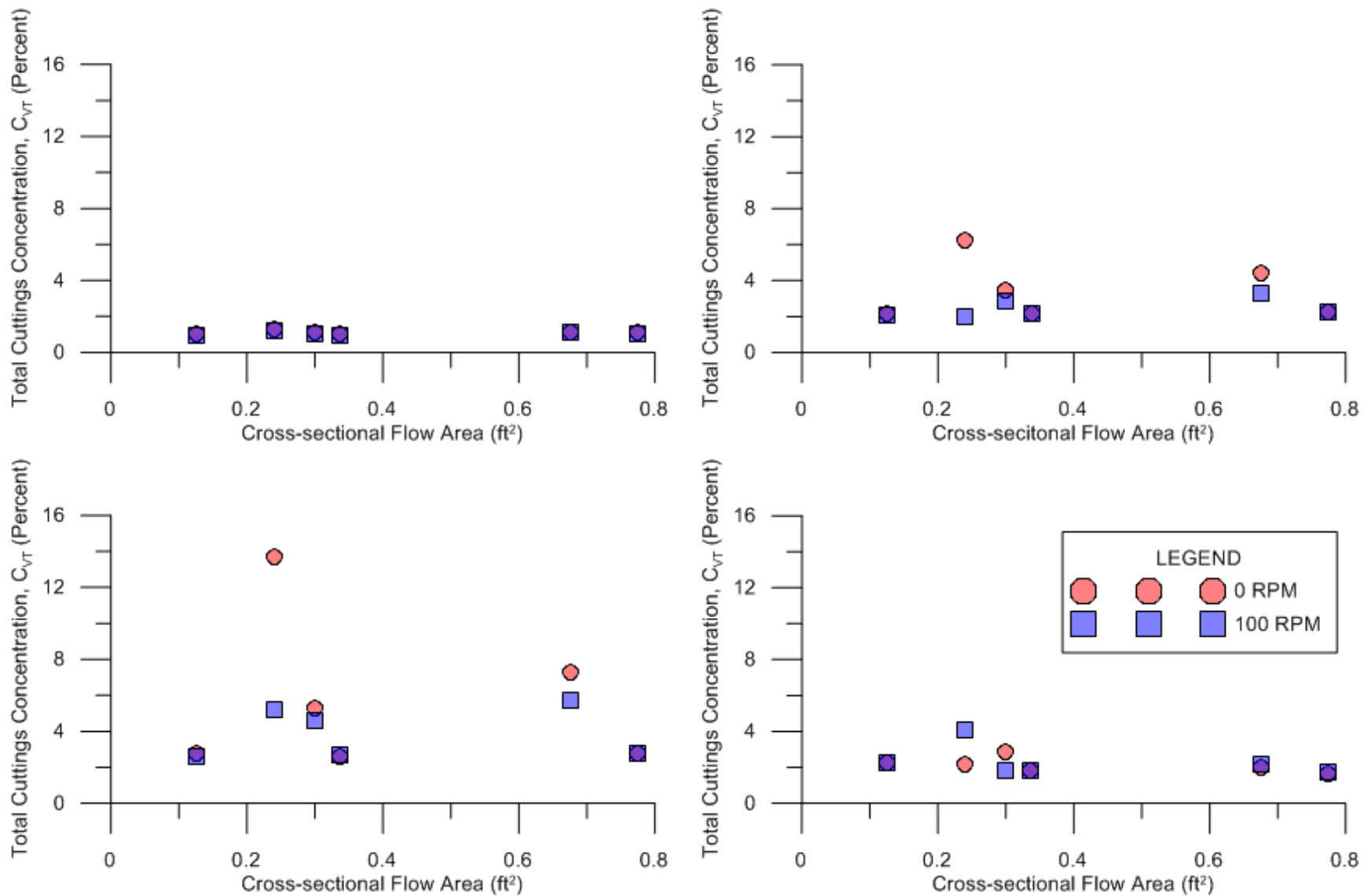


Figure 3.7: Results for applying drill pipe rotation at different wellbore inclinations. The top-left is at 0°, the top-right at 30°, the bottom-left at 60°, and the bottom-right at 90°.

Table 3.6: Model parameters for the ROP study

Parameter	List of Values
Drill Pipe OD (in.)	4.5, 3, 1.5
Casing ID (in.)	12, 8, 5
Eccentricity	Concentric
Average fluid velocity (ft/s)	2.5 ft/s
Rotary Speed (rpm)	0, 100
Inclination (degrees)	90
Rate of Penetration (ft/hr)	10, 50, 200

3.5.2 Results

Figure 3.8 contains the results for each ROP without drill pipe rotation. As expected, the cuttings accumulation increases with increased ROP. The relationship is approximately linear, proportionally increasing the remaining cuttings concentration with increased ROP. Similarly to the inclination results, however, some geometries are more sensitive to the increase in ROP than others. In fact, the same geometries that experience increased cuttings accumulations at 30° and 60° inclinations experience disproportionately increased cuttings accumulations at higher ROP's. Comparing the cuttings profiles in Appendix D, the same logic holds for this case as well. The larger drill pipe seems to stabilize the cuttings bed, allowing for increased accumulations.

Figure 3.9 contains the results for the low and high ROP cases with and without drill pipe rotation. The medium ROP case is shown in Section 3.2.2. Like the medium ROP case, the low ROP case shows very little effect from drill pipe rotation. The high ROP case shows vast improvement in the cases where the drill pipe stabilizes the cuttings bed without rotation and very little improvement in the cases where it does not.

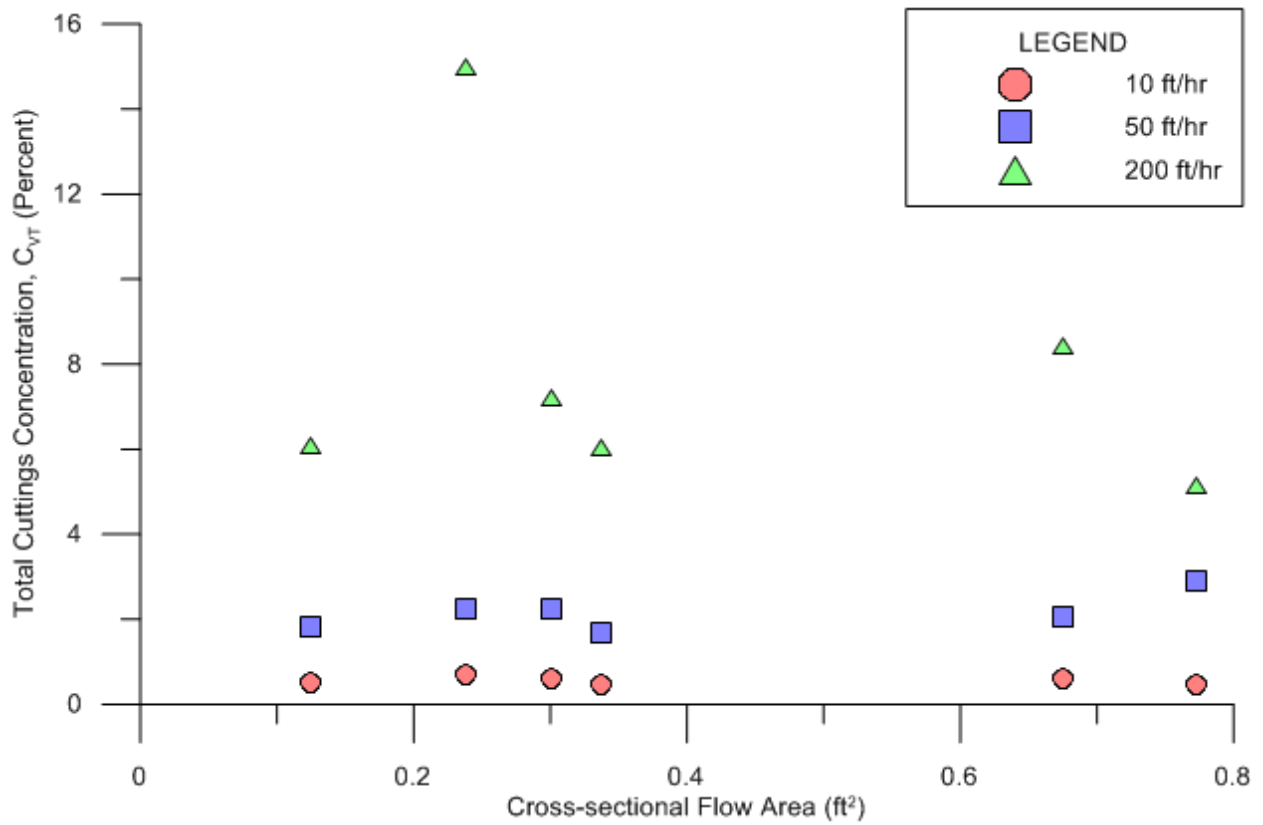


Figure 3.8: Resulting cuttings concentrations at low, moderate, and high rates of penetration.

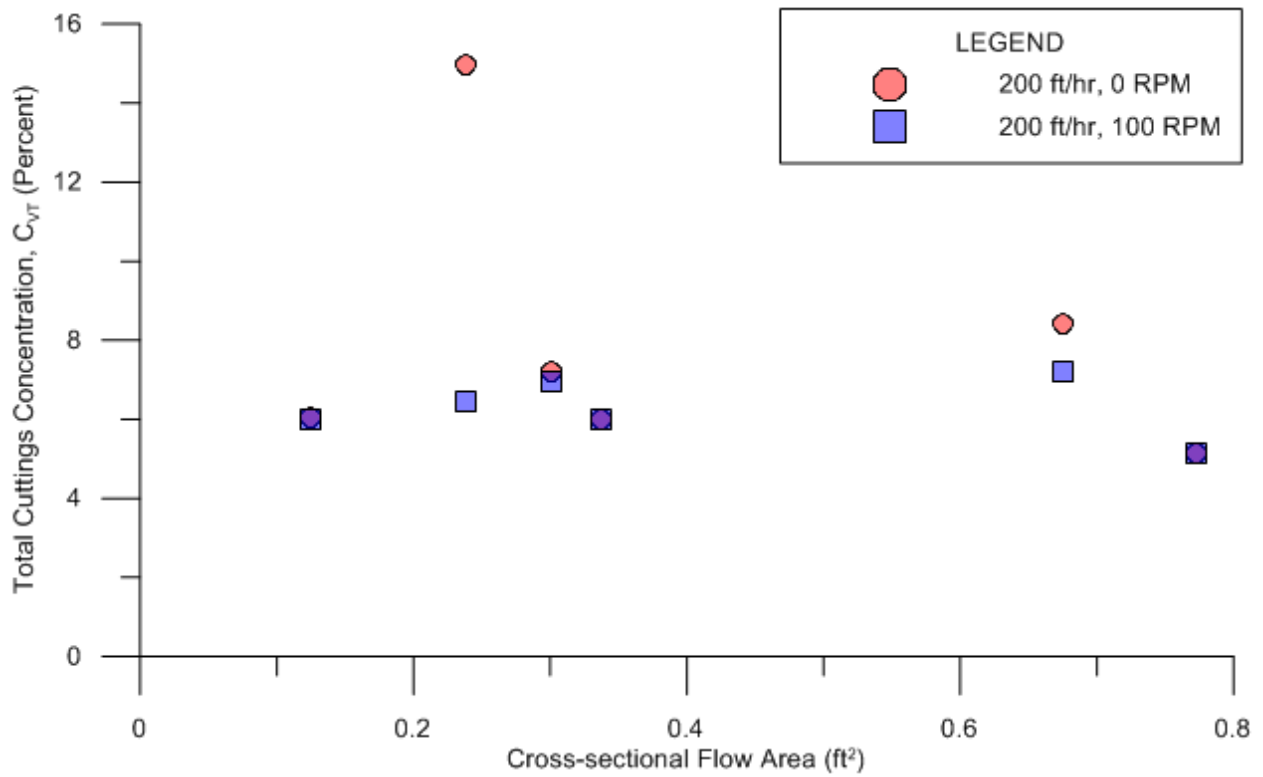
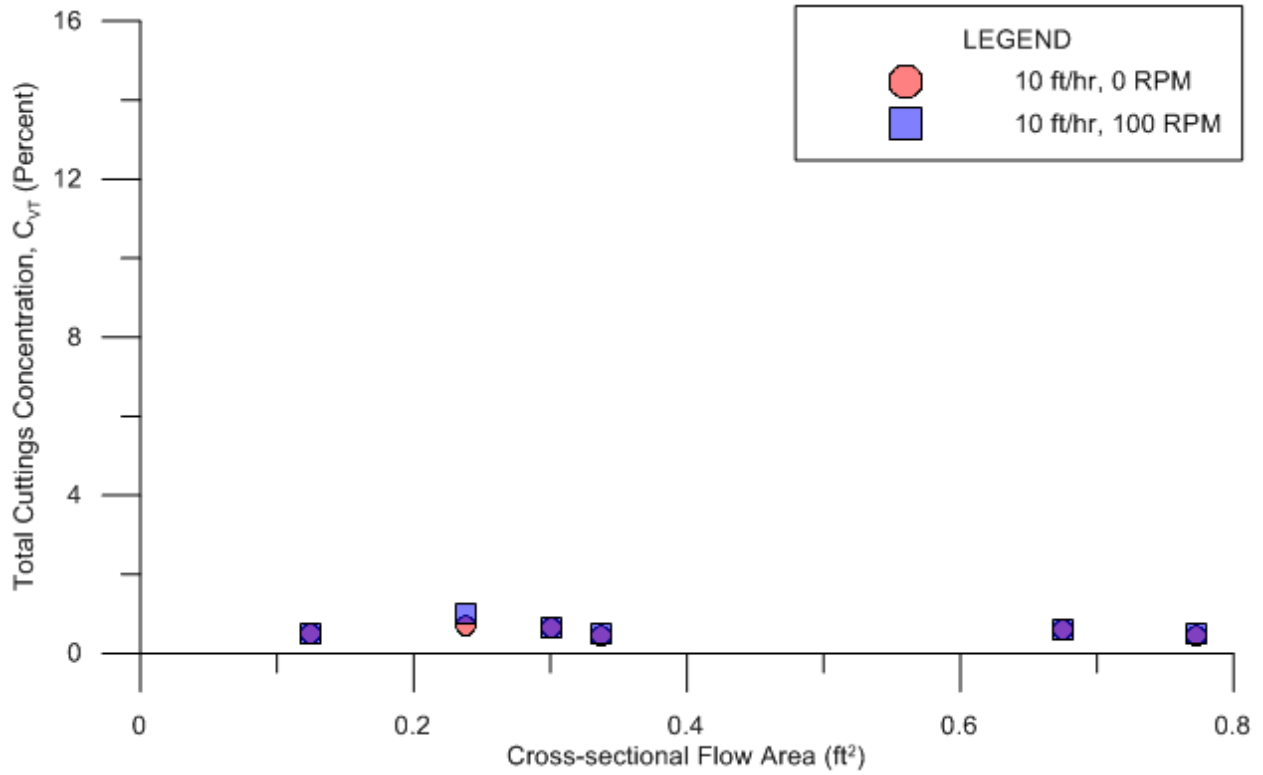


Figure 3.9: Results for applying drill pipe rotation at different rates of penetration. The top plot shows the effect at low (10 ft/hr) drilling rates, and the bottom shows the effect at high (200 ft/hr) drilling rates.

CHAPTER 4

DISCUSSION AND CONCLUSIONS

This chapter discusses implications of the results from the work presented in Chapters 2 and 3. Included are topics for future work that could further clarify ambiguous results and validate concepts that have not yet been thoroughly explored. Finally, the major findings are outlined in the conclusions.

4.1 Discussion

The combined results from the four studies suggest that the mechanisms for cuttings transport are more complicated than reported in previous studies. One notable example of this is the effect of drill pipe rotation. While many experimental studies suggest significant improvement in cuttings removal by the application of rotation (Sanchez et al. 1999), the simulations conducted in these studies suggest that improvement is highly dependent on other parameters. Referring back to the Simulation 2 results presented in Chapter 2, significant improvement only occurs when the flow rate is below a threshold. Other situations where improvement occurs include wellbore inclinations in the 30° to 60° range and high ROP's.

Additionally, the effect of eccentricity may also be highly dependent on the other system variables. Sufficient flow rates could yield positively eccentric cases beneficial, exposing more of the cuttings bed to high velocity fluid. This is in direct opposition to other reported claims (Nazari et al. 2010). However, the lower flow rates could contribute to the detrimental effects of eccentricity previously reported. In all, it is not likely that a clear positive or negative effect can be attributed to each system variable as previously attempted and reproduced in Chapter 1. Understanding each component and the combined effect is essential to understanding the physics.

4.2 Future Work

The work reported in this chapter has allowed for some observations that oppose the previously developed cuttings transport concepts. However, more research should be conducted to confirm and build off of these observations. Building out a larger data base with a greater range of drilling parameters and internal state variables will allow for more specific trends.

One of the specific model variables that should be more thoroughly investigated is the drill pipe roughness. Understanding the exact roll of drill pipe rotation is highly dependent on the roughness. With thorough tuning, it may be possible to determine the exact ranges that drill pipe rotation benefits hole cleaning. Additionally, the eccentricity study conducted in this chapter contained particularly poor convergence. Adjusting the mesh to obtain better results could lead to more observations and conclusions.

4.3 Conclusions

The following conclusions are drawn from the parameter implication study.

1. At a constant flow rate, cuttings accumulation is proportional to the square of the cross-sectional flow area.
2. At a constant average annular fluid velocity, cuttings accumulation is constant across all drill pipe and borehole sizes until the clearances become very small.
3. Maintaining sufficiently high average annular fluid velocity, approximately 2.0 ft/s, is the most important parameter for cuttings transport in a horizontal wellbore.
4. If the average annular fluid velocity is sufficiently maintained, the size of the drill pipe and borehole rarely affect the accumulation of cuttings in a wellbore.
5. Under some conditions, vertical eccentricity in either direction can decrease cuttings accumulations. The perfectly concentric scenario is not the ideal goal for cutting transport.
6. A wellbore inclination of 60° results in the worst cuttings accumulation, followed by 30° , 90° , and 0° . Drill pipe rotation can improve cuttings transport in the 60° and 30° scenarios.
7. Increasing ROP increases cuttings concentration in direct proportionality.
8. The effect of drill pipe rotation highly depends on other drilling parameters. Rotation does not always improve cuttings transport.
9. In cases of high cuttings accumulation such as inclined wellbores and high ROP, a motionless drill pipe can stabilize the cuttings bed, further increasing accumulation. Drill pipe rotation greatly improves these scenarios.
10. In the cases of high cuttings accumulation, larger drill pipes stabilize cuttings beds better than smaller drill pipes.

LIST OF SYMBOLS

A	=	Cross sectional area of duct (ft ²)
C_{VT}	=	Total volumetric cuttings concentration (%)
d_h	=	Hydraulic diameter (ft)
d_o, d_i	=	Outer diameter of annulus, inner diameter of annulus (ft)
p	=	Total perimeter of circular duct (ft)
Q	=	Flow rate (ft ³ /s)
r_{csg}	=	Casing radius (in.)
r_o, r_i	=	Outer radius of annulus, inner radius of annulus (ft)
Re	=	Reynolds number (dimensionless)
u	=	Average fluid velocity (ft/s)
ν	=	Kinematic viscosity (ft ² /s)
v_{avg}	=	Average annular fluid velocity (ft/s)
y_{dp}	=	Y-component of drill pipe center coordinate (in.)
ε	=	Eccentricity (dimensionless)
μ	=	Dynamic viscosity (lb _m /s/ft)
ρ	=	Fluid density (lbm/ft ³)

REFERENCES CITED

- ANSYS 2013a. ANSYS Fluent Theory Guide. Release 15.0. Canonsburg, PA: ANSYS, Inc.
- ANSYS 2013b. ANSYS Fluent User's Guide. Release 15.0. Canonsburg, PA: ANSYS, Inc.
- ANSYS 2014. Introduction to ANSYS Fluent R14.5 – Lecture 7: Turbulence Modeling. Online training video produced by ANSYS, Inc.
[https://support.ansys.com/AnsysCustomerPortal/en_us/Knowledge+Resources/Tutorials+&+Training+Materials/Training+Files/Introduction+to+ANSYS+Fluent+R14.5+-+Full+Course+Videos+\(BETA\)](https://support.ansys.com/AnsysCustomerPortal/en_us/Knowledge+Resources/Tutorials+&+Training+Materials/Training+Files/Introduction+to+ANSYS+Fluent+R14.5+-+Full+Course+Videos+(BETA)) (accessed 23 July 2014).
- Bilgesu, H.I, Mishra, N., and Ameri, S. 2007. Understanding the Effects of Drilling Parameters on Hole Cleaning in Horizontal and Deviated Wellbores Using Computational Fluid Dynamics. Paper SPE 111208 presented at the SPE Eastern Regional Meeting in Lexington, Kentucky, 17-19 October. <http://dx.doi.org/10.2118/111208-MS>.
- Campbell, J.A. 2001. Coiled Tubing Drilling - Has It Come of Age?. Paper presented at the Offshore Mediterranean Conference and Exhibition, Ravenna, Italy, 28-30 March.
- Feechan, M., Makselon, C., and Nolet, S. 2003. Field Experience with Composite Coiled Tubing. Paper SPE 82045 presented at the SPE/ICoTA Coiled Tubing Conference held in Houston, Texas, 8-9 April. <http://dx.doi.org/10.2118/82045-MS>.
- Gohel, S., Joshi, S. Azhar, A. et al. 2012. CFD Modeling of Solid Suspension in a Stirred Tank: Effect of Drag Models and Turbulent Dispersion on Cloud Height. *International Journal of Chemical Engineering* (2012): 1-9. <http://dx.doi.org/10.1155/2012/956975>.
- Hallundbæk, J. 1994. Well Tractors for Highly Deviated and Horizontal Wells. Paper SPE 28871 presented at the European Petroleum Conference held in London, United Kingdom, 25-27 October. <http://dx.doi.org/10.2118/28871-MS>.
- Leising, L.J. and Rike, E.A. 1994. Coiled-Tubing Case Histories. Paper SPE 27433 presented at the SPE/IADC Drilling Conference, Dallas, Texas, 15-18 February. <http://dx.doi.org/10.2118/27433-MS>.
- Li, Y., Bjordalen, N. , Kuru, E. 2004. Numerical Modelling of Cuttings Transport in Horizontal Wells Using Conventional Drilling Fluids. Paper SPE 2004-227 presented at the Canadian International Petroleum Conference, Calgary, Alberta, Canada, 8-10 June. <http://dx.doi.org/10.2118/2004-227>.
- Marker, R., Haukvik, J., Terry, J.B et al. 2000. Anaconda: Joint Development Project Leads to Digitally Controlled Composite Coiled Tubing Drilling System. Paper SPE 60750 presented at the SPE/ICoTA Coiled Tubing Roundtable, Houston, Texas, 5-6 April. <http://dx.doi.org/10.2118/60750-MS>.

- Montante, G. and Bakker, A. 2004. Solid-Liquid Multiphase Flow Validation in Tall Stirred Vessels with Multiple Impeller Systems. Technical notes produced by Fluent, Inc.
- Moore, N.B., Beaufort, R.E., Krueger, R.E. 1999. Puller-Thruster Downhole Tool. US Patent No. 6,003,606.
- Mitchell, R.F. and Miska, S.Z. 2011. *Fundamentals of Drilling Engineering*, Vol. 12, 2-5. Richardson, Texas: Textbook Series, SPE.
- Nazari, T., Hareland, G., and Azar, J.J. 2010. Review of Cuttings Transport in Directional Well Drilling: Systematic Approach. Paper SPE 132372 presented at the SPE Western Regional Meeting in Anaheim, California, 27-29 May. <http://dx.doi.org/10.2118/132372-MS>.
- Newman, K.R. and Stone, L.R. 1995. Final Report: Electric Drilling Motor for Coiled Tubing Drilling - Feasibility Study Phase 1. Chicago, Illinois: Gas Research Institute.
- Osorio, A. and Frisby, R. 2013. Zone Abandonment with E-Line Inflatable Bridge Plug Provides Work-Around for Platform with Coiled Tubing Access Limitations. Paper SPE 163922 presented at the SPE/ICoTA Coiled Tubing Conference held in The Woodlands, Texas, 26-27 March. <http://dx.doi.org/10.2118/163922-MS>.
- Pletcher, R.H., Tannehill, J.C., and Anderson, D.A. 2013. *Computational Fluid Mechanics and Heat Transfer*, third edition, 3-9, 66-82. Boca Raton, Florida: CRC Press.
- Sanchez, R.A., Azar, J.J., Bassal, A.A. et al. 1999. Effect of Drillpipe Rotation on Hole Cleaning During Directional-Well Drilling. *SPE Journal*4(2): 101-108. SPE-56406-PA. <http://dx.doi.org/10.2118/56406-PA>.
- Samuel, G.R. 2007. *Downhole Drilling Tools*, 615-631. Houston, Texas: Gulf Publishing Company.
- Sas-Jaworsky II, A. 1993. Coiled Tubing Operations and Services, Part 1. *World Oil's Coiled Tubing Handbook*. Houston, Texas: Gulf Publishing Company.
- Sifferman, T.R. and Becker, T.E. 1992. Hole Cleaning in Full-Scale Inclined Wellbores. *SPE Drilling Engineering* 7(2): 115-120. SPE-20422-PA. <http://dx.doi.org/10.2118/20422-PA>.
- Terry, J.B., Wilson, T.P., Eppink, J.M. et al. 2004. Well System. US Patent No. 7,172,038.
- Tomren, P.H., Iyoho, A.W., and Azar, J.J. 1986. Experimental Study of Cuttings Transport in Directional Wells. *SPE Drilling Engineering* 1(1): 43-56. SPE-12123-PA. <http://dx.doi.org/10.2118/12123-PA>.
- Zhou, Y. and Shah, S.N. 2003. Fluid Flow in Coiled Tubing: CFD Simulation. Paper Petroleum Society 2003-212 presented at the Canadian International Petroleum Conference in Calgary, Alberta, Canada, 10-12 June. <http://dx.doi.org/10.2118/2003-212>.

APPENDIX A
SUMMARY OF INPUTS

A.1 Simulation 1

Geometry		
Outer Diameter (in.)		5
Inner Diameter (in.)		1.9
Length (ft)		40
Mesh		
Radial Division Increments (degrees)		10
Sweep Type		Quad/Tri
Sweep Element Length (in.)		3
Inflation Layers		5
Inflation Growth Rate		1.8
First Layer Thickness (in.)		1
General		
Solver Type		Pressure-based
Velocity Formulation		Absolute
Time Domain		Steady-state
Gravitational Acceleration (ft/s ²)		32.14
CFD Models		
Multiphase Model		Euler-Euler
Number of Phases		2
Volume Fraction Scheme		Implicit
Viscous Model		Reynolds Stress
Reynolds Stress Model		Linear Pressure-Strain
Wall Reflection Effects		Enabled
Near-Wall Treatment		Standard Wall Functions
Reynolds Stress Model Multiphase Model		Dispersed
Reynolds Model Constant: Cmu		0.09
Reynolds Model Constant: C1-Epsilon		1.44
Reynolds Model Constant: C2-Epsilon		1.92
Reynolds Model Constant: C3-Epsilon		1.3
Reynolds Model Constant: C1-PS		1.8
Reynolds Model Constant: C2-PS		0.6
Reynolds Model Constant: C1'-PS		0.5
Reynolds Model Constant: C2'-PS		0.3
Reynolds Model Constant: TKE Prandtl Number		1
Reynolds Model Constant: TKR Prandtl Number		1.3
Reynolds Model Constant: Dispersion Prandtl Number		0.75
Materials		
Drilling Fluid Density (lb/ft ³)		62.3
Drilling Fluid Viscosity (lb/ft/s)		6.74x10 ⁻⁴
Drill Cuttings Density (lb/ft ³)		165.5
Phases		
Phase 1 – Material		Drilling Fluid (Water)
Phase 2 – Material		Drill Cuttings
Phase 2 – Granular		Enabled

A.1 Simulation 1 continued

Phase 2 – Granular Temperature Model	Phase Property
Phase 2 – Diameter	0.25 in
Phase 2 – Granular Viscosity Model	Gidaspow
Phase 2 – Granular Bulk Viscosity Model	Lun et al.
Phase 2 – Frictional Viscosity Model	Johnson et al.
Phase 2 – Angle of Internal Friction (degrees)	30.00007
Phase 2 – Frictional Pressure	Kinetic Theory
Phase 2 – Frictional Modulus	Derived
Phase 2 – Friction Packing Limit	0.05
Phase 2 – Granular Temperature	Algebraic
Phase 2 – Solids Pressure Model	Lun et al.
Phase 2 – Elasticity Modulus	Derived
Phase 2 – Packing Limit	0.63
Phase Interaction – Drag Coefficient	Gidaspow
Phase Interaction – Drag Modification Factor	Brucato
Phase Interaction – Turbulent Dispersion Model	Diffusion in Volume of Fluid
Phase Interaction – Restitution Coefficient	0.9
Boundary Conditions	
Inlet – Initial Gauge Pressure (lb/ft ²)	0
Inlet – Flow Direction	Normal to Boundary
Inlet – Phase 1 Turbulent Intensity (%)	5
Inlet – Phase 1 Turbulent Viscosity Ratio	10
Inlet – Phase 2 Velocity Ratio	1
Inlet – Simulation 1, Phase 1 Flow Rate (lb/s)	12.6 – 31.5
Inlet – Simulation 1, Phase 2 Flow Rate (lb/s)	0.333
Outlet – Gauge Pressure (lb/ft ²)	0
Outlet – Phase 1 Backflow Turbulent Intensity (%)	5
Outlet – Phase 1 Backflow Turbulent Viscosity Ratio	10
Outlet – Phase 2 Backflow Granular Temperature (ft ² /s ²)	0.00108
Outlet – Phase 2 Backflow Volume Fraction	0
Outer Wall – Wall Motion	Stationary
Outer Wall – Shear Condition	No Slip
Outer Wall – Wall Roughness Height (ft)	0
Outer Wall – Wall Roughness Constant	0.5
Inner Wall – Wall Motion	Stationary/ Rotational
Inner Wall – Rotation Speed (rad/s)	0 – 10.5
Inner Wall – Shear Condition	No Slip
Inner Wall – Wall Roughness Height (ft)	0
Inner Wall – Wall Roughness Constant	0.5
Solution	
Algorithm	Phase Coupled SIMPLE
Spatial Discretization – Gradient	Least Squares Cell Based
Spatial Discretization – Momentum	First Order Upwind
Spatial Discretization – Volume Fraction	First Order Upwind
Spatial Discretization – Turbulent Kinetic Energy	First Order Upwind
Spatial Discretization – Turbulent Dissipation Rate	First Order Upwind
Spatial Discretization – Reynolds Stresses	First Order Upwind

A.2 Simulation 2

Geometry

Outer Diameter (in.)	8
Inner Diameter (in.)	4.5
Length (ft)	25

Mesh

Radial Division Increments (degrees)	10
Sweep Type	Quad/Tri
Sweep Element Length (in.)	3
Inflation Layers	8
Inflation Growth Rate	1.2
Transition Ratio	0.3

General

Solver Type	Pressure-based
Velocity Formulation	Absolute
Time Domain	Steady-state
Gravitational Acceleration (ft/s ²)	32.14

CFD Models

Multiphase Model	Euler-Euler
Number of Phases	2
Volume Fraction Scheme	Implicit
Viscous Model	Reynolds Stress
Reynolds Stress Model	Linear Pressure-Strain
Wall Reflection Effects	Enabled
Near-Wall Treatment	Standard Wall Functions
Reynolds Stress Model Multiphase Model	Dispersed
Reynolds Model Constant: Cmu	0.09
Reynolds Model Constant: C1-Epsilon	1.44
Reynolds Model Constant: C2-Epsilon	1.92
Reynolds Model Constant: C3-Epsilon	1.3
Reynolds Model Constant: C1-PS	1.8
Reynolds Model Constant: C2-PS	0.6
Reynolds Model Constant: C1 ² -PS	0.5
Reynolds Model Constant: C2 ² -PS	0.3
Reynolds Model Constant: TKE Prandtl Number	1
Reynolds Model Constant: TKR Prandtl Number	1.3
Reynolds Model Constant: Dispersion Prandtl Number	0.75

Materials

Drilling Fluid Density (lb/ft ³)	62.3
Drilling Fluid Viscosity (lb/ft/s)	6.74x10 ⁻⁴
Drill Cuttings Density (lb/ft ³)	159.8

Phases

Phase 1 – Material	Drilling Fluid (Water)
Phase 2 – Material	Drill Cuttings
Phase 2 – Granular	Enabled
Phase 2 – Granular Temperature Model	Phase Property
Phase 2 – Diameter	0.25 in
Phase 2 – Granular Viscosity Model	Gidaspow
Phase 2 – Granular Bulk Viscosity Model	Lun et al.
Phase 2 – Frictional Viscosity Model	Johnson et al.
Phase 2 – Angle of Internal Friction (degrees)	30.00007
Phase 2 – Frictional Pressure	Kinetic Theory
Phase 2 – Frictional Modulus	Derived

A.2 Simulation 2 continued

Phase 2 – Friction Packing Limit	0.05
Phase 2 – Granular Temperature	Algebraic
Phase 2 – Solids Pressure Model	Lun et al.
Phase 2 – Elasticity Modulus	Derived
Phase 2 – Packing Limit	0.63
Phase Interaction – Drag Coefficient	Gidaspow
Phase Interaction – Drag Modification Factor	Brucato
Phase Interaction – Turbulent Dispersion Model	Diffusion in Volume of Fluid
Phase Interaction – Restitution Coefficient	0.9
Boundary Conditions	
Inlet – Initial Gauge Pressure (lb/ft ²)	0
Inlet – Flow Direction	Normal to Boundary
Inlet – Phase 1 Turbulent Intensity (%)	5
Inlet – Phase 1 Turbulent Viscosity Ratio	10
Inlet – Phase 2 Velocity Ratio	1
Inlet – Simulation 2, Phase 1 Flow Rate (lb/s)	17.4 – 31.3
Inlet – Simulation 2, Phase 2 Flow Rate (lb/s)	0.559
Outlet – Gauge Pressure (lb/ft ²)	0
Outlet – Phase 1 Backflow Turbulent Intensity (%)	5
Outlet – Phase 1 Backflow Turbulent Viscosity Ratio	10
Outlet – Phase 2 Backflow Granular Temperature (ft ² /s ²)	0.00108
Outlet – Phase 2 Backflow Volume Fraction	0
Outer Wall – Wall Motion	Stationary
Outer Wall – Shear Condition	No Slip
Outer Wall – Wall Roughness Height (ft)	0
Outer Wall – Wall Roughness Constant	0.5
Inner Wall – Wall Motion	Stationary/ Rotational
Inner Wall – Rotation Speed (rad/s)	0 – 18.3
Inner Wall – Shear Condition	No Slip
Inner Wall – Wall Roughness Height (ft)	0
Inner Wall – Wall Roughness Constant	0.5
Solution	
Algorithm	Phase Coupled SIMPLE
Spatial Discretization – Gradient	Least Squares Cell Based
Spatial Discretization – Momentum	First Order Upwind
Spatial Discretization – Volume Fraction	First Order Upwind
Spatial Discretization – Turbulent Kinetic Energy	First Order Upwind
Spatial Discretization – Turbulent Dissipation Rate	First Order Upwind
Spatial Discretization – Reynolds Stresses	First Order Upwind

APPENDIX B
DETERMINATION OF TURBULENCE

Turbulence is determined by calculating the Reynolds number. If the Reynolds number is greater than 4000, the flow is fully turbulent. The following equations are used to determine the Reynolds number for a flow between two concentric pipes.

$$Re = \frac{\rho u d_h}{\mu} = \frac{u d_h}{\nu} \quad \text{C.1}$$

$$d_h = \frac{4A}{p} = \frac{4(\pi r_o^2 - \pi r_i^2)}{2\pi r_o + 2\pi r_i} = 2(r_o - r_i) = d_o - d_i \quad \text{C.2}$$

$$u = \frac{Q}{A} = \frac{4Q}{\pi(d_o^2 - d_i^2)} \quad \text{C.3}$$

Where

Re	=	Reynolds number (dimensionless)
ρ	=	Fluid density (lbm/ft ³)
u	=	Average fluid velocity (ft/s)
d_h	=	Hydraulic diameter (ft)
μ	=	Dynamic viscosity (lb _m /s/ft)
ν	=	Kinematic viscosity (ft ² /s)
A	=	Cross sectional area of duct (ft ²)
p	=	Total perimeter of circular duct (ft)
r_o, r_i	=	Outer radius of annulus, inner radius of annulus (ft)
d_o, d_i	=	Outer diameter of annulus, inner diameter of annulus (ft)
Q	=	Flow rate (ft ³ /s)

The lowest Reynolds numbers occur at the lowest flow rates with no rotation. The inputs for Simulations 1 and 2 are shown in Table C.1.

Table B.1: Table of parameters used to determine minimum Reynolds number

Simulation 1		Simulation 2	
$Q =$	125 gpm	$Q =$	200 gpm
$d_o =$	5 in.	$d_o =$	8 in.
$d_i =$	1.9 in.	$d_i =$	4.5 in.
$\nu =$	1 cSt	$\nu =$	1 cSt

The lowest Reynolds number for Simulation 1 is 57,300, and the lowest for Simulation 2 is 50,600. Turbulent flow occurs at Reynolds numbers greater than 4,000. Therefore, all flows are fully turbulent.

APPENDIX C

LIST OF PARAMETERS FOR IMPLICATION STUDY SIMULATIONS

Table C.1 lists each simulation used in the parameter implication study with its relevant parameters. The simulations run in order of variable isolation studies, which include varied flow velocity, flow rate, rotary speed, eccentricity, inclination, and ROP. Simulations 98 through 111 consist of additional data gathered for each study for more complete results.

Table C.1: List of the parameters and results for each simulation in Chapter 3

Sim. #	Drill Pipe OD (in.)	Casing ID (in.)	Eccentricity (Fraction)	Flow Rate (gpm)	Average Annular Velocity (ft/s)	Rotary Speed (RPM)	Inclination (Degrees)	Rate of Penetration (ft/hr)	Resulting Cuttings Volume Percent (%)
1	4.5	12	0	300	1.0	0	90	50	6.87
2	4.5	8	0	300	2.8	0	90	50	2.90
3	4.5	5	0	300	25.8	0	90	50	0.29
4	3	12	0	300	0.9	0	90	50	8.49
5	3	8	0	300	2.2	0	90	50	2.36
6	3	5	0	300	7.7	0	90	50	0.33
7	1.5	12	0	300	0.9	0	90	50	10.54
8	1.5	8	0	300	2.0	0	90	50	2.98
9	1.5	5	0	300	5.4	0	90	50	0.42
10	4.5	12	0	757	2.5	0	90	50	2.04
11	4.5	8	0	268	2.5	0	90	50	2.23
12	4.5	5	0	29	2.5	0	90	50	10.27
13	3	12	0	826	2.5	0	90	50	1.93
14	3	8	0	337	2.5	0	90	50	2.91
15	3	5	0	98	2.5	0	90	50	0.68
16	1.5	12	0	868	2.5	0	90	50	1.68
17	1.5	8	0	378	2.5	0	90	50	1.82
18	1.5	5	0	139	2.5	0	90	50	2.24
19	4.5	12	0	757	2.5	100	90	50	2.16
20	4.5	8	0	268	2.5	100	90	50	4.07
21	4.5	5	0	29	2.5	100	90	50	6.79
22	3	12	0	826	2.5	100	90	50	1.91
23	3	8	0	337	2.5	100	90	50	1.78
24	3	5	0	98	2.5	100	90	50	3.31
25	1.5	12	0	868	2.5	100	90	50	1.70
26	1.5	8	0	378	2.5	100	90	50	1.82

27	1.5	5	0	139	2.5	100	90	50	2.23
28	4.5	12	-0.5	757	2.5	0	90	50	6.47
29	4.5	8	-0.375	268	2.5	0	90	50	0.80
30	1.5	12	-0.5	868	2.5	0	90	50	1.19
31	1.5	8	-0.5	378	2.5	0	90	50	1.28
32	1.5	5	-0.5	139	2.5	0	90	50	0.58
33	4.5	12	0.5	757	2.5	0	90	50	1.65
34	4.5	8	0.375	268	2.5	0	90	50	1.92
35	1.5	12	0.5	868	2.5	0	90	50	1.54
36	1.5	8	0.5	378	2.5	0	90	50	1.44
37	1.5	5	0.5	139	2.5	0	90	50	1.30
38	4.5	12	-0.5	757	2.5	100	90	50	5.05
39	4.5	8	-0.375	268	2.5	100	90	50	1.93
40	1.5	12	-0.5	868	2.5	100	90	50	1.15
41	1.5	8	-0.5	378	2.5	100	90	50	1.49
42	1.5	5	-0.5	139	2.5	100	90	50	1.83
43	4.5	12	0.5	757	2.5	100	90	50	1.68
44	4.5	8	0.375	268	2.5	100	90	50	1.86
45	1.5	12	0.5	868	2.5	100	90	50	1.56
46	1.5	8	0.5	378	2.5	100	90	50	1.45
47	1.5	5	0.5	139	2.5	100	90	50	1.34
48	4.5	12	0	757	2.5	0	0	50	1.14
49	4.5	8	0	268	2.5	0	0	50	1.29
50	1.5	12	0	868	2.5	0	0	50	1.07
51	1.5	8	0	378	2.5	0	0	50	0.99
52	1.5	5	0	139	2.5	0	0	50	1.00
53	4.5	12	0	757	2.5	0	30	50	4.40
54	4.5	8	0	268	2.5	0	30	50	6.27
55	1.5	12	0	868	2.5	0	30	50	2.28
56	1.5	8	0	378	2.5	0	30	50	2.20
57	1.5	5	0	139	2.5	0	30	50	2.18
58	4.5	12	0	757	2.5	0	60	50	7.23
59	4.5	8	0	268	2.5	0	60	50	13.68
60	1.5	12	0	868	2.5	0	60	50	2.73
61	1.5	8	0	378	2.5	0	60	50	2.56
62	1.5	5	0	139	2.5	0	60	50	2.69
63	4.5	12	0	757	2.5	100	0	50	1.12
64	4.5	8	0	268	2.5	100	0	50	1.26
65	1.5	12	0	868	2.5	100	0	50	1.07
66	1.5	8	0	378	2.5	100	0	50	0.99
67	1.5	5	0	139	2.5	100	0	50	1.00
68	4.5	12	0	757	2.5	100	30	50	3.33
69	4.5	8	0	268	2.5	100	30	50	1.98

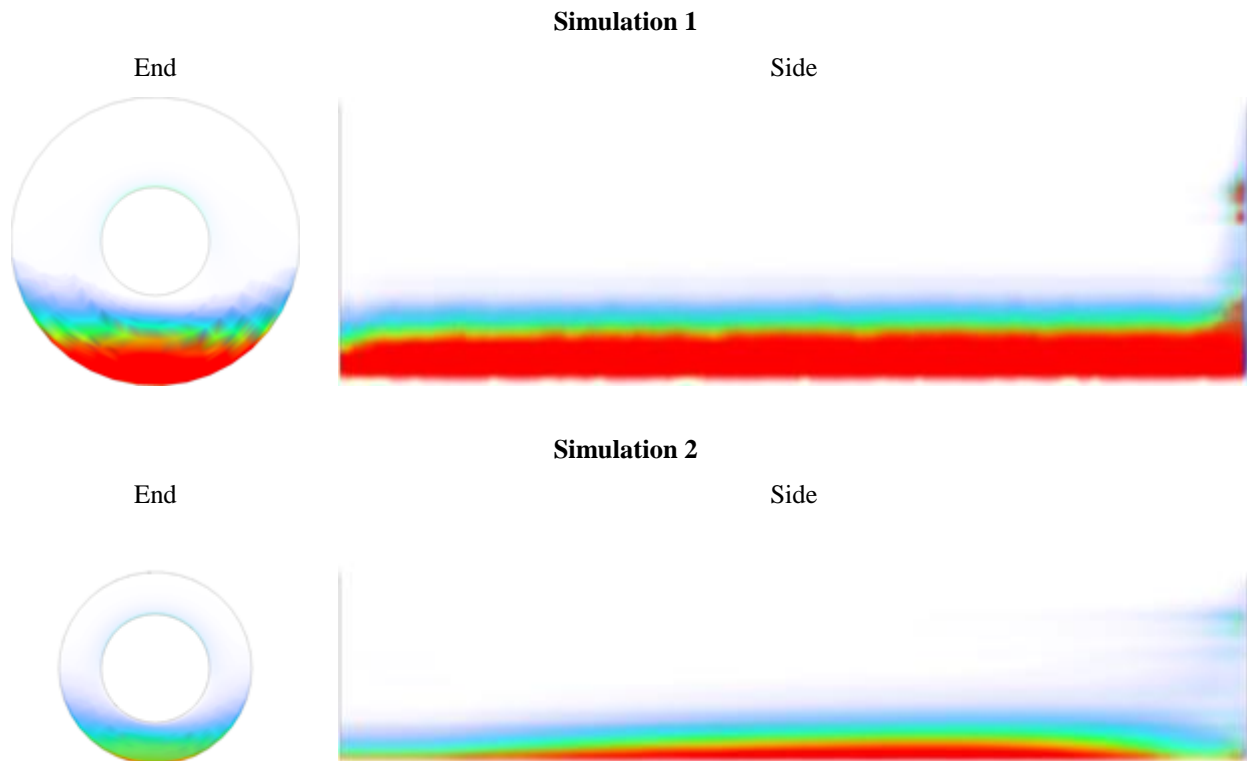
70	1.5	12	0	868	2.5	100	30	50	2.27
71	1.5	8	0	378	2.5	100	30	50	2.19
72	1.5	5	0	139	2.5	100	30	50	2.07
73	4.5	12	0	757	2.5	100	60	50	5.75
74	4.5	8	0	268	2.5	100	60	50	5.25
75	1.5	12	0	868	2.5	100	60	50	2.75
76	1.5	8	0	378	2.5	100	60	50	2.72
77	1.5	5	0	139	2.5	100	60	50	2.60
78	4.5	12	0	757	2.5	0	90	10	0.62
79	4.5	8	0	268	2.5	0	90	10	0.71
80	1.5	12	0	868	2.5	0	90	10	0.44
81	1.5	8	0	378	2.5	0	90	10	0.45
82	1.5	5	0	139	2.5	0	90	10	0.49
83	4.5	12	0	757	2.5	0	90	200	8.43
84	4.5	8	0	268	2.5	0	90	200	14.99
85	1.5	12	0	868	2.5	0	90	200	5.14
86	1.5	8	0	378	2.5	0	90	200	6.01
87	1.5	5	0	139	2.5	0	90	200	6.06
88	4.5	12	0	757	2.5	100	90	10	0.58
89	4.5	8	0	268	2.5	100	90	10	0.99
90	1.5	12	0	868	2.5	100	90	10	0.44
91	1.5	8	0	378	2.5	100	90	10	0.46
92	1.5	5	0	139	2.5	100	90	10	0.49
93	4.5	12	0	757	2.5	100	90	200	7.22
94	4.5	8	0	268	2.5	100	90	200	6.44
95	1.5	12	0	868	2.5	100	90	200	5.15
96	1.5	8	0	378	2.5	100	90	200	6.02
97	1.5	5	0	139	2.5	100	90	200	6.00
98	3	8	-0.5	337	2.5	0	90	50	0.87
99	3	8	0.5	337	2.5	0	90	50	1.46
100	3	8	-0.5	337	2.5	100	90	50	3.86
101	3	8	0.5	337	2.5	100	90	50	1.49
102	3	8	0	337	2.5	0	0	50	1.08
103	3	8	0	337	2.5	0	30	50	3.50
104	3	8	0	337	2.5	0	60	50	5.28
105	3	8	0	337	2.5	100	0	50	1.07
106	3	8	0	337	2.5	100	30	50	2.91
107	3	8	0	337	2.5	100	60	50	4.62
108	3	8	0	337	2.5	0	90	10	0.62
109	3	8	0	337	2.5	0	90	200	7.19
110	3	8	0	337	2.5	100	90	10	0.60
111	3	8	0	337	2.5	100	90	200	6.93

APPENDIX D

CUTTINGS VOLUME FRACTION PROFILES FOR PARAMETER IMPLICATIONS

Table D.1 shows the end and side views of the cuttings volume fractions for each of the simulations in the parameter implication study. Figure D.1 at the end of the table contains the color legend for interpreting the volume fractions. The side views are horizontally compressed for viewing ease.

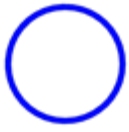
Table D.1: Volume fraction renderings



Simulation 3

End

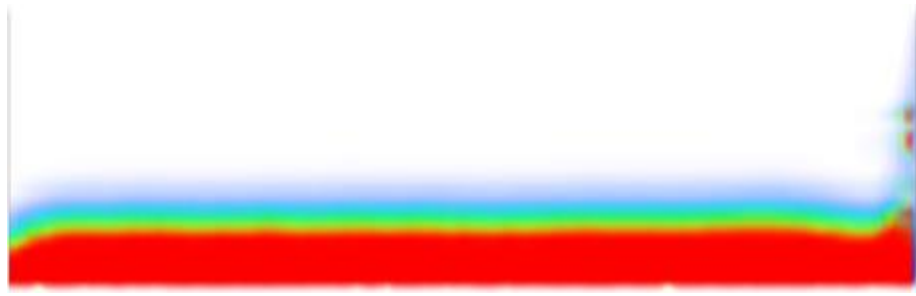
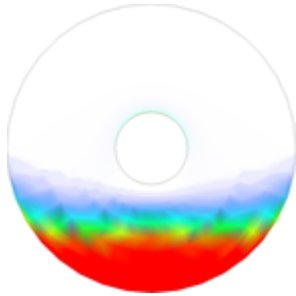
Side



Simulation 4

End

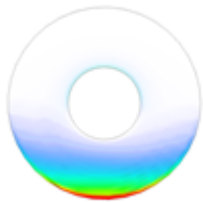
Side



Simulation 5

End

Side



Simulation 6

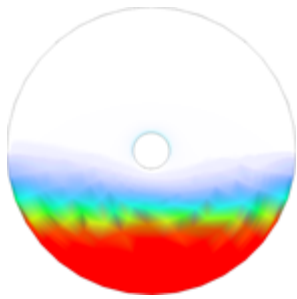
End

Side

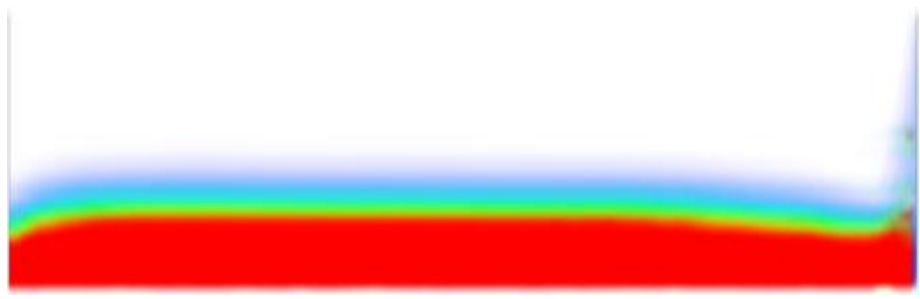


Simulation 7

End

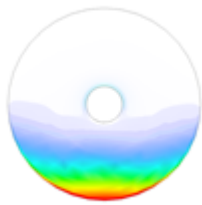


Side

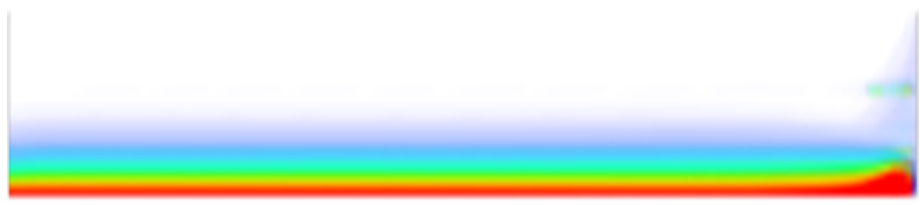


Simulation 8

End



Side



Simulation 9

End

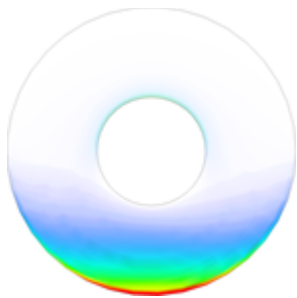


Side

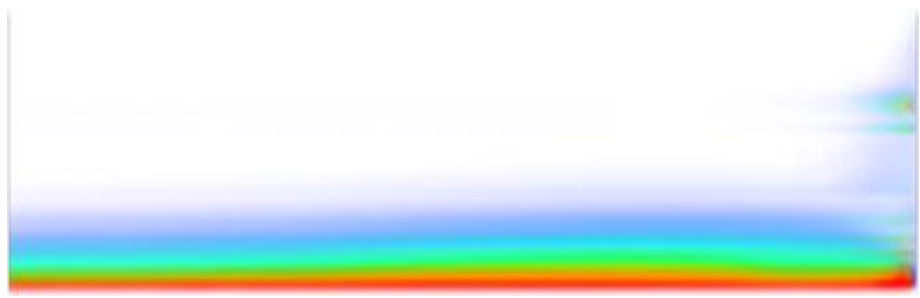


Simulation 10

End



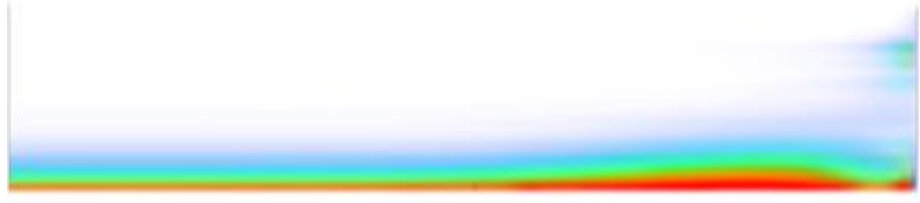
Side



Simulation 11

End

Side



Simulation 12

End

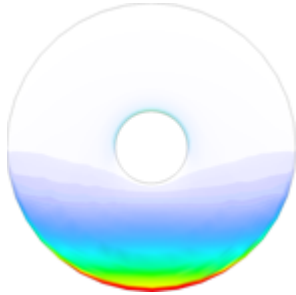
Side



Simulation 13

End

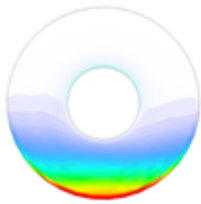
Side



Simulation 14

End

Side



Simulation 15

End

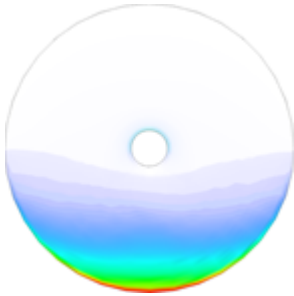
Side



Simulation 16

End

Side



Simulation 17

End

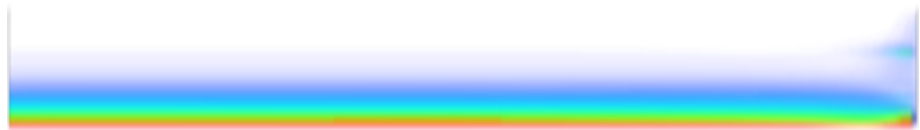
Side



Simulation 18

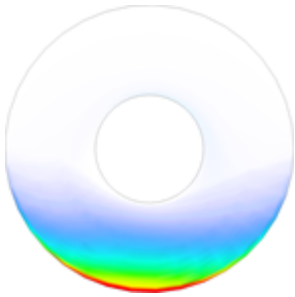
End

Side



Simulation 19

End



Side

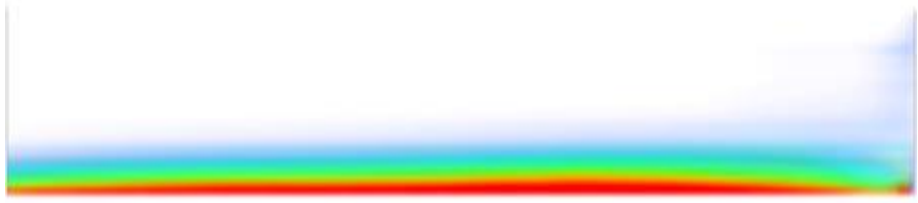


Simulation 20

End



Side



Simulation 21

End

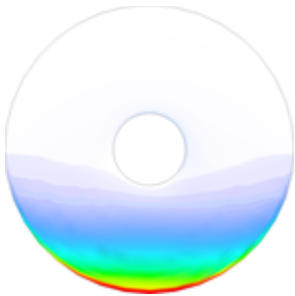


Side



Simulation 22

End



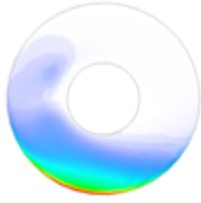
Side



Simulation 23

End

Side



Simulation 24

End

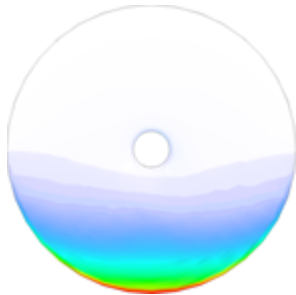
Side



Simulation 25

End

Side



Simulation 26

End

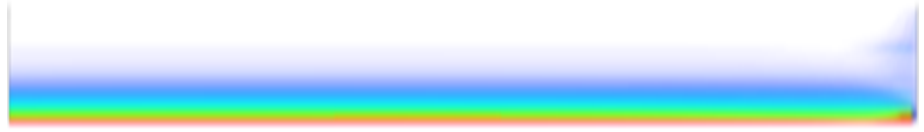
Side



Simulation 27

End

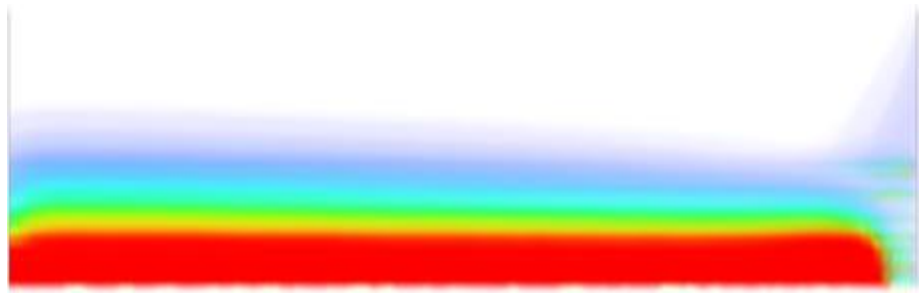
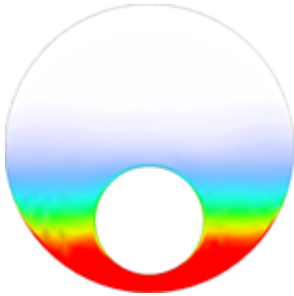
Side



Simulation 28

End

Side



Simulation 29

End

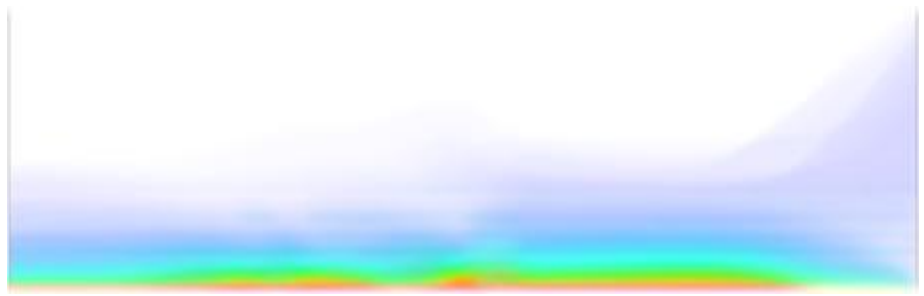
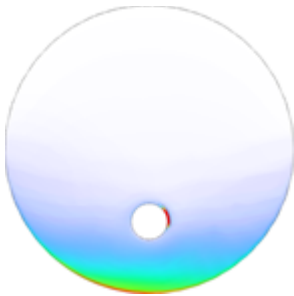
Side



Simulation 30

End

Side

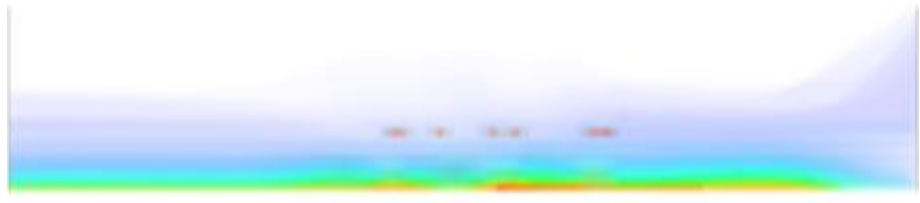


Simulation 31

End



Side



Simulation 32

End



Side



Simulation 33

End



Side



Simulation 34

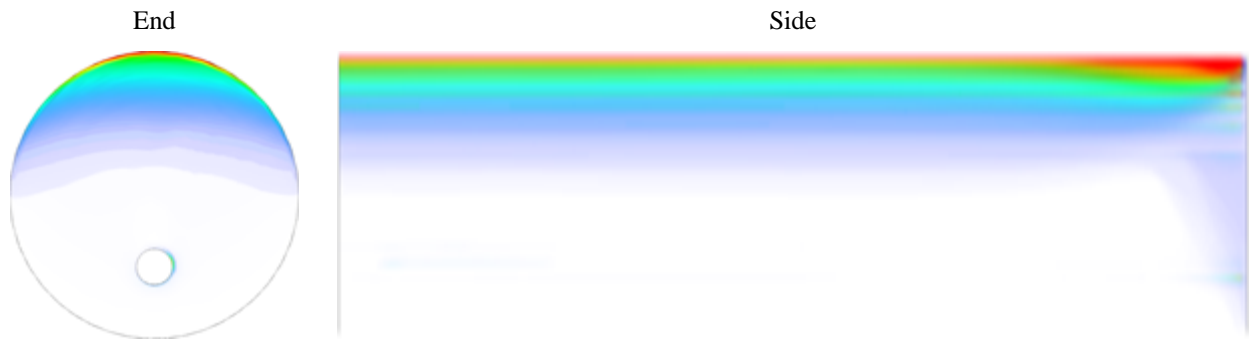
End



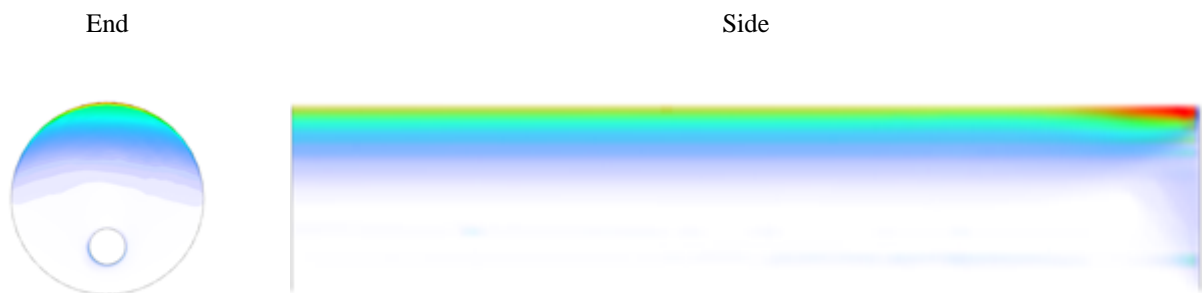
Side



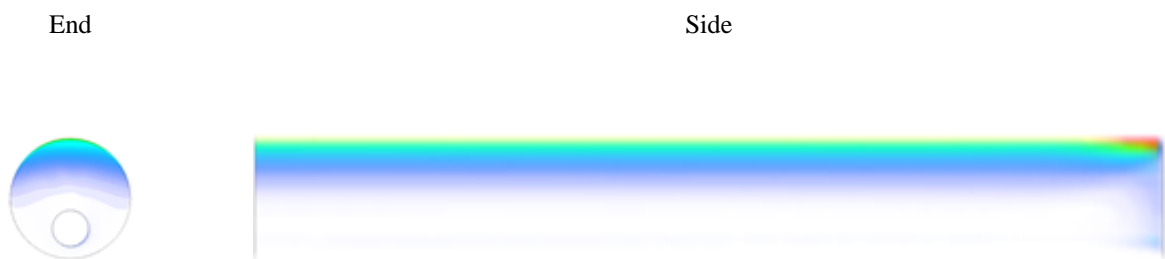
Simulation 35



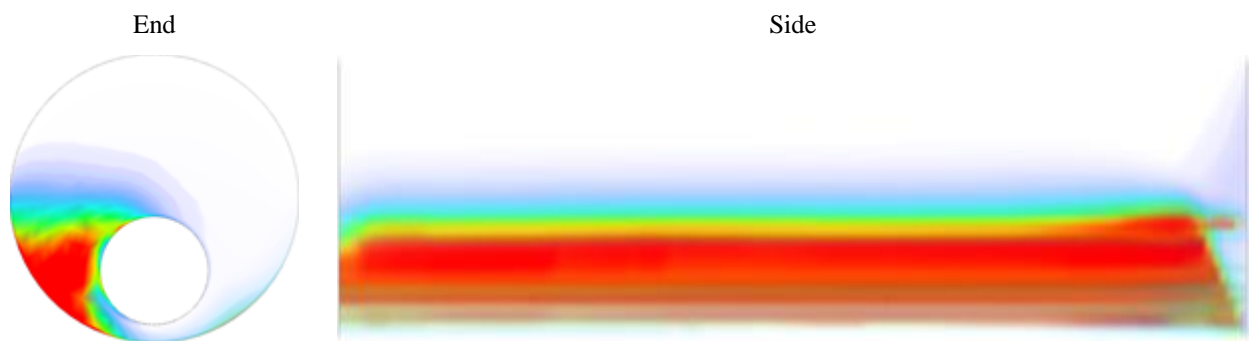
Simulation 36



Simulation 37



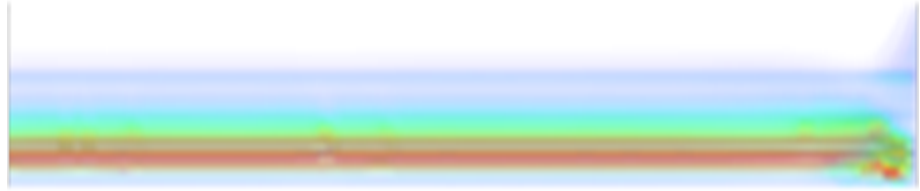
Simulation 38



Simulation 39

End

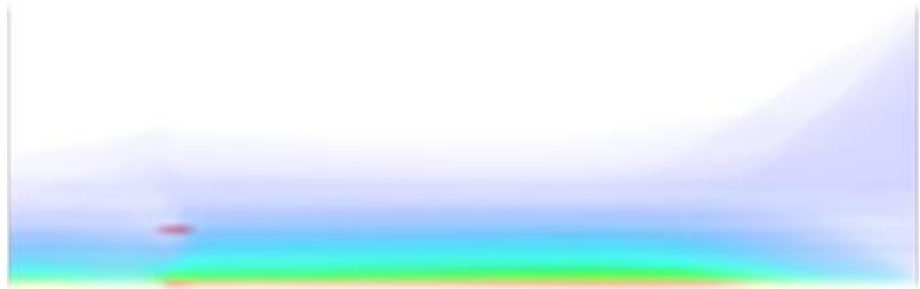
Side



Simulation 40

End

Side



Simulation 41

End

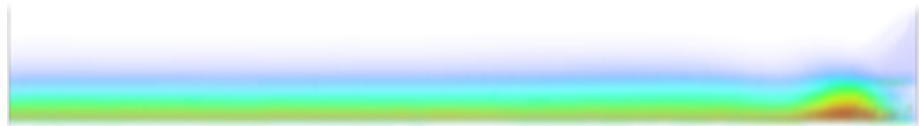
Side



Simulation 42

End

Side



Simulation 43

End



Side



Simulation 44

End



Side



Simulation 45

End



Side



Simulation 46

End



Side



Simulation 47

End

Side



Simulation 48

End

Side



Simulation 49

End

Side



Simulation 50

End

Side



Simulation 51

End

Side



Simulation 52

End

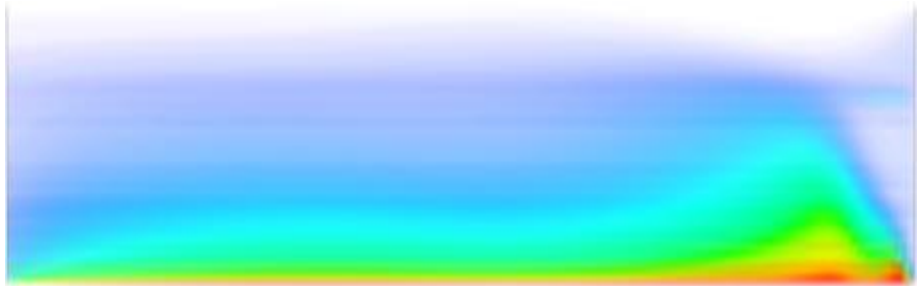
Side



Simulation 53

End

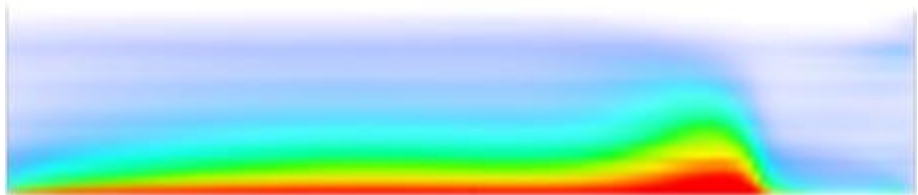
Side



Simulation 54

End

Side

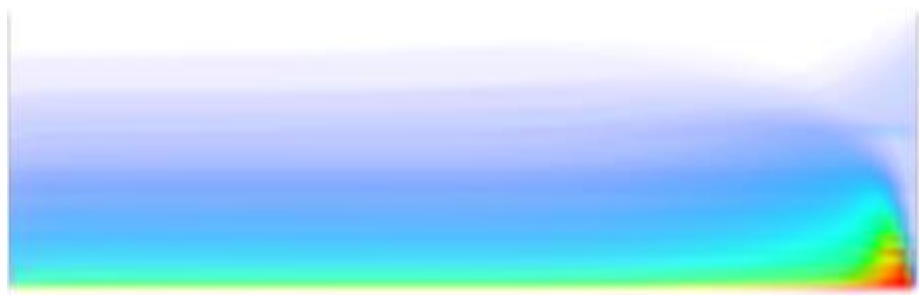


Simulation 55

End



Side



Simulation 56

End



Side

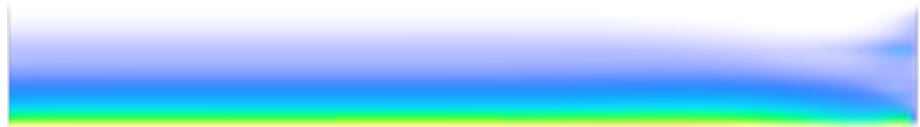


Simulation 57

End



Side

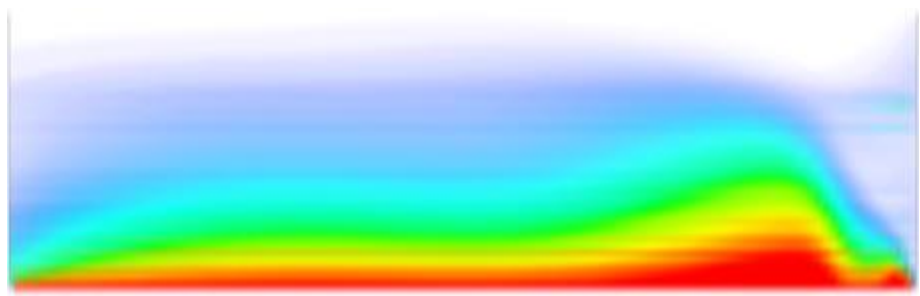


Simulation 58

End



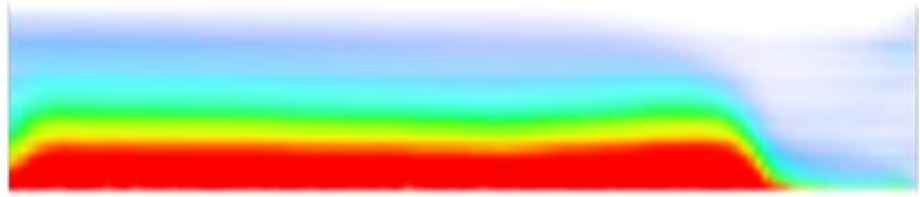
Side



Simulation 59

End

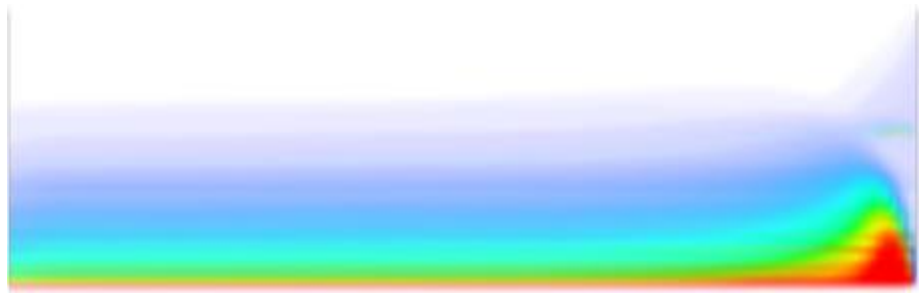
Side



Simulation 60

End

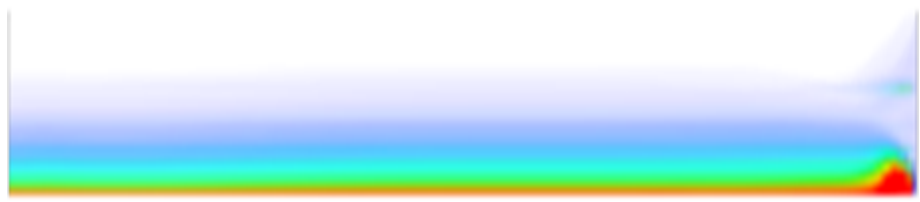
Side



Simulation 61

End

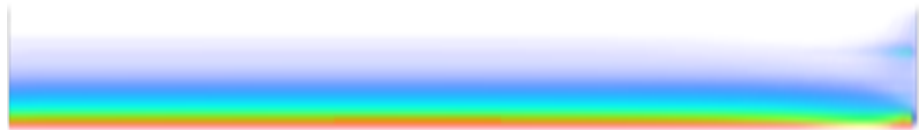
Side



Simulation 62

End

Side



Simulation 63

End

Side



Simulation 64

End

Side



Simulation 65

End

Side



Simulation 66

End

Side



Simulation 67

End

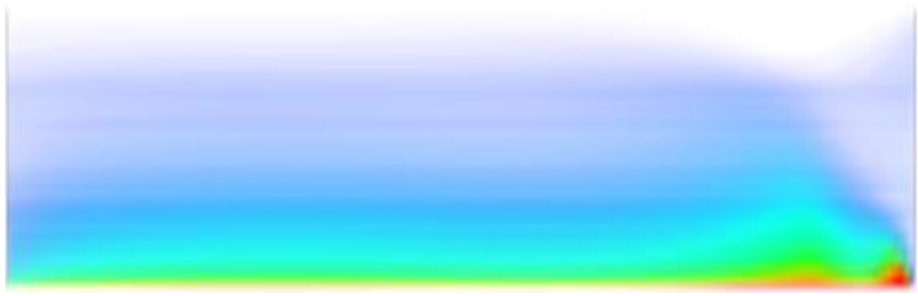
Side



Simulation 68

End

Side



Simulation 69

End

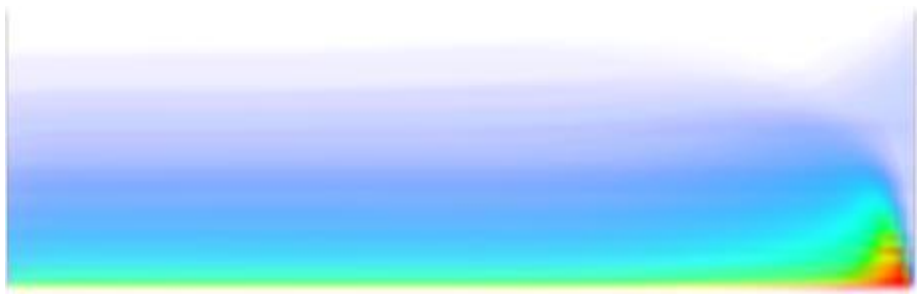
Side



Simulation 70

End

Side



Simulation 71

End

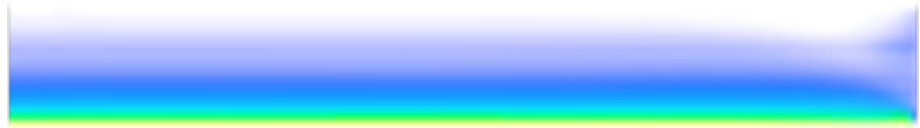
Side



Simulation 72

End

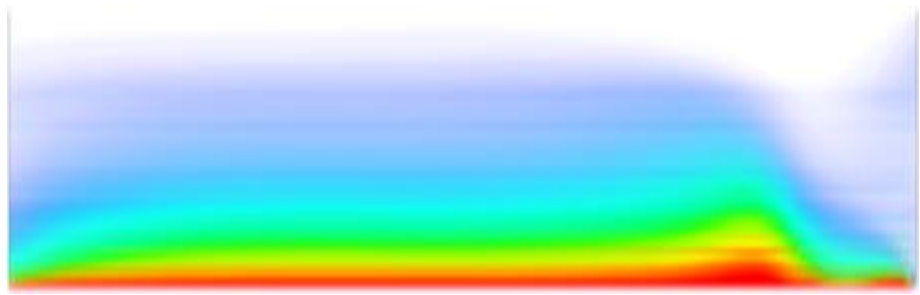
Side



Simulation 73

End

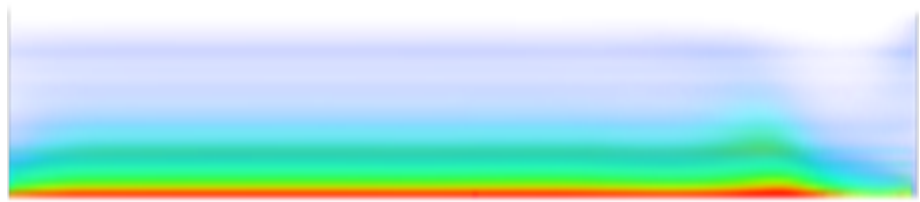
Side



Simulation 74

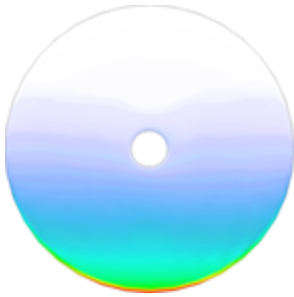
End

Side

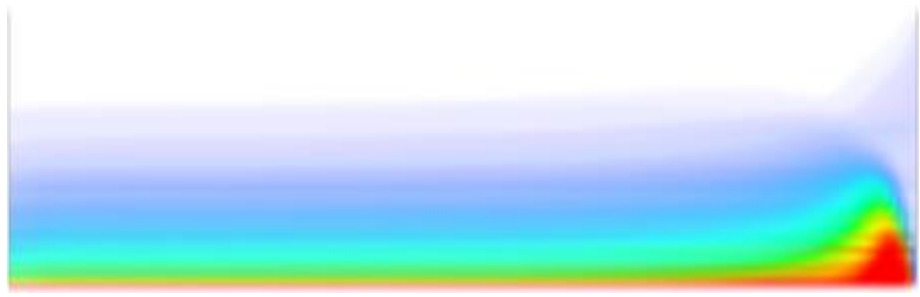


Simulation 75

End

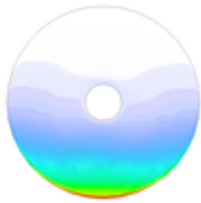


Side

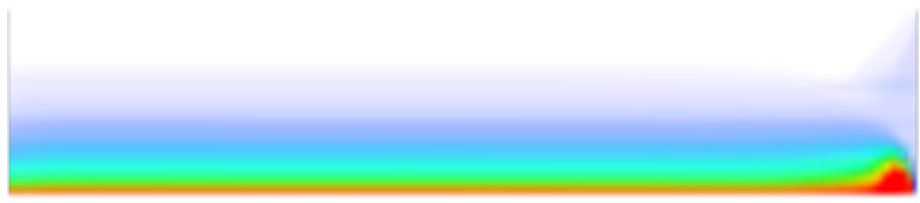


Simulation 76

End



Side

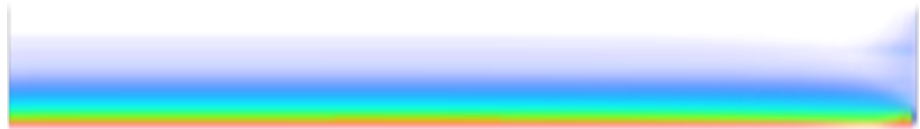


Simulation 77

End

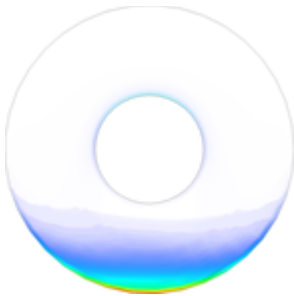


Side



Simulation 78

End



Side



Simulation 79

End

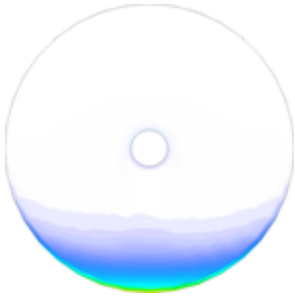
Side



Simulation 80

End

Side



Simulation 81

End

Side



Simulation 82

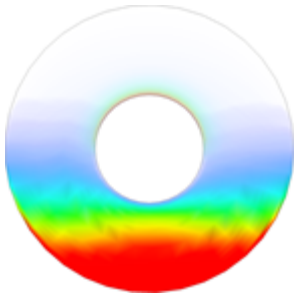
End

Side

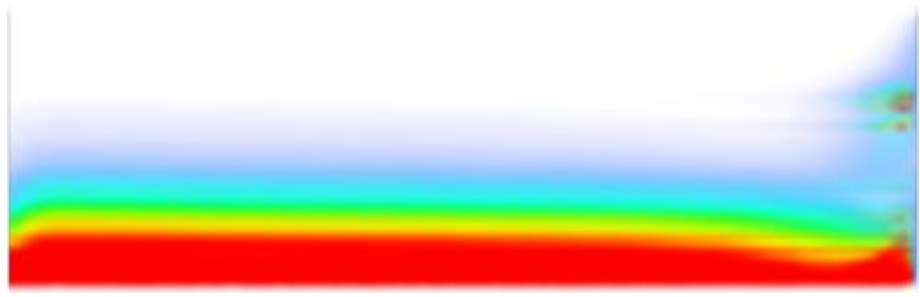


Simulation 83

End



Side

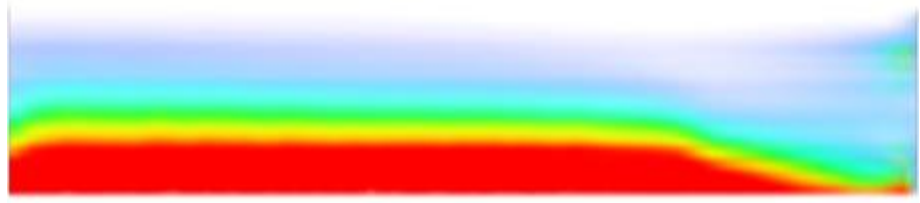


Simulation 84

End

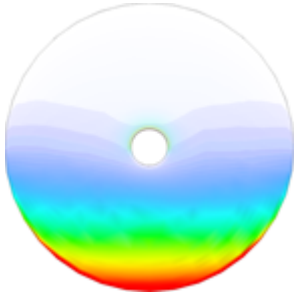


Side

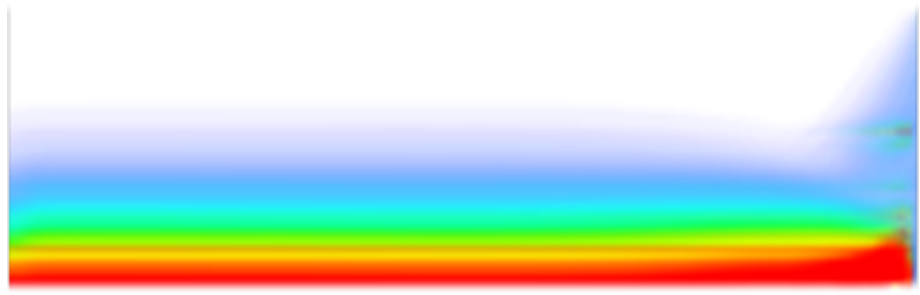


Simulation 85

End

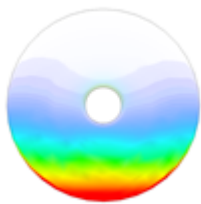


Side

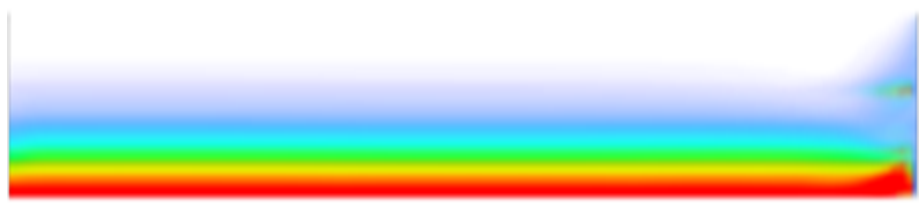


Simulation 86

End



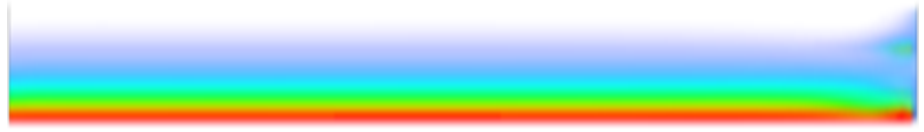
Side



Simulation 87

End

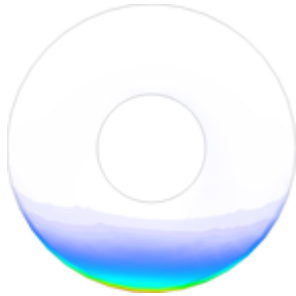
Side



Simulation 88

End

Side



Simulation 89

End

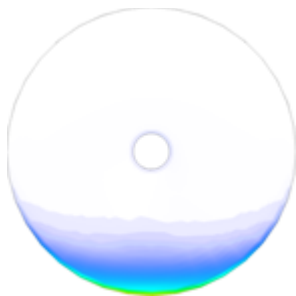
Side



Simulation 90

End

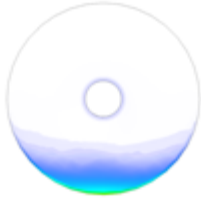
Side



Simulation 91

End

Side



Simulation 92

End

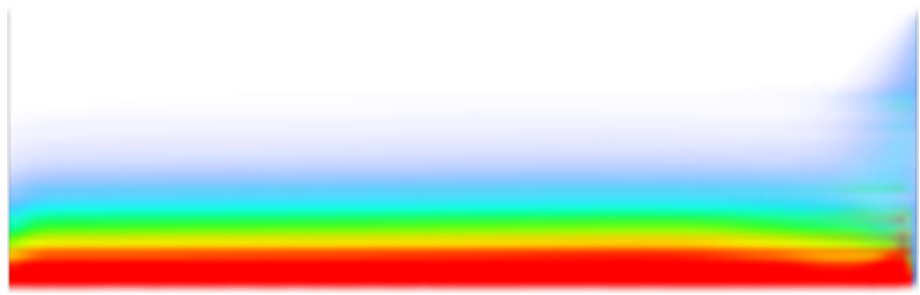
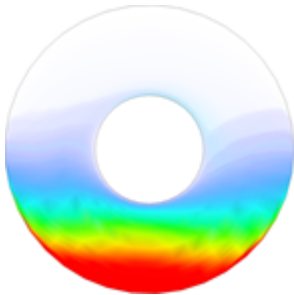
Side



Simulation 93

End

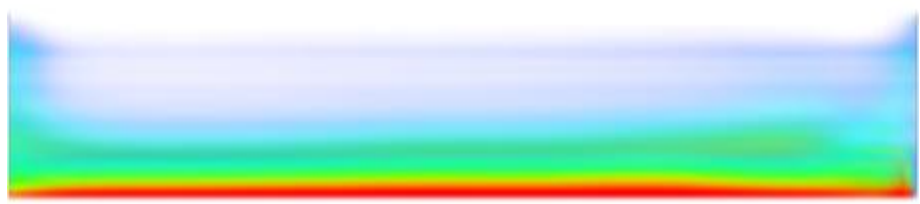
Side



Simulation 94

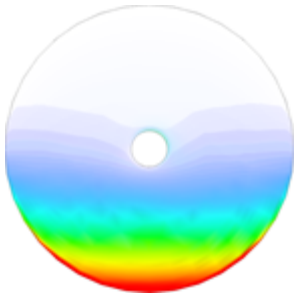
End

Side

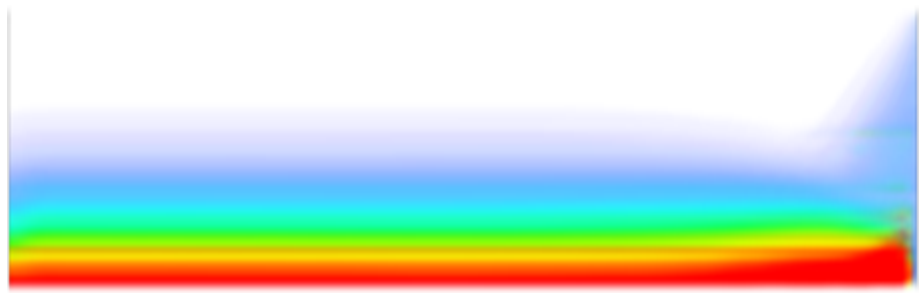


Simulation 95

End

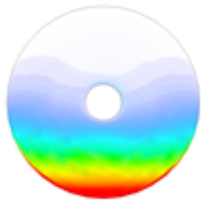


Side

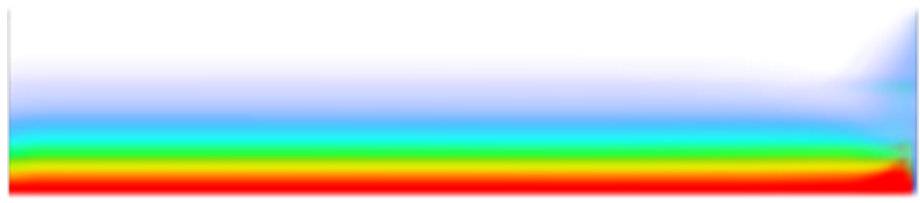


Simulation 96

End



Side

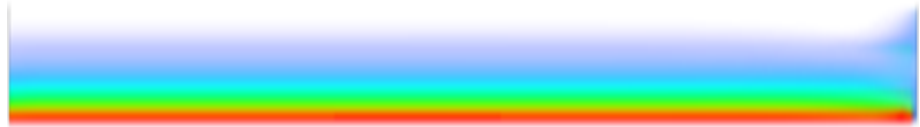


Simulation 97

End



Side



Simulation 98

End



Side



Simulation 99

End

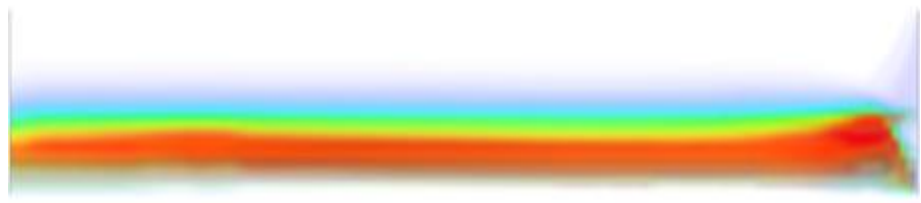
Side



Simulation 100

End

Side



Simulation 101

End

Side



Simulation 102

End

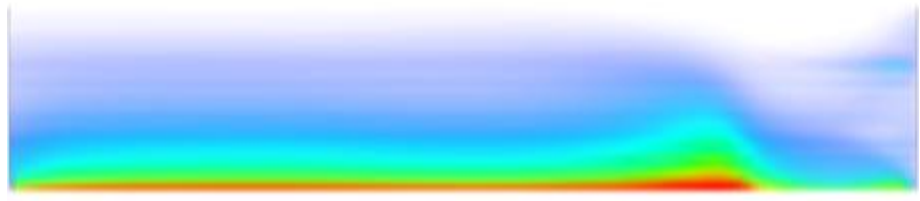
Side



Simulation 103

End

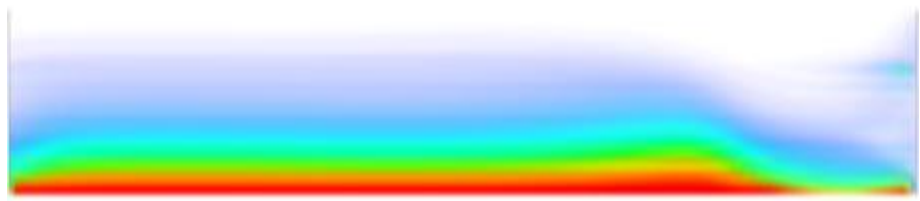
Side



Simulation 104

End

Side



Simulation 105

End

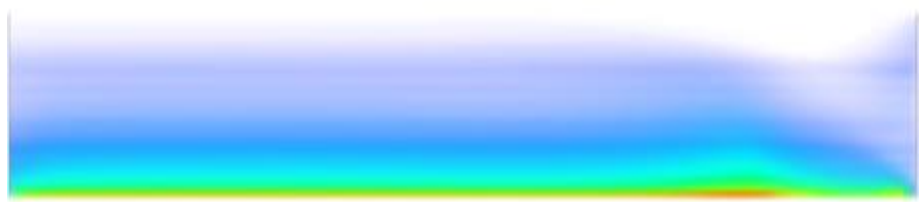
Side



Simulation 106

End

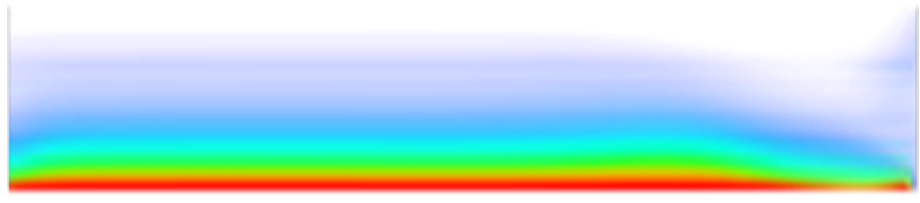
Side



Simulation 107

End

Side



Simulation 108

End

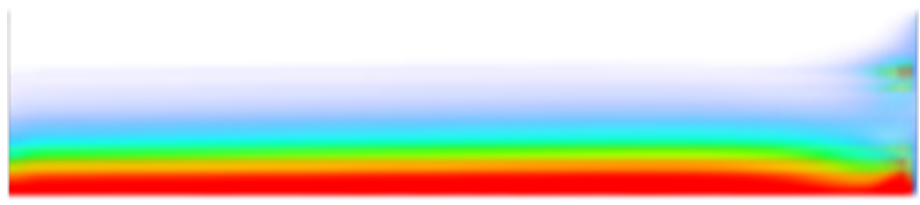
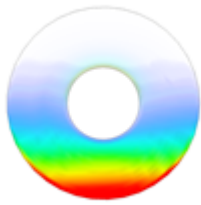
Side



Simulation 109

End

Side



Simulation 110

End

Side



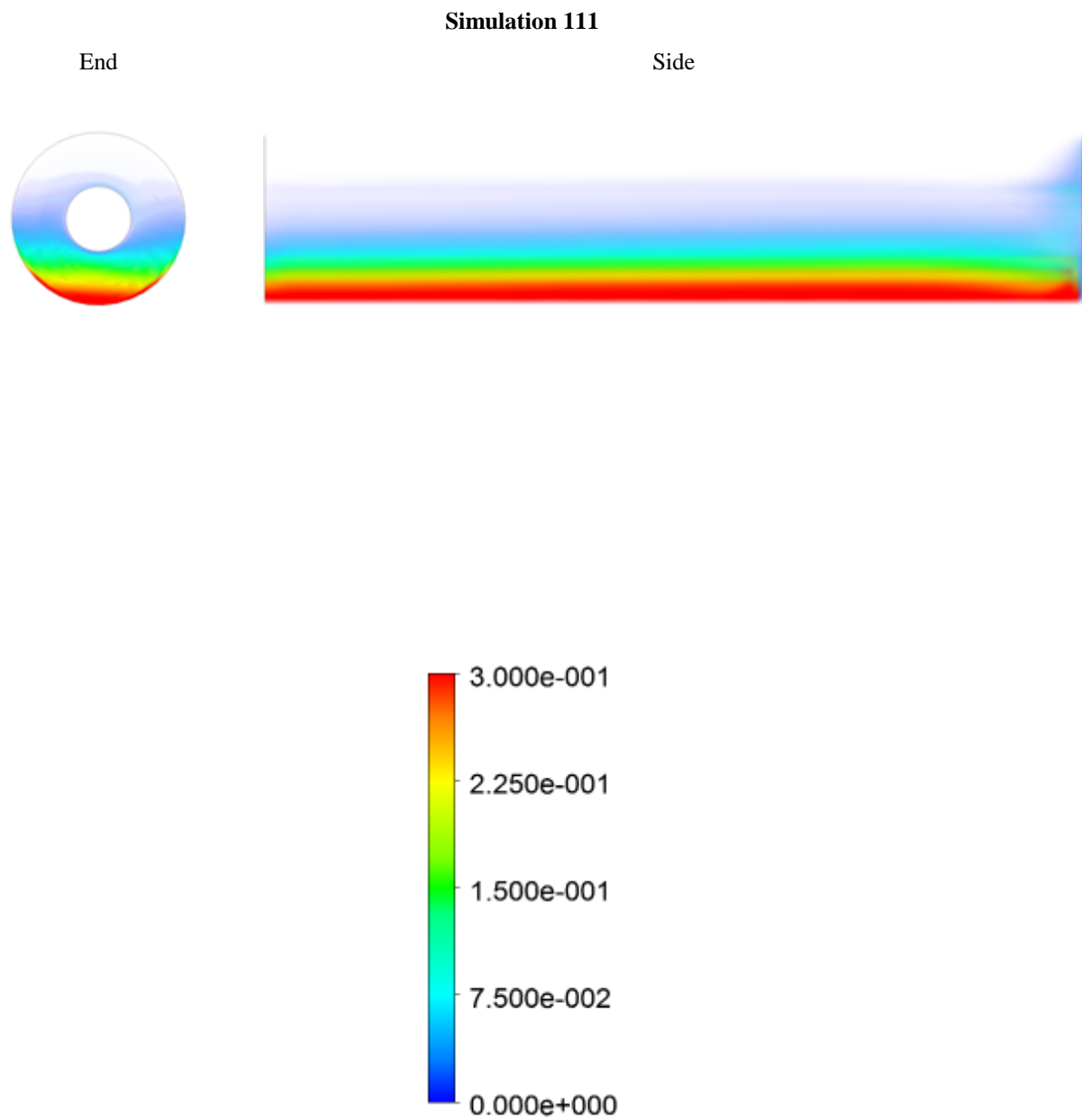


Figure D.1: Volume fractions of cuttings for the figures in Table D.1.